UNIVERSITATEA "BABES-BOLYAI" CLUJ-NAPOCA

Facultatea de Matematică şi Informatică

Catedra de Mecanică şi Astronomie

Sinteza finala a lucrarilor (2006-2008)

Grant de excelenta pentru tineri cercetatori: **cod 90**

Titlul grantului: **FENOMENE DE TRANSFER IN MEDII POROASE SI FLUIDE VASCOASE CU PROPRIETATI FIZICE VARIABILE**

Director de grant: Lect. dr. Teodor Groşan

S-au elaborat şi publicat, sau sunt în curs de publicare, următoarele lucrări ştiinţiifice:

1. A.J. Chamkha, C. Bercea (casatorita Revnic) and I. Pop, Free convection flow over a truncated cone embedded in a porous medium saturated with pure or saline water at low temperatures, *Mech. Res. Comm.,* Vol. 33, 433-440, 2006. (**ISI)**

2. T. Grosan, I. Pop, A note on the effect of radiation on free convection over a vertical flat plate embedded in a non-Newtonian fluid saturated porous media, Int. J. App. Mech. Engng., vol 11, pp. 715-722, 2006.

3. M. Kumari, T. Grosan, I. Pop, Rotating flow of power-law fluids over a stretching surface, *Technische Mechanik*, Vol. 26, pp.11-19, 2006.

4. T. Grosan, I. Pop, T. Mahmood, Thermal radiation effect on fully developed free convection in a vertical rectangular duct, Studia Univ. Babes-Bolyai, Mathematica, vol. 51, pp. 117-128, 2006.

5. T. Grosan, I. Pop, Non-linear density variation effects on the fully developed mixed convection flow in a vertical channel, Bulletin of Transilvania Universiy of Brasov, vol. 13, pp. 31-38, 2006.

6. C.Bercea (casatorita Revnic) and I. Pop: Forced convection boundary layer flow over a flat plate with variable thermal conductivity embedded in a porous medium, Bulletin of the Transilvania Univerity of BRAŞOV, Romania, ser. B1, vol 13, pp 31-38, 2006.

7. M. Kumari, C. Bercea (casatorita Revnic), I. Pop, Mixed convection along a vertical wavy surface with a discontinuous temperature profile in a porous medium, Proceedings of 3ICAPM 3rd International Conference on Applications of Porous Media, May 29–June 3, 2006, Marrakesch, Morocco, Paper number 4.

8. M.Kumari, C.Bercea (casatorita Revnic), I.Pop: Mixed convection flow along a thin vertical cylinder with localized cooling or heating in a porous medium, Int Jour Flud Mech Res, vol 34, 66-78, 2007.

9. T. Grosan, I. Pop, Thermal radiation effect on fully developed mixed convection flow in a vertical channel, *Technische Mechanik*, Vol. 27, pp. 37-47, 2007.

10. M. Kumari, C. Bercea (casatorita Revnic), I. Pop: Effect of non-uniform suction or injection on mixed convection boundary layer flow over a vertical permeable cylinder embedded in a porous medium, Malayasian J. Mathematical Sci., 1(2): 31-42 (2007)

11. M. Kumari, T. Grosan, I. Pop, Boundary layers growth on a moving surface due to an impulsive motion and sudden increase of wall heat flux, *Int. J. Appl. Mech. Engng*., Vol. 13, pp.203-215, 2008.

12. C. Bercea (casatorita Revnic), T. Grosan, I. Pop,. Heat Transfer in Axisymmetric Stagnation Flow on a Thin Cylinder, Studia Univ. Babes-Bolyai, Mathematica, vol. 53, pp. 119-132, 2008

13. Ş. M. Şoltuz, Teodor Grosan, Data Dependence for Ishikawa Iteration When Dealing with Contractive-Like Operators, *Fixed Point Theory and Applications*, Vol. 2008, Article ID 242916, 7 pages.(doi:10.1155/2008/242916).

14. T. Grosan, I. Pop and S.R. Pop, Radiation and variable viscosity effects in forced convection from a horizontal plate embedded in a porous medium, Stuida Univ. Babes-Bolyai, Mathematica, (in curs de publicare).

15. C. Revnic, T. Grosan, J. Merkin and I. Pop, Mixed convection near an axisymmetric stagnation point on a vertical cylinder, *Journal of Engineering Mathematics* (acceptata)

16. A. Postelnicu, T. Grosan and I. Pop, Brinkman Flow of a Viscous Fluid Through a Spherical Porous Medium Embedded in Another Porous Medium, *Transport in Porous Media* (sent for publication)

17. T. Grosan, C. Revnic, I. Pop, and D.B. Ingham, Magnetohydrodynamics oblique stagnation-point flow, *Meccanica* (sent for publication)

18. C.Revnic, T.Grosan and I.Pop: Unsteady boundary layer flow and heat transfer over a stretching sheet, International Conference of Numerical Analysis and Applied Mathematics (ICNAAM), Corfu, Grecia, 16-20 September 2007. In: *American Institut of Physics (AIP) – Conferences Proceedings*, November 2007(in press)

19. T. Grosan, C. Revnic, I. Pop, D.B. Ingham, Magnetic field and internal heat generation effects on the free convection in a rectangular cavity filled with a porous medium, Int. J. Heat Mass Transfer, (trimisa spre publicare)

Ca rezultat al grantului s-au publicat sau au fost trimise spre publicare un număr de 17 lucrari :

Juranale **ISI :** 2 lucrari publicată (1, 13)

2 lucrări acceptate (15,18)

3 lucrări trimise spre publicare (16, 17, 19)

Jurnale din străinătate:

6 lucrari publicate (2,3,7,8,9,10,11)

Jurnale din țară:

4 lucrări publicate (4,5,6,12)

o lucrare acceptată (14)

De asemenea membrii echipei de cercetare au participat la conferințe în țară (4 conferințe) şi străinătate (o conferință) şi la stagii de cercetare în străinătate (2 stagii).

S-au elaborat program numerice în Matlab şi Mathematica pentru rezolvarea sistemelor de ecuații diferențiale şi ecuații cu derivate parțiale.

Lucrările ISI au fost adăugate în extenso în anexă, pentru celelalte lucrari fiind adăugat abstractul.

Cluj-Napoca, 30 Iulie 2008

Director de proiect,

Lect. dr. Teodor Groşan

Anexa I

Articole şi preprinturi publicate sau trimise spre publicare în jurnale indexate ISI

Available online at www.sciencedirect.com
SCIENCE DIRECT®
ELSEVIER
Mechanics Research Communications 33 (2006) 433–440
MECHANICS RESEARCH COMMUNICATIONS
www.elsevier.com/locate/mechrescom

Free convection flow over a truncated cone embedded in a porous medium saturated with pure or saline water at low temperatures

A.J. Chamkha [a], C. Bercea [b], I. Pop [b,*]

[a] *Manufacturing Engineering Department, The Public Authority for Applied Education and Training, Shuweikh 70654, Kuwait*
[b] *Faculty of Mathematics, University of Cluj, R-3400 Cluj, CP 253, Romania*

Available online 17 November 2005

Abstract

Steady free convection boundary layer about a truncated cone embedded in a porous medium saturated with pure or saline water at low temperatures has been studied in this paper. The governing coupled partial differential equations are solved numerically using a very efficient finite-difference method. Several new parameters arise and the results are given for some specific values of these parameters. The obtained results for a Boussinesq fluid are compared with known results from the open literature and it is shown that the agreement between these results is very good.

Keywords: Truncated cone; Boundary layer; Porous medium; Cold or saline water

1. Introduction

Convective flow in porous media has been a subject of great interest for the last several decades due to its numerous thermal engineering applications in various disciplines, such as geophysical thermal insulation, modeling of packed sphere beds, cooling of electronic systems, groundwater hydrology, petroleum reservoirs, coal combustors, ground water pollution, ceramic processes, to name just a few of these applications. Some of the most important analytical, numerical and experimental studies with such applications, which present the current state-of-the-art in the area of convective heat transfer in porous media, have been gathered in the monographs by Nield and Bejan (1999), Ingham and Pop (1998, 2002), Vafai (2000), Pop and Ingham (2001), and Bejan and Kraus (2003).

Studies of convective heat transfer in porous media have been carried out in the past using the Boussinesq approximation, namely the fluid density ρ varies linearly with temperature. However, this is inappropriate for water at low temperatures because of the extremum at about 4 °C in pure water at 1 atm. Such conditions occur commonly in porous medium, such as permeable soils flooded by cold lake or sea water, water–ice

* Corresponding author. Tel.: +40 264 594315; fax: +40 264 591906.
E-mail address: popi@math.ubbcluj.ro (I. Pop).

0093-6413/$ - see front matter © 2005 Elsevier Ltd. All rights reserved.
doi:10.1016/j.mechrescom.2005.10.001

slurries, etc. A limited number of studies have been devoted in the past to the problem of convective boundary layer adjacent to heated or cooled bodies immersed in a porous medium saturated with cold water wherein a density extremum may arise. It should be mentioned that the buoyancy flow with an extremum may become very complicated, with local flow reversals and convective inversions. Density differences may then not be expressed as a linear function of the temperature. Ramilison and Gebhart (1980) examined the possible similarity solutions for vertical, buoyancy induced flow in a porous medium saturated with cold water. Lin and Gebhart (1986) have considered the corresponding case of a horizontal surface in a porous medium saturated with cold or saline water. Gebhart et al. (1983) obtained multiple steady state solutions for the problem considered by Lin and Gebhart (1986) using two numerical codes. A review of the convective flow in the vicinity of the maximum-density condition in water at low temperatures, along with relevant citations, is available in the survey by Kukula et al. (1987).

The present paper concerns the steady free convection boundary layer adjacent to a heated truncated cone embedded in an extensive porous medium saturated with either pure or saline water under the conditions in which a density extremum might occur. The density state equation used here is that proposed by Gebhart and Mollendorf (1977), which has been shown to be very accurate for both pure and saline water to a pressure level of 1000 bars up to 20 °C, and to 40% salinity. To the best of our knowledge, this problem has not been considered before. However, Yih (1999) made an analysis for free convection boundary layer about a truncated cone in a porous medium saturated with a Boussinesq fluid subjected to the coupled effects of thermal and mass diffusion.

2. Basic equations

Consider the steady free convection over a truncated cone (with half angle γ) embedded in a saturated porous medium filled with pure or saline water. It is assumed that the surface of the truncated cone is maintained at the constant temperature T_w, while the temperature of the ambient fluid is T_∞, where $T_w > T_\infty$. Fig. 1 shows the flow model and physical coordinate system. The governing boundary layer equations are given by, see Chamkha et al. (2004),

$$\frac{\partial}{\partial x}(ru) + \frac{\partial}{\partial y}(rv) = 0 \tag{1}$$

$$u = \frac{\rho_m g K}{\mu}\left[|T - T_m|^q - |T_\infty - T_m|^q\right]\cos\gamma \tag{2}$$

$$u\frac{\partial T}{\partial x} + v\frac{\partial T}{\partial y} = \alpha_m \frac{\partial^2 T}{\partial y^2} \tag{3}$$

subject to the boundary conditions

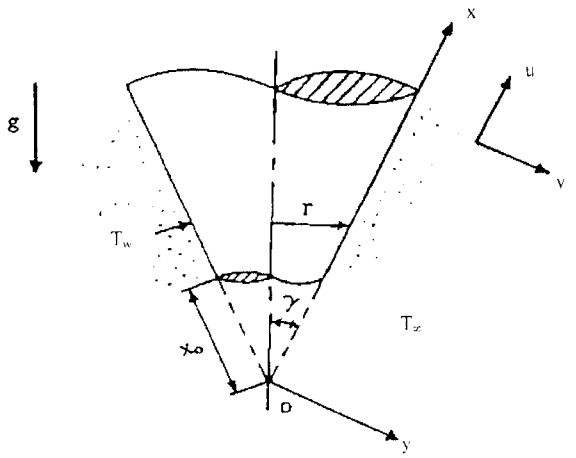

Fig. 1. Physical model and coordinate system.

$$v = 0, \quad T = T_w \quad \text{on } y = 0$$
$$T = T_\infty \quad \text{as } y \to \infty \tag{4}$$

where $r = x\sin\gamma$, x and y are the streamwise and transverse Cartesian coordinates, respectively, u and v are the velocity components in the x and y directions, respectively, T is the fluid temperature, K is the permeability of the porous medium, g is the magnitude of the gravitational acceleration, ρ, μ and α_m are the density, viscosity and effective thermal diffusivity of the porous medium. The new density equation, which applies to both pure and saline water is given by

$$\rho = \rho_m(s,p)[1 - \beta_m(s,p)|T - T_m(s,p)|^q] \tag{5}$$

where p is the pressure, s is the salinity and ρ_m and T_m denote the maximum density and temperature, respectively, for given pressure and salinity levels. The forms and values of q, β_m, ρ_m and T_m are given in the paper by Gebhart and Mollendorf (1977).

We now introduce the following new variables:

$$\xi = x^*/x_0, \quad x^* = (x - x_0)/x_0, \quad \eta = Ra_{x^*}^{1/2}(y/x^*)$$
$$\psi = \alpha_m r Ra_{x^*}^{1/2} f(\xi,\eta), \quad \theta(\xi,\eta) = (T - T_\infty)/(T_w - T_\infty) \tag{6}$$

where ψ is the stream function which is defined in the usual way as $u = (1/r)\partial\psi/\partial y$ and $v = -(1/r)\partial\psi/\partial x$, respectively and $Ra_{x^*} = \rho_m g K \beta_m |T_m - T_\infty|^q x^* \cos\gamma/\mu\alpha_m$ is the modified local Rayleigh number. Substituting (6) into Eqs. (1)–(3) we get

$$f' = |\theta - R|^q - |R|^q \tag{7}$$

$$\theta'' + \left(\frac{1}{2} + \frac{\xi}{1+\xi}\right) f\theta' = \xi\left(f'\frac{\partial\theta}{\partial\xi} - \theta'\frac{\partial f}{\partial\xi}\right) \tag{8}$$

subject to the boundary conditions (4), which become

$$f(\xi,0) = 0, \quad \theta(\xi,0) = 1, \quad \theta(\xi,\infty) = 0 \tag{9}$$

where primes denote partial differentiation with respect to η and the parameter R is defined as

$$R = \frac{T_m - T_\infty}{T_w - T_\infty} \tag{10}$$

It is worth mentioning that the parameter R places the prescribed temperature T_w and T_∞ with respect to $T_m(s,p)$. It also indicates the local direction of the buoyancy force across the thermal region and thus, also the direction of flow (see Ramilison and Gebhart, 1980).

In terms of the new variables, the velocity components in x- and y-directions are given by

$$u = (\alpha_m Ra_{x^*}/x^*)f'$$
$$v = -\left(\alpha_m Ra_{x^*}^{1/2}/x^*\right)\left[\left(\frac{1}{2} + \frac{\xi}{1+\xi}\right)f + \xi\frac{\partial f}{\partial\xi} - \frac{1}{2}\eta f'\right] \tag{11}$$

We are also interested in the local Nusselt number, which is given by

$$Nu_{x^*}/Ra_{x^*}^{1/2} = -\theta'(\xi,0) \tag{12}$$

It is worth mentioning to this end that Eqs. (7) and (8) become similar for $\xi = 0$ and $\xi = \infty$ and they describe the free convection over a vertical flat plate and, respectively, over a full cone embedded in a porous medium saturated with cold water.

3. Results and discussion

Eqs. (7) and (8) subject to the boundary conditions (9) have been solved numerically for some values of the temperature parameter R in the range between -10 and 0.194 at some upstream coordinates $\xi = 0.0$–1.0 using the finite-difference scheme developed by Blottner (1970). The values of q used are $q = 1$, 1.727147 and

Table 1
Comparison of the values of $-\theta'(\xi,0)$

ξ	Cheng et al. (1985)	Yih (1999)	Present
0	0.4437	0.4439	0.4444
0.5	0.5412	0.5285	0.5294
1.0	0.5991	0.5807	0.5812
2.0	0.6572	0.6373	0.6399
6.0	0.7219	0.7123	0.7130
10.0	0.7391	0.7330	0.7336
20.0	0.7532	0.7500	0.7507
40.0	0.7607	0.7592	0.7596
∞	0.7685	0.7686	0.7690

1.894816 (cold water approximation) also considered by Ramilison and Gebhart (1980). It should be mentioned that close to $R = 0.194$ the convergence of the numerical solution is very slow. This is expected due to the occurrence of the flow reversal across the convective layer. A comparison of the present results for the local Nusselt number, $-\theta'(\xi,0)$, with those reported by Cheng et al. (1985) and Yih (1999) is given in Table 1 for $R = 0$ and $q = 1$ (classical Boussinesq approximation), and some values of the streamwise parameter ξ. It can be seen from Table 1 and Fig. 8 that the present results are in excellent agreement with those of Cheng et al. (1985) and Yih (1999), and we are, therefore, confident that the present numerical results are very accurate.

The non-dimensional velocity $f'(\xi,\eta)$ and non-dimensional temperature $\theta(\xi,\eta)$ profiles are shown in Figs. 2–8. Also, the variation of the local Nusselt number given by Eq. (12) is plotted in Figs. 9 and 10. It is seen from Figs. 2 and 3 that for a fixed value of q and ξ, the velocity profiles increase, while the temperature profiles decrease as the parameter R decreases from zero. The same happens for these profiles when q increases for a fixed value of R and ξ as can be seen from Figs. 4 and 5. However, Figs. 6 and 7 show that both the velocity and temperature profiles decrease as the streamwise coordinate ξ increase from $\xi = 0$ to $\xi = \infty$ (full cone). The present results are also compared in Fig. 8 with those of Ramilison and Gebhart (1980) for the corresponding problem of a vertical flat plate ($\xi = 0$) embedded in a porous medium saturated with cold water. An excellent agreement between these results can be again noticed. We notice that a small flow reversal occurs for the values of R in the range $0.1 < R \leqslant 0.194$ that confirms the findings of Ramilison and Gebhart (1980). Further, Figs. 9 and 10 show that the values of the local Nusselt number increases with a decrease from zero of the temperature parameter R and with the increase of the parameter q. The variation of the heat transfer is very large over the whole range of R for the value of q considered. However, the variation of the local Nusselt number is almost linear with ξ.

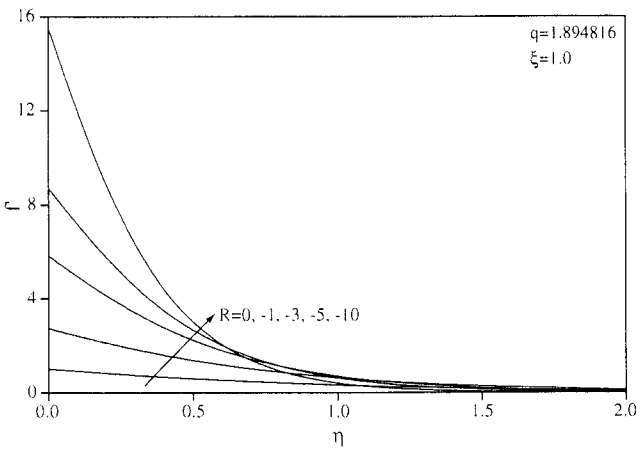

Fig. 2. Effects of R on the tangential velocity profiles.

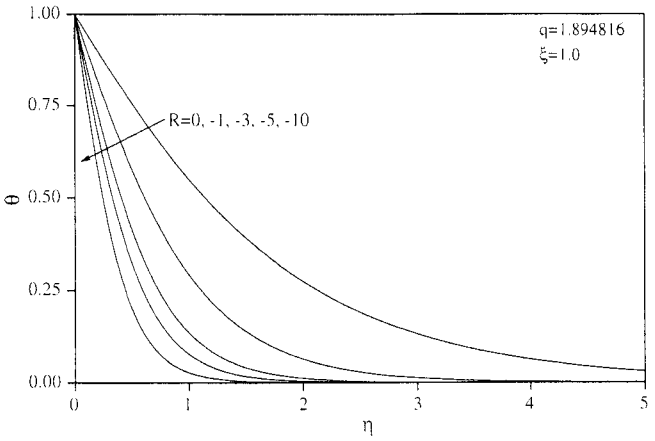

Fig. 3. Effects of R on the temperature profiles.

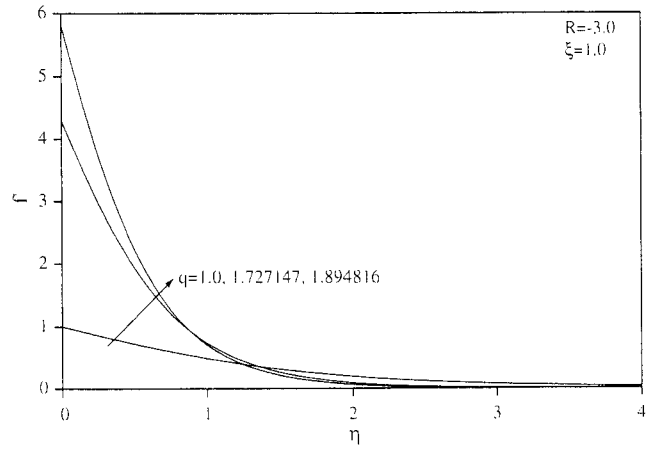

Fig. 4. Effects of q on the tangential velocity profiles.

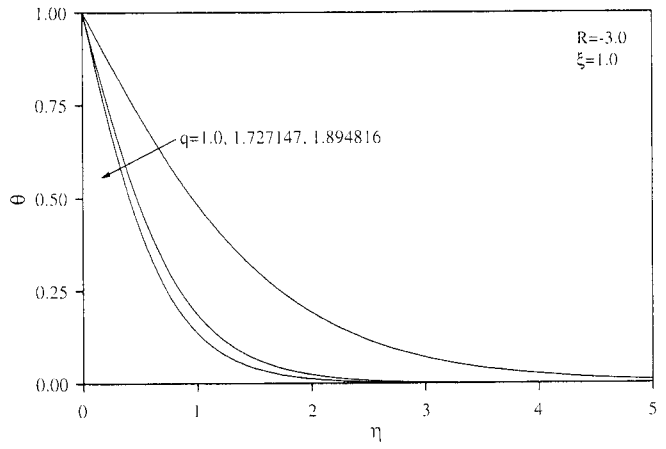

Fig. 5. Effects of q on the temperature profiles.

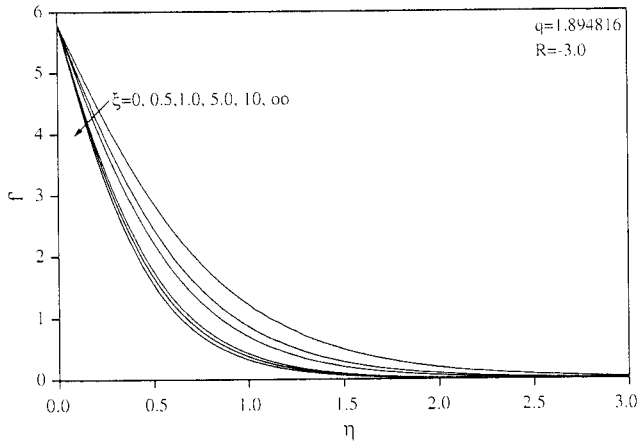

Fig. 6. Development of the tangential velocity profiles.

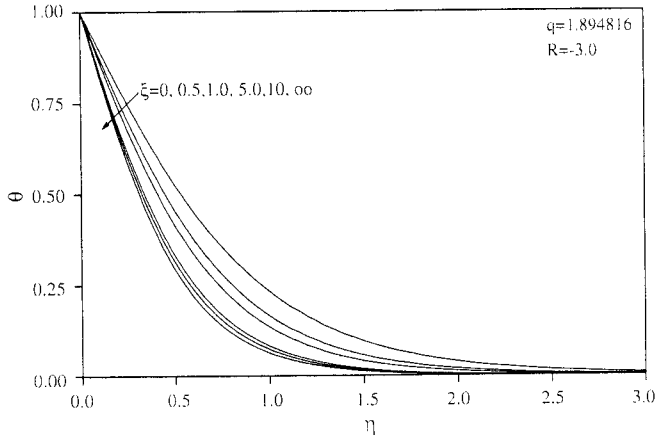

Fig. 7. Development of the temperature profiles.

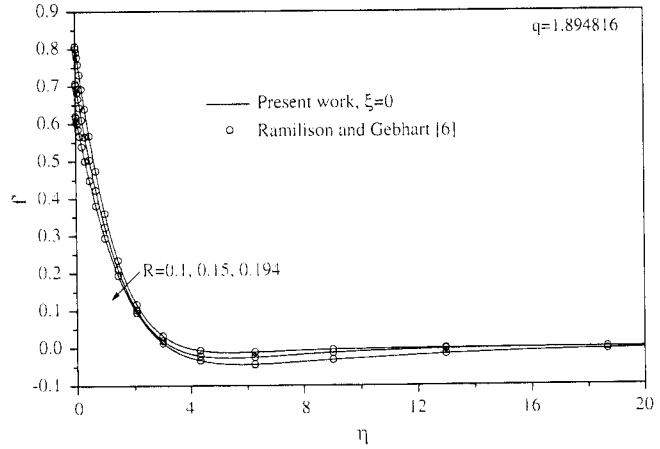

Fig. 8. Reserved flow conditions for various values of R.

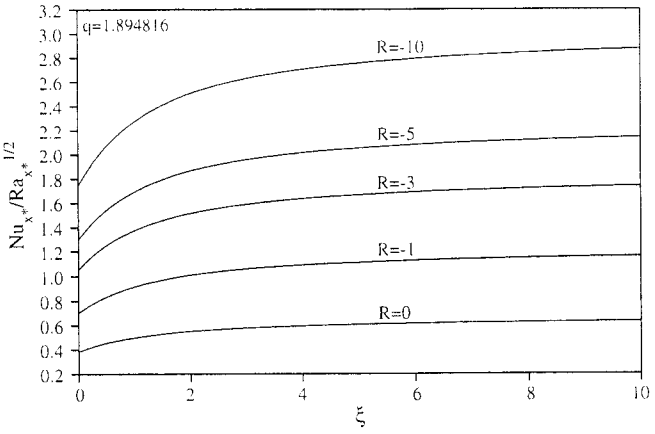

Fig. 9. Effects of R on the local Nusselt number.

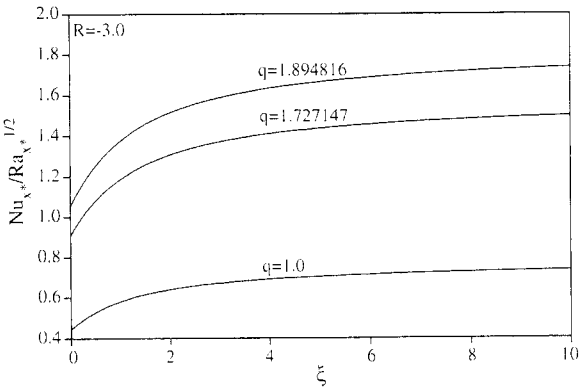

Fig. 10. Effects of q on the local Nusselt number.

4. Conclusions

The free convection boundary layer flow over a heated vertical truncated cone embedded in a porous medium saturated with cold water wherein a density extremum may arise is investigated. Numerical investigations supported by an exact analysis with the finite-difference are made for an isothermal surface and over a wide range of the temperature parameter R and three values of the exponent q in density Eq. (5). Two parameters R, and q arise and they determine the fundamental nature of the density field and the effects of the pressure and salinity levels, respectively. The conventional free convection approximation is also included in the present formulation by choosing $q = 1$ in those flows for which $R = 0$ (classical Boussinesq approximation). It is shown that the effect of q on heat transfer is great when $|R|$ is high, and it increases with an increase of $|R|$.

References

Bejan, A., Kraus, A.D. (Eds.), 2003. Heat Transfer Handbook. Wiley, New York.
Blottner, F.C., 1970. AIAA J. 8, 193.
Chamkha, A.J., Bercea, C., Pop, I., 2004. Int. J. Appl. Math. Eng. 9, 273.
Cheng, P., Le, T.T., Pop, I., 1985. Int. Commun. Heat Mass Transfer 12, 717.
Gebhart, B., Mollendorf, J.C., 1977. Deep Sea Res. 24, 831.
Gebhart, B., Hassard, B., Hastings, S.P., Kazarinoff, N., 1983. Numer. Heat Transfer 6, 337.
Ingham, D.B., Pop, I. (Eds.), 1998. Transport Phenomena in Porous Media. Pergamon, Oxford, vol. II, 2002.

Kukula, D.J., Gebhart, B., Mollendorf, J.C., 1987. Adv. Heat Transfer 18, 325.
Lin, D.-S., Gebhart, B., 1986. Int. J. Heat Mass Transfer 29, 611.
Nield, D.A., Bejan, A., 1999. Convection in Porous Media, 2nd ed. Springer, New York.
Pop, I., Ingham, D.B., 2001. Convective Heat Transfer: Computational and Mathematical Modelling of Viscous Fluids and Porous Media. Pergamon, Oxford.
Ramilison, J.M., Gebhart, B., 1980. Int. J. Heat Mass Transfer 23, 1521.
Vafai, K. (Ed.), 2000. Handbook of Porous Media. Marcel Dekker, New York.
Yih, K.A., 1999. Acta Mech. 137, 83.

Hindawi Publishing Corporation
Fixed Point Theory and Applications
Volume 2008, Article ID 242916, 7 pages
doi:10.1155/2008/242916

Research Article

Data Dependence for Ishikawa Iteration When Dealing with Contractive-Like Operators

Ş. M. Şoltuz[1,2] and Teodor Grosan[3]

[1] *Departamento de Matematicas, Universidad de los Andes, Carrera 1 No. 18A-10, Bogota, Colombia*
[2] *The Institute of Numerical Analysis, P.O. Box 68-1, Cluj-Napoca, Romania*
[3] *Department of Applied Mathematics, Babes-Bolyai University, Cluj-Napoca, Romania*

Correspondence should be addressed to Teodor Grosan, tgrosan@math.ubbcluj.ro

Received 13 February 2008; Accepted 27 May 2008

Recommended by Hichem Ben-El-Mechaiekh

We prove a convergence result and a data dependence for Ishikawa iteration when applied to contraction-like operators. An example is given, in which instead of computing the fixed point of an operator, we approximate the operator with a contractive-like one. For which it is possible to compute the fixed point, and therefore to approximate the fixed point of the initial operator.

1. Introduction

Let X be a real Banach space; let $B \subset X$ be a nonempty convex closed and bounded set. Let $T, S : B \to B$ be two maps. For a given $x_0, u_0 \in B$, we consider the Ishikawa iteration (see [1]) for T and S:

$$x_{n+1} = (1-\alpha_n)x_n + \alpha_n T y_n, \quad y_n = (1-\beta_n)x_n + \beta_n T x_n, \tag{1.1}$$

$$u_{n+1} = (1-\alpha_n)u_n + \alpha_n S v_n, \quad v_n = (1-\beta_n)u_n + \beta_n S u_n, \tag{1.2}$$

where $\{\alpha_n\} \subset (0,1)$, $\{\beta_n\} \subset 0,1)$, and

$$\lim_{n\to\infty} \alpha_n = \lim_{n\to\infty} \beta_n = 0, \ \sum_{n=1}^{\infty} \alpha_n = \infty. \tag{1.3}$$

Set $\beta_n = 0$, $\forall n \in N$, to obtain the Mann iteration, see [2].

The map T is called Kannan mappings, see [3], if there exists $b \in (0, 1/2)$ such that for all $x, y \in B$,

$$\|Tx - Ty\| \leq b\left(\|x - Tx\| + \|y - Ty\|\right). \tag{1.4}$$

Similar mappings are Chatterjea mappings, see [4], for which there exists $c \in (0,1/2)$ such that for all $x, y \in B$,

$$\|Tx - Ty\| \leq c\left(\|x - Ty\| + \|y - Tx\|\right). \tag{1.5}$$

Zamfirescu collected these classes. He introduced the following definition, see [5].

Definition 1.1 (see [5, 6]). The operator $T : X \to X$ satisfies condition Z (Zamfirescu condition) if and only if there exist the real numbers a, b, c satisfying $0 < a < 1$, $0 < b,\ c < 1/2$ such that for each pair x, y in X, at least one condition is true:

(i) (z_1) $\|Tx - Ty\| \leq a\|x - y\|$,

(ii) (z_2) $\|Tx - Ty\| \leq b\left(\|x - Tx\| + \|y - Ty\|\right)$,

(iii) (z_3) $\|Tx - Ty\| \leq c\left(\|x - Ty\| + \|y - Tx\|\right)$.

It is known, see Rhoades [7], that (z_1), (z_2), and (z_3) are independent conditions. Consider $x, y \in B$. Since T satisfies condition Z, at least one of the conditions from (z_1), (z_2), and (z_3) is satisfied. If (z_2) holds, then

$$\|Tx - Ty\| \leq b\left(\|x - Tx\| + \|y - Ty\|\right) \leq b\left(\|x - Tx\| + \left(\|y - x\| + \|x - Tx\| + \|Tx - Ty\|\right)\right). \tag{1.6}$$

Thus

$$(1 - b)\|Tx - Ty\| \leq b\|x - y\| + 2b\|x - Tx\|. \tag{1.7}$$

From $0 \leq b < 1$ one obtains,

$$\|Tx - Ty\| \leq \frac{b}{1 - b}\|x - y\| + \frac{2b}{1 - b}\|x - Tx\|. \tag{1.8}$$

If (z_3) holds, then one gets

$$\|Tx - Ty\| \leq c\left(\|x - Ty\| + \|y - Tx\|\right) \leq c\left(\|x - Tx\| + \|Tx - Ty\| + \|x - y\| + \|x - Tx\|\right) \tag{1.9}$$

Hence,

$$(1 - c)\|Tx - Ty\| \leq c\|x - y\| + 2c\|x - Tx\|, \tag{1.10}$$

that is,

$$\|Tx - Ty\| \leq \frac{c}{1 - c}\|x - y\| + \frac{2c}{1 - c}\|x - Tx\|. \tag{1.11}$$

Denote

$$\delta := \max\left\{a, \frac{b}{1 - b}, \frac{c}{1 - c}\right\}, \tag{1.12}$$

to obtain

$$0 \leq \delta < 1. \tag{1.13}$$

Finally, we get

$$\|Tx - Ty\| \leq \delta\|x - y\| + 2\delta\|x - Tx\|, \quad \forall x, y \in B. \tag{1.14}$$

Formula (1.14) was obtained as in [8].

Osilike and Udomene introduced in [9] a more general definition of a quasicontractive operator; they considered the operator for which there exists $L \geq 0$ and $q \in (0,1)$ such that

$$\|Tx - Ty\| \leq q\|x - y\| + L\|x - Tx\|, \quad \forall x, y \in B. \tag{1.15}$$

Imoru and Olatinwo considered in [10], the following general definition. Because they failed to name them, we will call them here contractive-like operators.

Definition 1.2. One calls *contractive-like* the operator T if there exist a constant $q \in 0,1)$ and a strictly increasing and continuous function $\phi : [0,\infty) \to [0,\infty)$ with $\phi(0) = 0$ such that for each $x, y \in X$,

$$\|Tx - Ty\| \leq q\|x - y\| + \phi\big(\|x - Tx\|\big). \tag{1.16}$$

In both papers [9, 10], the T-stability of Picard and Mann iterations was studied.

2. Preliminaries

The data dependence abounds in literature of fixed point theory when dealing with Picard-Banach iteration, but is quasi-inexistent when dealing with Mann-Ishikawa iteration. As far as we know, the only data-dependence result concerning Mann-Ishikawa iteration is in [11]. There, the data dependence of Ishikawa iteration was proven when applied to contractions. In this note, we will prove data-dependence results for Ishikawa iteration when applied to the above contractive-like operators. Usually, Ishikawa iteration is more complicated but nevertheless more stable as Mann iteration. There is a classic example, see [12], in which Mann iteration does not converge while Ishikawa iteration does. This is the main reason for considering Ishikawa iteration in Theorem 3.2.

The following remark is obvious by using the inequality $(1 - x) \leq \exp(x),\ \forall x \geq 0$.

Remark 2.1. Let $\{\theta_n\}$ *be a nonnegative sequence such that* $\theta_n \in (0,1],\ \forall n \in \mathbb{N}$. *If* $\sum_{n=1}^{\infty}\theta_n = \infty$, *then* $\prod_{n=1}^{\infty}(1 - \theta_n) = 0$.

The following is similar to lemma from [13]. (Note that another proof for this lemma [13] can be found in [11].)

Lemma 2.2. *Let* $\{a_n\}$ *be a nonnegative sequence for which one supposes there exists* $n_0 \in \mathbb{N}$, *such that for all* $n \geq n_0$ *one has satisfied the following inequality:*

$$a_{n+1} \leq (1 - \lambda_n)a_n + \lambda_n\sigma_n, \tag{2.1}$$

where $\lambda_n \in (0,1),\ \forall n \in \mathbb{N}, \sum_{n=1}^{\infty}\lambda_n = \infty$, *and* $\sigma_n \geq 0\ \forall n \in \mathbb{N}$. *Then,*

$$0 \leq \limsup_{n\to\infty} a_n \leq \limsup_{n\to\infty} \sigma_n. \tag{2.2}$$

Proof. There exists $n_1 \in \mathbb{N}$ such that $\sigma_n \leq \limsup \sigma_n$, $\forall n \geq n_1$. Set $n_2 = \max\{n_0, n_1\}$ such that the following inequality holds, for all $n \geq n_2$:

$$a_{n+1} \leq (1-\lambda_n)(1-\lambda_{n-1})\cdots(1-\lambda_{n_1})a_{n_1} + \limsup_{n\to\infty} \sigma_n. \tag{2.3}$$

Using the above Remark 2.1 with $\theta_n = \lambda_n$, we get the conclusion. In order to prove (2.3), consider (2.1) and the induction step:

$$\begin{aligned} a_{n+2} &\leq (1-\lambda_{n+1})a_{n+1} + \lambda_{n+1}\sigma_{n+1} \leq (1-\lambda_{n+1})(1-\lambda_n)(1-\lambda_{n-1})\cdots(1-\lambda_{n_1})a_{n_1} \\ &\quad + (1-\lambda_{n+1})\limsup_{n\to\infty}\sigma_n + \lambda_{n+1}\sigma_{n+1} \\ &= (1-\lambda_{n+1})(1-\lambda_n)(1-\lambda_{n-1})\cdots(1-\lambda_{n_1})a_{n_1} + \limsup_{n\to\infty}\sigma_n. \end{aligned} \tag{2.4}$$

□

3. Main results

Theorem 3.1. *Let X be a real Banach space, $B \subset X$ a nonempty convex and closed set, and $T : B \to B$ a contractive-like map with x^* being the fixed point. Then for all $x_0 \in B$, the iteration* (1.1) *converges to the unique fixed point of T.*

Proof. The uniqueness comes from (1.16); supposing we have two fixed points x^* and y^*, we get

$$\|x^* - y^*\| = \|Tx^* - Ty^*\| \leq q\|x^* - y^*\| + \phi(\|x^* - Tx^*\|) = q\|x^* - y^*\|, \tag{3.1}$$

that is, $(1-q)\|x^* - y^*\| = 0$. From (1.1) and (1.16) we obtain

$$\begin{aligned} \|x_{n+1} - x^*\| &\leq (1-\alpha_n)\|x_n - x^*\| + \alpha_n\|Ty_n - Tx^*\| \\ &\leq (1-\alpha_n)\|x_n - x^*\| + \alpha_n q\|y_n - x^*\| \\ &\leq (1-\alpha_n)\|x_n - x^*\| + \alpha_n q(1-\beta_n)\|x_n - x^*\| + q\alpha_n\beta_n\|Tx_n - Tx^*\| \\ &\leq (1-\alpha_n(1-q))(1-(1-q)\beta_n))\|x_n - x^*\| \\ &\leq (1-\alpha_n(1-q))\|x_n - x^*\| \leq \cdots \leq \left(\prod_{k=1}^{n}(1-\alpha_k q)\right)\|x_0 - x^*\|. \end{aligned} \tag{3.2}$$

Use Remark 2.1 with $\theta_k = \alpha_k q$ to obtain the conclusion. □

This result allows us to formulate the following data dependence theorem.

Theorem 3.2. *Let X be a real Banach space, let $B \subset X$ be a nonempty convex and closed set, and let $\varepsilon > 0$ be a fixed number. If $T : B \to B$ is a contractive-like operator with the fixed point x^* and $S : B \to B$ is an operator with a fixed point u^*, (supposed nearest to x^*) , and if the following relation is satisfied:*

$$\|Tz - Sz\| \leq \varepsilon, \quad \forall z \in B, \tag{3.3}$$

then

$$\|x^* - u^*\| \leq \frac{\varepsilon}{1-q}. \tag{3.4}$$

Proof. From (1.1) and (1.2), we have

$$x_{n+1} - u_{n+1} = (1-\alpha_n)(x_n - u_n) + \alpha_n(Ty_n - Sv_n). \tag{3.5}$$

Thus

$$\begin{aligned}
\|x_{n+1} - u_{n+1}\| &= \|(1-\alpha_n)(x_n - u_n) + \alpha_n(Sv_n - Ty_n)\| \\
&\leq (1-\alpha_n)\|x_n - u_n\| + \alpha_n\|Sv_n - Tv_n + Tv_n - Ty_n\| \\
&\leq (1-\alpha_n)\|x_n - u_n\| + \alpha_n\|Tv_n - Sv_n\| + \alpha_n\|Tv_n - Ty_n\| \\
&\leq (1-\alpha_n)\|x_n - u_n\| + \alpha_n\varepsilon + q\alpha_n\|y_n - v_n\| + \alpha_n\phi(\|y_n - Ty_n\|) \\
&\leq (1-\alpha_n)\|x_n - u_n\| + \alpha_n\varepsilon + q\alpha_n(1-\beta_n)\|x_n - u_n\| + q\alpha_n\beta_n\|Tx_n - Su_n\| + \alpha_n\phi(\|y_n - Ty_n\|) \\
&\leq (1-\alpha_n)\|x_n - u_n\| + \alpha_n\varepsilon + q\alpha_n(1-\beta_n)\|x_n - u_n\| \\
&\quad + \alpha_n\beta_n q(\|Tx_n - Tu_n\| + \|Tu_n - Su_n\|) + \alpha_n\phi(\|y_n - Ty_n\|) \\
&\leq (1-\alpha_n)\|x_n - u_n\| + \alpha_n\varepsilon + q\alpha_n(1-\beta_n)\|x_n - u_n\| \\
&\quad + q^2\alpha_n\beta_n\|x_n - u_n\| + q\alpha_n\beta_n\phi(\|x_n - Tx_n\|) + q\alpha_n\beta_n\varepsilon + \alpha_n\phi(\|y_n - Ty_n\|) \\
&= (1 - \alpha_n(1 - q(1-\beta_n) - \beta_n q^2))\|x_n - u_n\| + \alpha_n\varepsilon + q\alpha_n\beta_n\varepsilon \\
&\quad + q\alpha_n\beta_n\phi(\|x_n - Tx_n\|) + \alpha_n\phi(\|y_n - Ty_n\|) \\
&= (1-\alpha_n(1-q)(1+q\beta_n))\|x_n - u_n\| + \alpha_n(q\beta_n\phi(\|x_n - Tx_n\|) + \phi(\|y_n - Ty_n\|) + q\beta_n\varepsilon + \varepsilon) \\
&\leq (1-\alpha_n(1-q))\|x_n - u_n\| + (\alpha_n(1-q))\frac{q\beta_n\phi(\|x_n - Tx_n\|) + \phi(\|y_n - Ty_n\|) + q\beta_n\varepsilon + \varepsilon}{1-q}.
\end{aligned} \tag{3.6}$$

Note that $\lim_{n\to\infty}\phi(\|x_n - Tx_n\|) = \lim_{n\to\infty}\phi(\|y_n - Ty_n\|) = 0$ because ϕ is a continuous map and both $\{x_n\}, \{y_n\}$ converge to the fixed point of T. Set

$$\begin{aligned}
\lambda_n &:= \alpha_n(1-q), \\
\sigma_n &:= \frac{q\beta_n\phi(\|x_n - Tx_n\|) + \phi(\|y_n - Ty_n\|) + q\beta_n\varepsilon + \varepsilon}{1-q},
\end{aligned} \tag{3.7}$$

and use Lemma 2.2 to obtain the conclusion

$$\|x^* - u^*\| \leq \frac{\varepsilon}{1-q}. \tag{3.8}$$

□

Remark 3.3. (i) Set $\beta_n = 0,\ \forall n \in \mathbb{N}$, to obtain the data dependence for Mann iteration.

(ii) The Zamfirescu operators and implicitly (Chatterjea and Kannan) are contractive-like operators, therefore our Theorem 3.2 remains true for these classes.

4. Numerical example

The following example follows the example from [8].

Example 4.1. Let $T : \mathbb{R} \to \mathbb{R}$ be given by

$$\begin{aligned} Tx &= 0, \quad \text{if } x \in (-\infty, 2] \\ &= -0.5, \quad \text{if } x \in (2, +\infty). \end{aligned} \tag{4.1}$$

Then T is contractive-like operator with $q = 0.2$ and ϕ = identity.

Note the unique fixed point is 0. Consider now the map $S : R \to R$,

$$\begin{aligned} Sx &= 1, \quad \text{if } x \in (-\infty, 2] \\ &= -1.5, \quad \text{if } x \in (2, +\infty) \end{aligned} \tag{4.2}$$

with the unique fixed point 1. Take ε to be the distance between the two maps as follows:

$$\|Sx - Tx\| \leq 1, \quad \forall x \in \mathbb{R}. \tag{4.3}$$

Set $u_0 = x_0 = 0$, $\alpha_n = \beta_n = 1/(n+1)$. Independently of above theory, the Ishikawa iteration applied to S, leads to

Iteration step	Ishikawa iteration
1	0.5
10	0.9
100	0.99

(4.4)

Note that for $n = 1$,

$$0.5 = \frac{1}{n+1}0 + \frac{1}{n+1}S\left(\frac{1}{2}\right), \tag{4.5}$$

since $y_1 = (1/(n+1))0 + (1/n+1)1 = 1/2$. (The above computations can be obtained also by using a Matlab program.) This leads us to "conclude" that Ishikawa iteration applied to S converges to fixed point, $(x^* = 1)$. Eventually, one can see that the distance between the two fixed points is one. Actually, without knowing the fixed point of S (and without computing it), via Theorem 3.2, we can do the following estimate for it:

$$\|x^* - u^*\| \leq \frac{1}{1-q} = \frac{1}{1-0.2} = \frac{10}{8} = 1.2. \tag{4.6}$$

As a conclusion, instead of computing fixed points of S, choose T more closely to S and the distance between the fixed points will shrink too.

Acknowledgments

The authors are indebted to referee for carefully reading the paper and for making useful suggestions. This work was supported by CEEX ET 90/2006-2008.

References

[1] S. Ishikawa, "Fixed points by a new iteration method," *Proceedings of the American Mathematical Society*, vol. 44, no. 1, pp. 147–150, 1974.
[2] W. R. Mann, "Mean value methods in iteration," *Proceedings of the American Mathematical Society*, vol. 4, no. 3, pp. 506–510, 1953.
[3] R. Kannan, "Some results on fixed points," *Bulletin of the Calcutta Mathematical Society*, vol. 60, pp. 71–76, 1968.
[4] S. K. Chatterjea, "Fixed-point theorems," *Comptes Rendus de l'Académie Bulgare des Sciences*, vol. 25, pp. 727–730, 1972.
[5] T. Zamfirescu, "Fix point theorems in metric spaces," *Archiv der Mathematik*, vol. 23, no. 1, pp. 292–298, 1972.
[6] B. E. Rhoades, "Fixed point iterations using infinite matrices," *Transactions of the American Mathematical Society*, vol. 196, pp. 161–176, 1974.
[7] B. E. Rhoades, "A comparison of various definitions of contractive mappings," *Transactions of the American Mathematical Society*, vol. 226, pp. 257–290, 1977.
[8] V. Berinde, "On the convergence of the Ishikawa iteration in the class of quasi contractive operators," *Acta Mathematica Universitatis Comenianae*, vol. 73, no. 1, pp. 119–126, 2004.
[9] M. O. Osilike and A. Udomene, "Short proofs of stability results for fixed point iteration procedures for a class of contractive-type mappings," *Indian Journal of Pure and Applied Mathematics*, vol. 30, no. 12, pp. 1229–1234, 1999.
[10] C. O. Imoru and M. O. Olatinwo, "On the stability of Picard and Mann iteration processes," *Carpathian Journal of Mathematics*, vol. 19, no. 2, pp. 155–160, 2003.
[11] Ş. M. Şoltuz, "Data dependence for Ishikawa iteration," *Lecturas Matemáticas*, vol. 25, no. 2, pp. 149–155, 2004.
[12] C. E. Chidume and S. A. Mutangadura, "An example of the Mann iteration method for Lipschitz pseudocontractions," *Proceedings of the American Mathematical Society*, vol. 129, no. 8, pp. 2359–2363, 2001.
[13] J. A. Park, "Mann-iteration process for the fixed point of strictly pseudocontractive mapping in some Banach spaces," *Journal of the Korean Mathematical Society*, vol. 31, no. 3, pp. 333–337, 1994.

Journal of Applied Mathematics and Decision Sciences

Special Issue on
Intelligent Computational Methods for Financial Engineering

Call for Papers

As a multidisciplinary field, financial engineering is becoming increasingly important in today's economic and financial world, especially in areas such as portfolio management, asset valuation and prediction, fraud detection, and credit risk management. For example, in a credit risk context, the recently approved Basel II guidelines advise financial institutions to build comprehensible credit risk models in order to optimize their capital allocation policy. Computational methods are being intensively studied and applied to improve the quality of the financial decisions that need to be made. Until now, computational methods and models are central to the analysis of economic and financial decisions.

However, more and more researchers have found that the financial environment is not ruled by mathematical distributions or statistical models. In such situations, some attempts have also been made to develop financial engineering models using intelligent computing approaches. For example, an artificial neural network (ANN) is a nonparametric estimation technique which does not make any distributional assumptions regarding the underlying asset. Instead, ANN approach develops a model using sets of unknown parameters and lets the optimization routine seek the best fitting parameters to obtain the desired results. The main aim of this special issue is not to merely illustrate the superior performance of a new intelligent computational method, but also to demonstrate how it can be used effectively in a financial engineering environment to improve and facilitate financial decision making. In this sense, the submissions should especially address how the results of estimated computational models (e.g., ANN, support vector machines, evolutionary algorithm, and fuzzy models) can be used to develop intelligent, easy-to-use, and/or comprehensible computational systems (e.g., decision support systems, agent-based system, and web-based systems)

This special issue will include (but not be limited to) the following topics:

- **Computational methods**: artificial intelligence, neural networks, evolutionary algorithms, fuzzy inference, hybrid learning, ensemble learning, cooperative learning, multiagent learning
- **Application fields**: asset valuation and prediction, asset allocation and portfolio selection, bankruptcy prediction, fraud detection, credit risk management
- **Implementation aspects**: decision support systems, expert systems, information systems, intelligent agents, web service, monitoring, deployment, implementation

Authors should follow the Journal of Applied Mathematics and Decision Sciences manuscript format described at the journal site http://www.hindawi.com/journals/jamds/. Prospective authors should submit an electronic copy of their complete manuscript through the journal Manuscript Tracking System at http://mts.hindawi.com/, according to the following timetable:

Manuscript Due	December 1, 2008
First Round of Reviews	March 1, 2009
Publication Date	June 1, 2009

Guest Editors

Lean Yu, Academy of Mathematics and Systems Science, Chinese Academy of Sciences, Beijing 100190, China; Department of Management Sciences, City University of Hong Kong, Tat Chee Avenue, Kowloon, Hong Kong; yulean@amss.ac.cn

Shouyang Wang, Academy of Mathematics and Systems Science, Chinese Academy of Sciences, Beijing 100190, China; sywang@amss.ac.cn

K. K. Lai, Department of Management Sciences, City University of Hong Kong, Tat Chee Avenue, Kowloon, Hong Kong; mskklai@cityu.edu.hk

Mixed convection flow near an axisymmetric stagnation point on a vertical cylinder

Cornelia Revnic[1], Teodor Grosan[2], John Merkin[3], Ioan Pop[2]

January 17, 2008

[1]Tiberiu Popoviciu Mathematical Institute, P.O.Box. 68-1, 400110, Cluj, Romania
[2]Babes-Bolyai University, Applied Mathematics, R-3400 Cluj, CP 253, Romania
[3]Department of Applied Mathematics, University of Leeds, Leeds LS2 9JT, UK

Abstract

The mixed convection flow near an axisymmetric stagnation point on a vertical cylinder is considered. The equations for the fluid flow and temperature fields reduce to similarity form that involve a Reynolds number R and a mixed convection parameter λ, as well as the Prandtl number σ. Numerical solutions are obtained for representative values of these parameters, which show the existence of a critical value $\lambda_c = \lambda_c(R, \sigma)$ for the existence of solutions in the opposing ($\lambda < 0$) case. The variation of λ_c with R is considered. In the aiding ($\lambda > 0$) case solutions are possible for all λ and the asymptotic limit $\lambda \to \infty$ is obtained. The limits of large and small R are also treated and the nature of the solution for large Prandtl number is briefly discussed.

Keywords: Boundary layers, axisymmetric stagnation flow, mixed convection, dual solutions, asymptotic solutions.

1 Introduction

Combined forced and free convection flows (mixed convection) are encountered in many technological and industrial applications including solar receivers exposed to wind currents, electronic devices cooled by fans, nuclear reactors cooled during emergency shutdown, heat exchanges placed in a low-velocity environment and many more. Two-dimensional stagnation point flows arise in the vicinity of a stagnation line resulting from a two-dimensional flow impinging on a curved surface at right angles to it and thereafter flowing symmetrically about the stagnation line. Hiemenz [1] was the first to study two-dimensional stagnation-point flows. Later Eckert [2] and Gorla [3] considered the corresponding forced convection heat transfer problem. Three-dimensional stagnation-point flows have been studied by Homann [4] and the axisymmetric stagnation-point flow on circular cylinder by Wang [5] and Gorla [6]. The three-dimensional flow resulting from an axisymmetric stagnation flow impinging obliquely on a body surface has been treated by Weidman and Putkaradze [7]. The problem of axisymmetric stagnation-point flow acting on a porous flat plate oscillating transversely in its own plane has been investigated by Weidman and Mahalingam [8]. In this case a three-dimensional flow results from a stagnation-point flow on a flat plate oscillating in its own plane. Gorla [9] has studied the unsteady viscous flow in the vicinity of an axisymmetric stagnation point on a circular cylinder.

The steady mixed convection flow near the stagnation region of a vertical flat plate has been studied by Ramachandran *et al.* [10] and by Gorla [11] for the flow near an axisymmetric stagnation point on a slender impermeable vertical cylinder. Mixed convection flows arise when the buoyancy forces resulting from temperature differences within the flow become comparable to the pressure gradient forces arising from the forced flow. As a consequence, both the flow and thermal fields are significantly affected by the buoyancy forces. The study of thick axisymmetric free convection boundary layers along slender bodies has been shown by Kuiken [12] to have an unusual structure at large distances along the cylinder. When the boundary-layer variables are scaled so as to be of order unity within the boundary layer, the boundary conditions that hold on the surface of the slender body are given at a value of the independent variable which is close to zero. As a result, when a perturbation analysis is used to obtain the solution at large distances along the cylinder, the body is reduced to a line at the first approximation.

Recently several papers have been published on axisymmetric mixed convection boundary-layer flows along slender bodies. Naraian and Uberoi [13, 14] have studied the mixed convection boundary layer on a vertical needle. These are bodies of revolution whose diameter is of the same order as the thickness of the velocity or thermal boundary layers that develop on it. By appropriately varying the radius of the needle, the boundary-layer equations admit similarity solutions. Wang [16] found a similarity solution for the mixed convection boundary layer on an adiabatic vertical needle with a heat source at the tip, a situation that arises, for example, for a stick burning at its lower end.

The present paper considers the steady mixed convection flow that develops near an axisymmetric stagnation point on a vertical isothermal cylinder in the case when the boundary layer is thick compared to the radius of the cylinder. We start by describing

the governing equations, following closely [8, 11] for the forced convection problem. This results in two ordinary differential equations for the flow and temperature fields that involve, as well as the Prandtl number σ, the two further parameters R, which is measure of the forced flow, and a mixed convection parameter λ. We start by giving numerical solutions to these equationsfor representative values of λ and R, finding dual solutions for negative λ with critical points $\lambda_c < 0$, requiring $\lambda \geq \lambda_c$ for the existence of a solution. We determine how λ_c varies with R, before considering the asymptotic limits of $\lambda \to \infty$ (free convection limit) and $R \to \infty$ and $R \to 0$.

2 Equations

We consider the steady mixed convection flow near an axisymmetric stagnation point on an infinite cylinder. The cylinder is taken as mounted vertically and the flow is assumed to be axisymmetric about the x-axis, which measures distance along the cylinder in a vertical direction with gravity acting in the negative x direction. The stagnation point is at $x = 0$, $r = a$, where r measures distance radially from the centre of the cylinder of radius a. The ambient fluid has a constant temperature T_∞ and the cylinder is maintained at a temperature $T_w(x) = T_0 \left(\frac{x}{a}\right) + T_\infty$. Having $T_w > T_\infty$ corresponds to assisting flow, with $T_w < T_\infty$ corresponding to opposing flow. The outer flow in this situation, taken directly from [11], is

$$u = -\left(\frac{U_\infty}{a}\right)\left(r - \frac{a^2}{r}\right), \qquad v = 2U_\infty\left(\frac{x}{a}\right) \tag{1}$$

where U_∞ is the planar flow at large distances from the cylinder and where u and v are the velocity components in the x and r directions respectively.

Again following [11], we introduce the variables

$$\eta = \left(\frac{r}{a}\right)^2, \quad u = -U_\infty \eta^{-1/2} f(\eta), \quad v = 2U_\infty\left(\frac{x}{a}\right) f'(\eta), \quad \theta(\eta) = \frac{T - T_\infty}{T_w - T_\infty} \tag{2}$$

where T is the temperature of the fluid. Applying (2) in the governing equations and making the standard Boussinesq approximation, we find that our flow is described by the similarity equations, again from [11],

$$\eta f''' + f'' + R(f\, f'' + 1 - f'^2) + \lambda\theta = 0 \tag{3}$$

$$\eta\theta'' + \theta' + \sigma\, R(f\,\theta' - f'\,\theta) = 0 \tag{4}$$

subject to the boundary conditions, from (1), that

$$f(1) = 0,\ f'(1) = 0,\ \theta(1) = 1, \qquad f' \to 1,\ \theta \to 0 \ \text{ as } \ \eta \to \infty \tag{5}$$

(primes denote differentiation with respect to η) where σ is the Prandtl number and where

$$R = \frac{U_\infty a}{2\nu}, \qquad \lambda = \frac{g\beta a^2 T_0}{8U_\infty \nu} \tag{6}$$

are, respectively, a Reynolds number and a mixed convection parameter, with $\lambda > 0$ corresponding to assisting flow and $\lambda < 0$ corresponding to opposing flow. In (6) ν is the kinematic viscosity of the fluid, g the acceleration due to gravity and β the coefficient of thermal expansion.

The parameters perhaps of most physical interest are the skin friction parameter C_f and the Nusselt number Nu, defined as

$$C_f = \frac{\tau_w}{\rho U_\infty^2}, \quad Nu = \frac{aq_w}{k(T_w - T_\infty)} \quad \text{where} \quad \tau_w = \mu \left(\frac{\partial v}{\partial r}\right)_{r=a} \quad q_w = -k \left(\frac{\partial T}{\partial r}\right)_{r=a} \tag{7}$$

and where μ and k are the dynamic viscosity and thermal conductivity respectively. From (2), we have that

$$C_f = 2\left(\frac{x}{a}\right) f''(1), \qquad Nu = -2\theta'(1) \tag{8}$$

We start by describing numerical solutions to equations (3, 4) subject to boundary conditions (5). Throughout we assume that the Prandtl number σ is of $O(1)$, our numerical results are all for the case when $\sigma = 1$.

3 Numerical results

Equations (3, 4) subject to boundary conditions (5) were solved numerically using a standard shooting method for solving boundary-value problems (D02AGF in the NAG library). In figure 1 we plot $f''(1)$ and $\theta'(1)$ against λ for $R = 1, 5, 10$ (with $\sigma = 1$). This figure shows that, for $\lambda < 0$, there is a critical value λ_c with solutions possible only for $0 > \lambda \geq \lambda_c$ and for $\lambda > \lambda_c$ there are dual solutions. The value of λ_c decreases as R is increased, thus giving a greater range of negative λ for possible solutions. For $\lambda > 0$ there is only one solution with the values of $f''(1)$ increasing and $\theta'(1)$ decreasing as λ is increased (for a given value of R). For the larger values of λ, the values of $f''(1)$ for $R = 1$ becomes greater than those for the larger values of R (= 5, 10), indicating that, for sufficiently large values of λ, $f''(1)$ increases as R is decreased. However, the values of $-\theta'(1)$ increase as R is increased (for a given value of λ).

In figure 2 we take values for λ ($\lambda = 1, -2$) representative respectively of aiding and opposing mixed convection and plot the corresponding values of $f''(1)$ and $\theta'(1)$ against R. We see that in both cases $\theta'(1)$ decreases as R is increased. However, for $\lambda = 1$, $f''(1)$ has a minimum value, of $f''(1) = 1.6648$ at $R = 0.272$, before increasing again for the larger values of R. For $\lambda = -2$ there is a critical value R_c of R ($R_c \simeq 0.622$) below which there are no solutions, as might be expected from figure 1.

3.1 Critical points

We saw in figure 1 the existence of a critical value λ_c of λ, requring $\lambda \geq \lambda_c$ for a solution to exist. We can calculate how λ_c varies with R using the appproach described in [17, 18]. Essentially we perturb about the solution given by equations (3, 4) to obtain a linear homogeneous problem. It is then the existence of a nontrivial solution to this homogeneous problem that determines λ_c for a given value of R (and σ). In figure 3 we

plot λ_c against R, with the figure showing that λ_c decreases as R is increased, seemingly in a linear manner for the larger values of R, and increases towards zero as R is reduced. The region in the (λ, R) parameter space where solutions exist is labelled on this figure.

Our numerical solutions suggest considering various limiting forms and we now discuss these in more detail, starting with the free convection limit, $\lambda \to \infty$.

4 Asymptotic results

4.1 λ large

To obtain a solution valid for λ large we start by putting

$$f = \lambda^{1/4} F, \qquad \zeta = \lambda^{1/4}(\eta - 1) \tag{9}$$

leaving θ unscaled. This results in the equations

$$(1 + \lambda^{-1/4}\zeta)F''' + \lambda^{-1/4}F'' + R(FF'' - F'^2) + \lambda^{-1}R + \theta = 0 \tag{10}$$

$$(1 + \lambda^{-1/4}\zeta)\theta'' + \lambda^{-1/4}\theta' + \sigma R(F\theta' - F'\theta) = 0 \tag{11}$$

where primes now denote differentiation with respect to ζ, subject to the boundary conditions

$$F(0) = 0,\ F'(0) = 0,\ \theta(0) = 1, \qquad F' \to \lambda^{-1/2},\ \theta \to 0 \ \text{ as } \ \zeta \to \infty \tag{12}$$

Equations (10, 11) suggest looking for a solution by expanding

$$F = F_0 + \lambda^{-1/4}F_1 + \cdots, \qquad \theta = \theta_0 + \lambda^{-1/4}\theta_1 + \cdots \tag{13}$$

We can scale the leading-order problem obtained by substituting expansion (13) into equations (10, 11) by putting

$$F_0 = R^{-3/4}\overline{F}_0, \qquad \overline{\zeta} = R^{1/4}\zeta \tag{14}$$

This results in

$$\overline{F}_0''' + \overline{F}_0\overline{F}_0'' - \overline{F}_0'^2 + \theta_0 = 0 \tag{15}$$

$$\theta_0'' + \sigma(\overline{F}_0\theta_0' - \overline{F}_0'\theta_0) = 0 \tag{16}$$

subject to

$$\overline{F}_0(0) = 0,\ \overline{F}_0'(0) = 0,\ \theta_0(0) = 1, \qquad \overline{F}_0' \to 0,\ \theta_0 \to 0 \ \text{ as } \ \overline{\zeta} \to \infty \tag{17}$$

where primes now denote differentiation with respect to $\overline{\zeta}$. A numerical solution of (15 – 17) gives, for $\sigma = 1$, $\overline{F}_0''(0) = 0.73950$, $\theta_0'(0) = -0.59509$.

We can continue to the next order by first rescaling

$$F_1 = R^{-1}\,\overline{F}_1, \qquad \theta_1 = R^{-1/4}\,\overline{\theta}_1 \tag{18}$$

This gives, with (14),

$$\overline{F}_1''' + \overline{F}_0\overline{F}_1'' + \overline{F}_1\overline{F}_0'' - 2\overline{F}_0'\overline{F}_1' + \overline{\theta}_1 = -(\overline{F}_0'' + \overline{\zeta}\,\overline{F}_0''') \tag{19}$$

$$\overline{\theta}_1'' + \sigma(\overline{F}_0\overline{\theta}_1'' + \overline{F}_1\theta_0' - \overline{F}_0'\overline{\theta}_1 - \overline{F}_1\theta_0) = -(\theta_0' + \overline{\zeta}\,\theta_0'') \tag{20}$$

subject to

$$\overline{F}_1(0) = 0,\ \overline{F}_1'(0) = 0,\ \overline{\theta}_1(0) = 0, \qquad \overline{F}_1' \to 0,\ \overline{\theta}_1 \to 0 \ \text{ as } \ \overline{\zeta} \to \infty \tag{21}$$

A numerical solution gives, again for $\sigma = 1$, that $\overline{F}_1''(0) = 0.06888$, $\overline{\theta}_1'(0) = -0.23452$.

From (9, 14) and (18) we have

$$\begin{aligned} \left(\frac{d^2 f}{d\eta^2}\right)_{\eta=1} &\sim \left(\frac{\lambda^3}{R}\right)^{1/4} \left(0.7395 + 0.0689(R\lambda)^{-1/4} + \cdots\right), \\ \left(\frac{d\theta}{d\eta}\right)_{\eta=1} &\sim -(R\lambda)^{1/4}\left(0.5951 + 0.2345(R\lambda)^{-1/4} + \cdots\right) \qquad \text{as } \lambda \to \infty \end{aligned} \tag{22}$$

Expressions (22) show that, for sufficiently large values of λ, $-\theta'(1)$ increases as R is increased and that $f''(1)$ decreases as R is increased, in line with figure 1. In figure 4 we plot the values of $(\lambda^3/R)^{-1/4} f''(1)$ and $-(\lambda R)^{-1/4}\theta'(1)$ obtained from the numerical solution of equations (3, 4) against λ for $R = 1$, 10. In both cases the asymptotic limit for λ large given by (22) is approached as λ increases, though more slowly for $R = 10$ than for $R = 1$ as might be expected from (22).

4.2 R large

To obtain a solution for R large we follow the approach given in [7] for the forced convection case and start by writing

$$f = R^{-1/2}\phi, \qquad \xi = R^{1/2}(\eta - 1) \tag{23}$$

and leaving θ unscaled. This results in the equations

$$(1 + R^{-1/2}\xi)\phi''' + R^{-1/2}\phi'' + 1 + \phi\phi'' - \phi'^2 + \lambda R^{-1}\theta = 0 \tag{24}$$

$$(1 + R^{-1/2}\xi)\theta'' + R^{-1/2}\theta' + \sigma(\phi\theta' - \phi'\theta) = 0 \tag{25}$$

subject to the boundary conditions given in (5) and where primes now denote differentiation with respect to ξ. Equations (24, 25) suggest an expansion in powers of $R^{-1/2}$, the leading-order term just being the forced convection limit discussed in [7].

For convection to have an effect at leading order we require λ to be large, specifically of $O(R)$. This leads us to put

$$\lambda = \mu\, R \qquad \text{with } \ \mu \ \text{ of } \ O(1) \tag{26}$$

The problem for the leading-order terms ϕ_0, θ_0 is now

$$\phi_0''' + 1 + \phi_0\phi_0'' - \phi_0'^2 + \mu\theta_0 = 0 \tag{27}$$

$$\theta_0'' + \sigma(\phi_0\theta_0' - \phi_0'\theta_0) = 0 \tag{28}$$

still subject to the boundary conditions that

$$\phi_0(0) = 0,\ \phi_0'(0) = 0,\ \theta_0(0) = 1, \qquad \phi_0' \to 1,\ \theta_0 \to 0 \ \text{ as } \ \xi \to \infty \tag{29}$$

Equations (27 - 29) have to solved numerically and graphs of $\phi_0''(0)$ and $\theta_0'(0)$ for $\sigma = 1$ plotted against μ are shown in figure 5. From these figures we see that there is a critical value μ_c of μ with dual solutions for $0 > \mu > \mu_c$ and no solutions for $\mu < \mu_c$. For $\sigma = 1$, we find that $\mu_c = -2.3618$, giving

$$\lambda_c \sim -2.3618R + \cdots \qquad \text{as } \ R \to \infty \tag{30}$$

For $\mu > 0$ there is only one solution with both $\phi_0''(0)$ and $-\theta_0'(0)$ increasing as μ is increased.

Expression (30) shows a linear increase in $|\lambda_c|$ with R, as noted previously about figure 3, and to confirm this asymptotic behaviour we plot the values of $\lambda_c R^{-1}$ obtained from our numerical integrations to find λ_c against R in figure 6. The numerically determined values approach this asymptotic limit (shown by the broken line), though only slowly as R is increased, suggesting that the $O(R^{-1/2})$ correction has a significant effect even at moderately large values of R.

For μ large we can recover expressions (22) by putting

$$\phi_0 = \mu^{1/4}\,\overline{\phi}_0, \qquad \overline{\xi} = \mu^{1/4}\,\xi \tag{31}$$

When (31) is substituted into equations (27 - 29) and then $\mu \to \infty$, we obtain equations (15 - 17) and, on using (26), the leading-order terms in (22).

4.3 R small

The behaviour of the solution for R small depends on whether λ is small or of $O(1)$. We start with the latter case, assuming that $\lambda > 0$.

4.3.1 λ of O(1)

For this case we start in an inner region where η is of $O(1)$ and scale

$$f = A(R)\,g, \qquad \theta = 1 + B(R)\,h \tag{32}$$

The scaling factors A and B are to be determined, though we assume that

$$A(R) \gg 1, \qquad B(R) \ll 1, \qquad \frac{RA}{B} \ll 1, \qquad AR \ll 1 \tag{33}$$

When (32) is substituted into equations (3, 4) and (33) is taken, the leading-order terms g_0, h_0 are given by, on satisfying the boundary condtions on $\eta = 1$,

$$g_0 = a_0(\eta\log\eta - \eta + 1) \qquad h_0 = b_0\log\eta \tag{34}$$

for constants a_0, b_0 to be determined. Before continuing the solution in the inner region, we next consider the outer region.

For the outer region we write

$$f = R^{-1}G, \quad \theta = \frac{\beta^2}{R}H, \quad Y = \beta\,\eta, \qquad \text{where } \beta = \beta(R) \ll 1, \ \frac{R}{\beta} \ll 1 \tag{35}$$

with the scaling factor $\beta(R)$ also to be determined. When (35) is substituted into equations (3, 4) and the assumptions for β given in (35) applied, we find that the leading-order problem in the outer region is

$$YG''' + G'' + GG'' - G'^2 + \lambda H = 0, \qquad YH'' + H' + \sigma(GH' - G'H) = 0 \tag{36}$$

subject to the outer boundary conditions at leading order that

$$G' \to 0, \quad H \to 0 \quad \text{as } Y \to \infty \tag{37}$$

To find the inner boundary conditions for (36) we need to match with the inner region.

We can express the inner solution (34) as, on using (35),

$$\begin{aligned} f &\sim \frac{A(R)}{\beta}\, a_0 Y[\log Y + (-\log\beta) - 1] + \cdots \\ \theta &\sim [1 + b_0 B(R)(-\log\beta)] + b_0 B(R)\log Y + \cdots \end{aligned} \tag{38}$$

From (38) we choose

$$A(R) = \frac{\beta}{R(-\log\beta)}, \qquad B(R) = \frac{1}{(-\log\beta)} = \frac{\beta^2}{R}, \qquad b_0 = -1 \tag{39}$$

Hence $\beta(R)$ is given implicitly by

$$\beta^2(-\log\beta) = R, \qquad \text{with} \quad \beta \sim \frac{\sqrt{2}\,R^{1/2}}{(-\log R)^{1/2}} + \cdots \quad \text{as } R \to 0 \tag{40}$$

We note that (39, 40) are consistent with the assumptions in (33) and (35). Expressions (38) then give, at leading order,

$$G \sim a_0 Y + \cdots, \qquad H \sim -\log Y + \cdots \quad \text{as } Y \to 0 \tag{41}$$

To get higher order terms in (41) we need to consider the inner region again. On using (39) we see that an expansion of the form

$$g = g_0 + \frac{g_1}{(-\log\beta)} + \cdots + O(\beta), \qquad h = h_0 + \frac{h_1}{(-\log\beta)} + \cdots + O(\beta) \tag{42}$$

is required, where the $O(\beta)$ terms in (42) also include terms in

$$\beta(-\log\beta)^2, \qquad \beta(-\log\beta), \qquad \beta(-\log\beta)^{-1}$$

and $h_1 = b_1 \log\eta$ for some constant b_1. When (42) is substituted into equations (3, 4) and using (32, 35) we find, after some calculation, that the inner boundary condition (41) for the outer region becomes modified to

$$\begin{aligned} G &\sim a_0 Y + \frac{\lambda}{2} Y^2 \log Y + \frac{1}{2}(a_0^2 - \frac{5\lambda}{2} - \lambda b_1) Y^2 + \cdots , \\ H &\sim -\log Y + b_1 - \sigma a_0 Y \log Y + \sigma a_0 (b_1 + 2) Y + \cdots \qquad \text{as} \quad Y \to 0 \end{aligned} \tag{43}$$

We can remove the parameter λ from this problem by writing $\overline{Y} = \lambda^{1/2} Y$ and then the problem in the outer region becomes

$$\overline{Y} G''' + G'' + G G'' - G'^2 + H = 0, \qquad \overline{Y} H'' + H' + \sigma(G H' - G' H) = 0 \tag{44}$$

subject to the conditions that

$$G' \to 0, \quad H \to 0 \quad \text{as} \quad \overline{Y} \to \infty \tag{45}$$

and

$$\begin{aligned} G &\sim \overline{a}_0 \overline{Y} + \frac{\overline{Y}^2}{2} \log \overline{Y} + \frac{1}{2}(\overline{a}_0^2 - \frac{5}{2} - \overline{b}_1) \overline{Y}^2 + \cdots , \\ H &\sim -\log \overline{Y} + \overline{b}_1 - \sigma \overline{a}_0 \overline{Y} \log \overline{Y} + \sigma \overline{a}_0 (\overline{b}_1 + 2) \overline{Y} + \cdots \qquad \text{as} \quad \overline{Y} \to 0 \end{aligned} \tag{46}$$

where $\overline{a}_0 = \lambda^{-1/2} a_0$ and $\overline{b}_1 = b_1 + \frac{1}{2} \log \lambda$.

The problem given by (44 – 46) has to be solved numerically to determine the constants $\overline{a}_0$ and $\overline{b}_1$ and we find, for $\sigma = 1$, that $\overline{a}_0 = 1.0016$, $\overline{b}_1 = -1.2396$. This then gives for small R and $\sigma = 1$,

$$\begin{aligned} \left(\frac{d^2 f}{d\eta^2}\right)_{\eta=1} &= \frac{1}{\beta(-\log\beta)^2}(1.0016 \lambda^{1/2} + \cdots) \\ \left(\frac{d\theta}{d\eta}\right)_{\eta=1} &= -\frac{1}{(-\log\beta)}(1 + \frac{1.2396 + \frac{1}{2}\log\lambda}{(-\log\beta)} + \cdots) \end{aligned} \tag{47}$$

with β given in terms of R by (40). Equations (3, 4) were solved numerically with $\lambda = 1$ for small values of R. The solution domain increases as R is decreased, in line with (35), and the outer boundary condition had to be applied at increasingly larger values of $\eta = \eta_\infty$ as R was decreased, the results shown in figure 7 were obtained using $\eta_\infty = 250$. In figure 7 we give plots of $f''(1)$ and $\theta'(1)$ against R obtained from our numerical integrations, the values obtained from (47) are shown by broken lines. The agreement with the asymptotic forms for small R is not particularly good, though both solutions are following the same trend. This difference can, perhaps, be explained by the fact that the approach to the asymptotic forms (47) is only very slow, with correction terms of $(-\log\beta)^{-1} \sim (-\log R)^{-1}$ and hence R has to be extremely small for these correction terms to have only a small effect. In practice we probably require values of R too small for obtaining reasonably accurate numerical solutions. At these very small values of R, η_∞ needs to be extremely large leading to errors in the shooting method employed to solve the two-point boundary-value problem.

4.3.2 λ small

We can see, particularly from (36, 37), that, when λ is of $O(1)$, the flow is driven at leading order only by the natural convection effects. The forced flow enters the solution at higher order. However, when λ is small, this cannot be the case and to get an estimate on λ when the forced convection effects have an influence at leading order, we see from (35) that the buoyancy term included in equation (36) is of $O(\lambda\beta^2 R^{-1})$ whereas the forced convection term is of $O(R)$. This suggests, on using (40), that these two effects will be comparable when $\lambda \sim R(-\log R)$ and leads us to put

$$\lambda = R(-\log R)\,\nu \qquad \text{with } \nu \text{ of } O(1) \text{ for } R \text{ small.} \tag{48}$$

We start our solution for this case in the inner region where we have at leading order, motivated by our previous solution for λ of $O(1)$,

$$f \sim \frac{1}{(-\log R)}\, c_0(\eta\log\eta - \eta + 1) + \cdots, \quad \theta \sim 1 + \frac{1}{(-\log R)}\left(-\log\eta + \frac{d_1}{(-\log R)}\log\eta + \cdots\right) \tag{49}$$

for constants c_0 and d_1 to be determined. For the outer region we now put

$$f = \frac{1}{R}\,G, \qquad \theta = \frac{1}{(-\log R)}\,H, \qquad Y = R\,\eta \tag{50}$$

Applying (50) in equations (3, 4) gives, at leading order

$$YG''' + G'' + 1 + GG'' - G'^2 + \nu H = 0, \qquad YH'' + H' + \sigma(GH' - G'H) = 0 \tag{51}$$

now subject to the outer boundary conditions

$$G' \to 1, \quad H \to 0 \quad \text{as } Y \to \infty \tag{52}$$

and, on matching with the inner region,

$$G \sim c_0 Y + \cdots, \quad H \sim -\log Y + d_1 + \cdots \quad \text{as } Y \to 0 \tag{53}$$

We note that ν cannot be scaled out of problem (51 – 53) (as it could previously) and that, for $\nu = 0$ (forced convection limit)

$$c_0 = 1, \quad G = Y, \quad H = -\frac{\mathrm{e}^{-\sigma Y}\log(\sigma Y)}{(1+\sigma Y)} + (1+\sigma Y)\int_{\sigma Y}^{\infty} \frac{\mathrm{e}^{-v}(3+v)\log v}{(1+v)^3}\,dv \tag{54}$$

giving

$$d_1 = \int_0^{\infty} \frac{\mathrm{e}^{-v}(3+v)\log v}{(1+v)^3}\,dv - \log\sigma = -1.4448 - \log\sigma$$

Plots of c_0 against ν obtained by solving (51 – 53) numerically are given in figure 8. This figure shows that there is a critical value ν_c of ν, with $\nu_c = -0.9832$ for $\sigma = 1$, and dual solutions for $0 > \nu > \nu_c$. This gives

$$\lambda_c \sim -0.9832R(-\log R) + \cdots \qquad \text{as } R \to 0 \tag{55}$$

For $\nu > 0$ there is only one solution and the problem given by (44 – 46) can be recovered for ν large by putting $\overline{Y} = \nu^{1/2}Y$ in (51 – 53) and letting $\nu \to \infty$.

5 Conclusions

We have considered the mixed convection boundary-layer flow around an axisymmetric stagnation point. The equations for the flow and temperature fields reduce to similarity form (3 – 5) and involve the three parameters, the Prandtl number σ, a Reynolds number R and a mixed convection parameter λ, defined in (6). The similarity equations were solved numerically for representative values of the parameters R and λ, see figures 1 and 2. The main conclusions from these numerical integrations were that, for $\lambda < 0$ (opposing flow), there was a critical value λ_c of λ with dual solutions for $\lambda_c < \lambda < 0$ and no solutions for $\lambda < \lambda_c$. For $\lambda \geq 0$ (aiding flow) there was a single solution for all λ. An asymptotic solution for λ large was derived, with the results summarized in (22).

The occurrence of dual solutions for opposing flows is not unexpected and is consistent with many previous studies of similarity solutions in mixed convection, see [17, 18, 19] for example. The critical value λ_c was seen to depend on R (and on σ), see figure 3. A solution for R large was obtained which showed that λ_c is of $O(R)$ in this case, as given in (30) for $\sigma = 1$. Thus for strong external flows (large R) boundary-layer flows are still possible even when there are strongly opposing buoyancy forces. For R small the flow was seen to be driven predominantly by the buoyancy forces when λ is of $O(1)$, as summarized in (47). However, for λ small both buoyancy and the external flow have comparable effects, giving a critical value of $O(R(-\log R))$ for R small, as given by (55) for $\sigma = 1$. The effect of weak external flows is to severely limit the range of λ where there can be opposing flows.

Our numerical results were for the case $\sigma = 1$ and we expect qualitatively similar behaviour when σ is of $O(1)$, typical of gases. For liquids (water) σ is somewhat larger and it is thus worth briefly considering the large σ limit. Following the treatment in [20, 21] we expect that, for σ large, the solution to involve a relatively thin thermal inner layer and a thicker outer viscous flow region. In the inner region we have

$$\eta = 1 + \sigma^{-1/3}\tau, \qquad f = \sigma^{-2/3}\Phi \tag{56}$$

with θ left unscaled. At leading order, for σ large, we obtain

$$\Phi''' = 0, \qquad \theta'' + R(\Phi\theta' - \Phi'\theta) = 0 \tag{57}$$

subject to

$$\Phi(0) = 0, \quad \Phi'(0) = 0, \quad \theta(0) = 1, \qquad \theta \to 0 \ \text{ as } \ \tau \to \infty \tag{58}$$

with the outer condition on Φ relaxed at this stage and where primes denote differentiation with respect to τ.

Equations (57, 58) give

$$\Phi = A_0\tau^2 \tag{59}$$

for some constant $A_0 = A_0(R)$ to be determined and

$$\theta = \frac{\left(\frac{2}{3}\right)!}{3\left(\frac{1}{3}\right)!}\,\mathrm{e}^{-s}\,U(\frac{4}{3};\frac{2}{3};s) \qquad \text{where} \quad s = \frac{1}{3}\,(RA_0)\tau^3 \tag{60}$$

in terms of confluent hypergeometric functions [22]. Expressions (56) and (60) give

$$\left(\frac{d\theta}{d\eta}\right)_{\eta=1} = -\sigma^{1/3}(RA_0)^{1/3}\,\frac{3^{2/3}\left(\frac{2}{3}\right)!^2}{2\left(\frac{1}{3}\right)!^2} + \cdots \qquad \text{as} \quad \sigma \to \infty \tag{61}$$

Expression (61) shows that the heat transfer increases as σ is increased, being of $O(\sigma^{1/3})$ for σ large.

To determine the constant A_0 we need to consider the outer region, in which we can neglect the temperature and write $\eta = 1 + \overline{\eta}$. This leads to

$$(1+\overline{\eta})f''' + f'' + R(1 + ff'' - f'^2) = 0 \tag{62}$$

and, on matching with the inner region, that

$$f \sim A_0\overline{\eta}^2 + \cdots \quad \text{as} \quad \overline{\eta} \to 0, \qquad f' \to 0 \quad \text{as} \quad \overline{\eta} \to \infty \tag{63}$$

Equations (62, 63) are essentially the forced convection limit with the solution given by [7]. Their solution then gives A_0 in terms of R. For R large [7] show that $A_0 \sim 0.6163\,R^{1/2} + \cdots$, giving $\left(\dfrac{d\theta}{d\eta}\right)_{\eta=1}$ of $O(R^{1/2}\sigma^{1/3}$ for R and σ large.

The leading order problem (57 – 60, 62, 63) for σ large does not give a critical value for λ. In fact the solution is independent of λ at leading order, with the buoyancy forces arising at $O(\sigma^{-1/3})$ in the inner region. This suggests that the critical value λ_c will, for a given value of R, decrease to large negative values as σ is increased. We illustrate this in figure 9 with a plot of $\theta'(1)$ against λ for $R = 1$ and $\sigma = 10$ to compare with the results for $\sigma = 1$. This figure clearly shows that the critical values λ_c has decreased for $\sigma = 10$ over that for $\sigma = 1$, giving a greater range of λ for solutions in the opposing case. The values of $\theta'(1)$ have, for a given λ, also decreased for $\sigma = 10$, in line with expression (61). In figure 10 we plot λ_c against σ again for $R = 1$, showing that λ_c decreases relatively slowly as σ is increased, as can be expected from the above analysis for the large λ case.

Acknowledgements
CR was supported by UEFISCSU grant PN-02-ID-PCE-1/525 and TG by CEEX grant 90. JM and IP were both supported by a Royal Society (London) Joint Project Grant.

References

1. K. Hiemenz, Die Grenzschicht an einem in den gleich formigen Flussigkeitsstrom eingetacuhten geraden Kreisszylinder. *Dinglers Polytech. J.* **326**, 1911, 321-324.

2. E.R.G. Eckert, Die Berechnung des Wärmeüberganges in der laminaren Grenzschicht um stromter Korper. *VDI - Forchungsheft* **416**, 1942, 1-24.

3. R.S.R. Gorla, Heat transfer in an axisymmetric stagnation flow on a cylinder. *Appl. Sci. Res.* **32**, 1976, 541-553.

4. F. Hommann, Der Einfluss grosser Zähigkeit bei der Stromung um den Cylinder und um die Kugel. *J. Appl. Math. Phys. (ZAMP)* **16**, 1936, 153-164.

5. C. Y. Wang, Axisymmetric stagnation flow on a cylinder. *Quart. Appl. Math.* **32**, 1974, 207-213.

6. R.S.R. Gorla, Nonsimilar axisymetric stagnation flow on a moving cylinder. *Int. J. Engng. Sci.* **16**, 1978, 392-400.

7. P.D. Weidman, V. Putkaradze. Axisymmetric stagnation flow obliquely impinging on a circular cylinder. *European J. Mechanics B/Fluids* **22**, 123–131, 2003.

8. P.D. Weidman and S. Mahalingam, Axisymmetric stagnation-point flow impinging on a transversely oscillating plate with suction. *J. Engng. Math.* **31**, 1997, 305-318.

9. R.S.R. Gorla, Unsteady viscous flow in the vicinity of an axisymmetric stagnation point on a circular cylinder. *Int. J. Engng. Sci.* **17**, 1979, 87-93.

10. N. Ramachandran, T.S. Chen and B.F. Armaly, Mixed convection in stagnation flows adjacent to vertical surface. *J. Heat Transfer* **110**, 1988, 173-177.

11. R.S.R. Gorla, Mixed convection in an axisymmetric stagnation flow on a vertical cylinder. *Acta Mechanica* **99**, 1993, 113-123.

12. H.K. Kuiken, The thick free-convective boundary-layer along a semi-infinite isothermal vertical cylinder. *J. Appl. Math. Phys. (ZAMP)* **25**, 1974, 497-514.

13. I.P. Naraian and M.S. Uberoi, Combined forced and free convection heat transfer from thin needles in a uniform stream. *Phys. Fluids* **15**, 1972, 1879-1882.

14. I.P. Naraian and M.S. Uberoi, Combined forced and free convection over thin needles. *Int. J. Heat Mass Transfer* **16**, 1973, 1505-1511.

15. I.L.S. Chen, Mixed convection flow about slender bodies of revolution. *J. Heat Transfer* **109**, 1987, 1033-1036.

16. C.Y. Wang, Mixed convection on a vertical needle with heated tip. *Phys. Fluids A* **2**, 1990, 622-625.

17. J.H. Merkin. On dual solutions occurring in mixed convection in a porous medium. *J. Engng. Math.* **20**, 171–179, 1985.

18. J.H. Merkin, T. Mahmood. Mixed convection boundary layer similarity solutions: prescribed wall heat flux. *J. Applied Mathematics and Physics (ZAMP)* **40**, 51–68, 1989.

19. G. Wilks, J.S. Bramley. Dual solutions in mixed convection. *Proc. Roy. Soc. Edinburgh* **87A**, 1981, 349–358.

20. K. Stewartson, L.T. Jones. The heated vertical plate at high Prandtl number. *J. Aeronautical Sciences* **24**, 1957, 379–380.

21. H.K. Kuiken. The heated vertical plate at high Prandtl number free convection. *J. Engineering Math.* **2**, 1968, 355–371.

22. L.J. Slater. *Confluent hypergeometric functions.* Cambridge University Press, Cambridge, 1960.

Captions for figures

Figure 1 Plots of (a) $f''(1)$ and (b) $\theta'(1)$ against λ for $R = 1$, 5, 10 obtained from the numerical solution of equations (3, 4) subject to boundary conditions (5) for $\sigma = 1$.

Figure 2 Plots of (a) $f''(1)$ and (b) $\theta'(1)$ against R for $\lambda = 1, -2$ obtained from the numerical solution of equations (3, 4) subject to boundary conditions (5) for $\sigma = 1$.

Figure 3 A plot of the critical value λ_c of λ against R (for $\sigma = 1$). The region in the (λ, R) parameter plane where solutions exist is labelled on the figure.

Figure 4 Plots of $(\lambda^3/R)^{-1/4} f''(1)$ and $-(\lambda R)^{-1/4}\theta'(1)$ obtained from the numerical solution of equations (3, 4) against λ for $R = 1$, 10 and $\sigma = 1$.

Figure 5 Plots of (a) $\phi_0''(0)$ and (b) $\theta_0'(0)$ against $\mu = \lambda R^{-1}$ for the solution for large R given by (27 - 29) for $\sigma = 1$.

Figure 6 A plot of $\lambda_c R^{-1}$ against R for $\sigma = 1$. The asymptotic limit (30) for R large is shown by the broken line.

Figure 7 Plots of (a) $f''(1)$ and (b) $\theta'(1)$ against R for $\lambda = 1$, $\sigma = 1$ for small R obtained from the numerical solution of equations (3, 4) subject to boundary conditions (5). The asymptotic expressions (47) are shown by the broken lines.

Figure 8 A plot of c_0 against ν, defined in (48), for $\sigma = 1$ arising in the small R, small λ problem (51 – 53).

Figure 9 Plots of $\theta'(1)$ against λ for $R = 1$ and $\sigma = 1$, 10 obtained from the numerical solution of equations (3, 4) subject to boundary conditions (5).

Figure 10 A plot of the critical value λ_c of λ against σ for $R = 1$. The region in the (λ, σ) parameter plane where solutions exist is labelled on the figure.

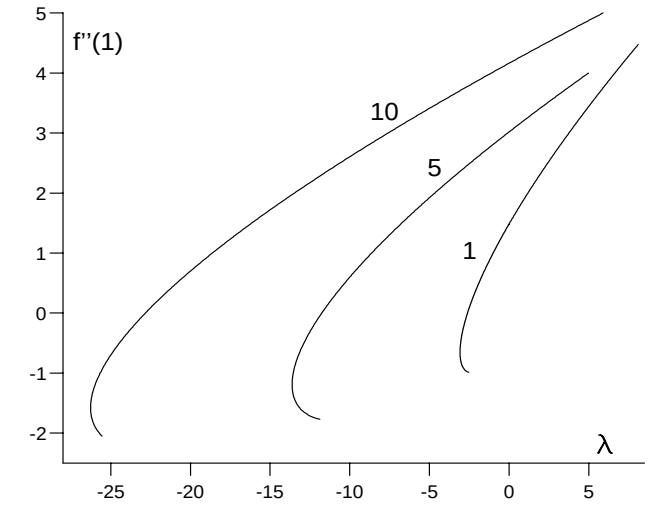

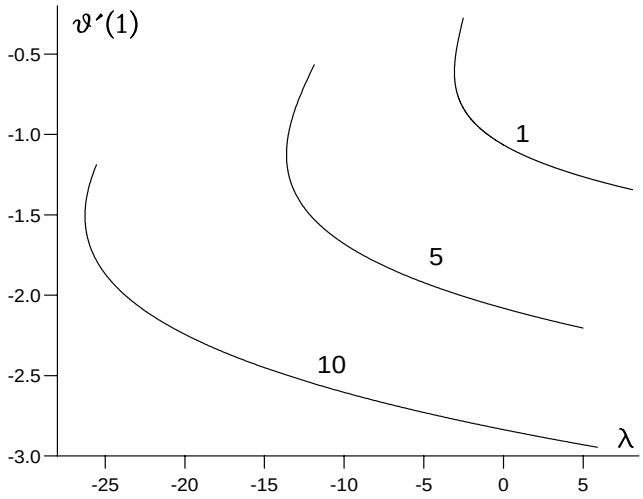

Figure 1: Plots of (a) $f''(1)$ and (b) $\theta'(1)$ against λ for $R = 1$, 5, 10 obtained from the numerical solution of equations (3, 4) subject to boundary conditions (5) for $\sigma = 1$.

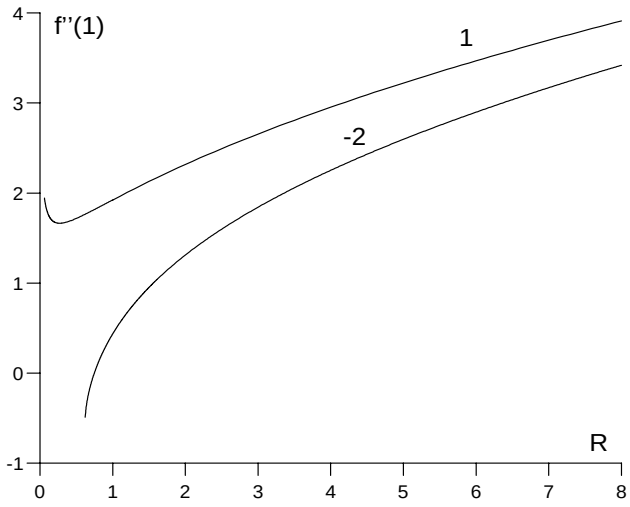

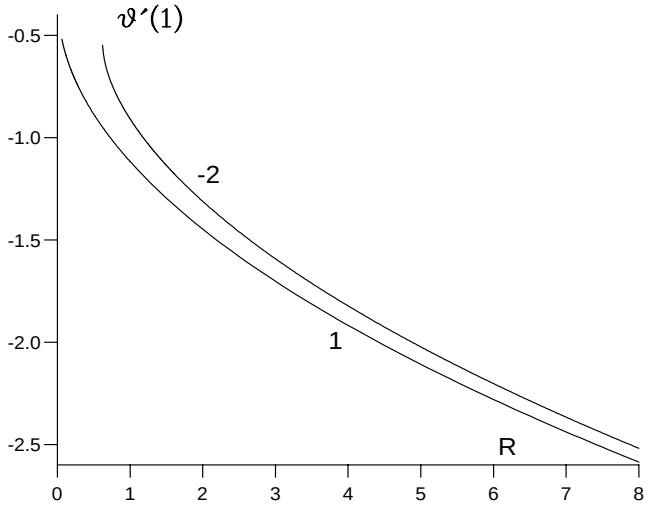

Figure 2: Plots of (a) $f''(1)$ and (b) $\theta'(1)$ against R for $\lambda = 1, -2$ obtained from the numerical solution of equations (3, 4) subject to boundary conditions (5) for $\sigma = 1$.

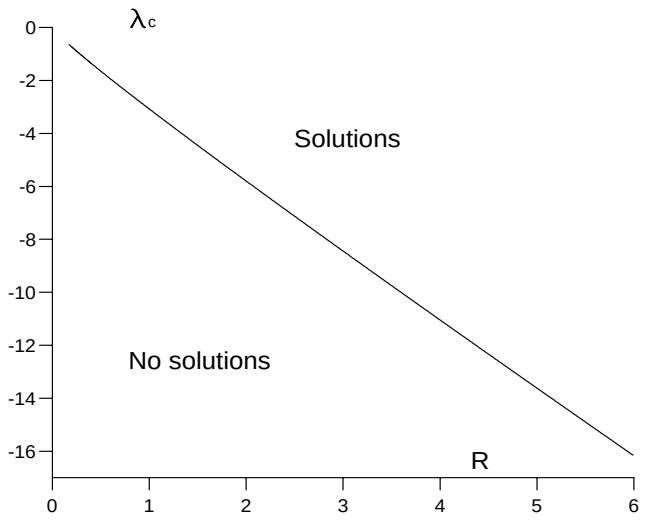

Figure 3: A plot of the critical value λ_c of λ against R (for $\sigma = 1$). The region in the (λ, R) parameter plane where solutions exist is labelled on the figure.

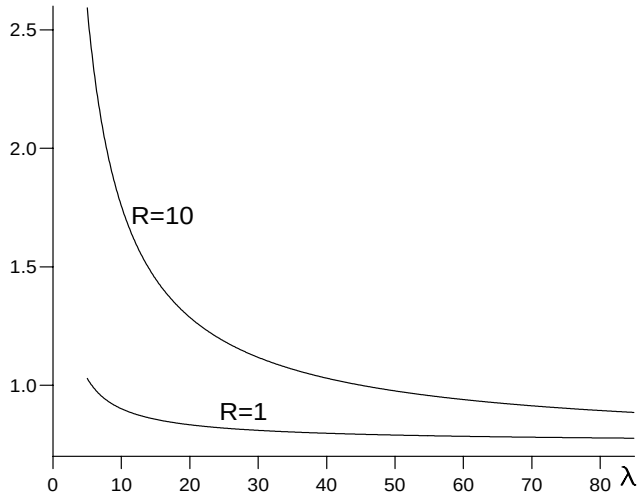

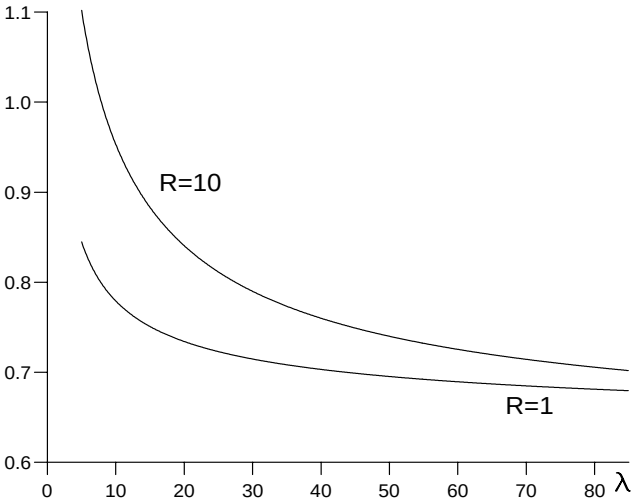

Figure 4: Plots of $(\lambda^3/R)^{-1/4} f''(1)$ and $-(\lambda R)^{-1/4}\theta'(1)$ obtained from the numerical solution of equations (3, 4) against λ for $R = 1$, 10 and $\sigma = 1$.

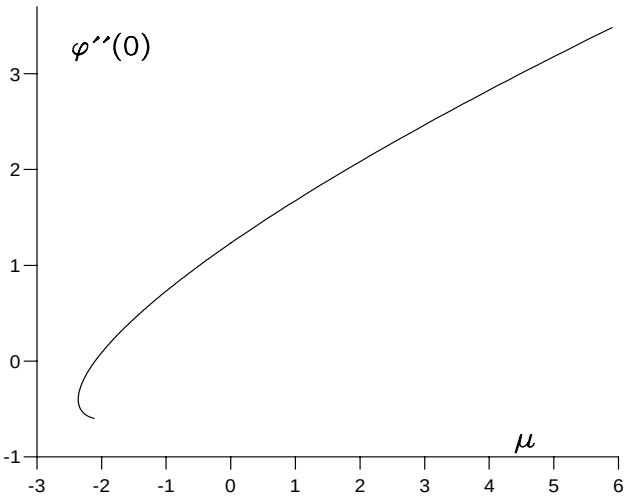

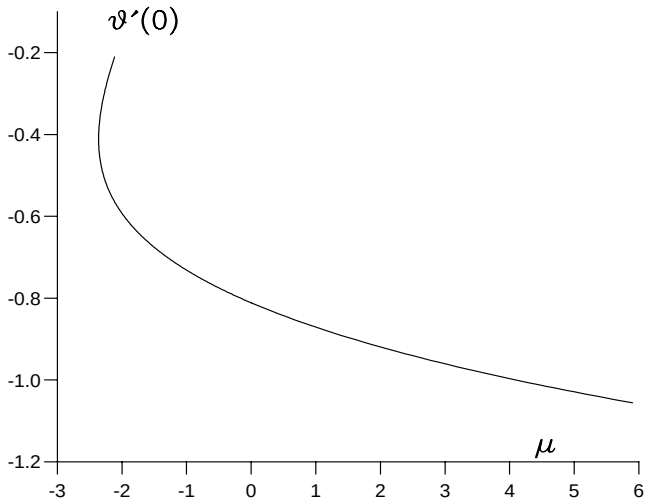

Figure 5: Plots of (a) $\phi_0''(0)$ and (b) $\theta_0'(0)$ against $\mu = \lambda\, R^{-1}$ for the solution for large R given by (27 - 29) for $\sigma = 1$.

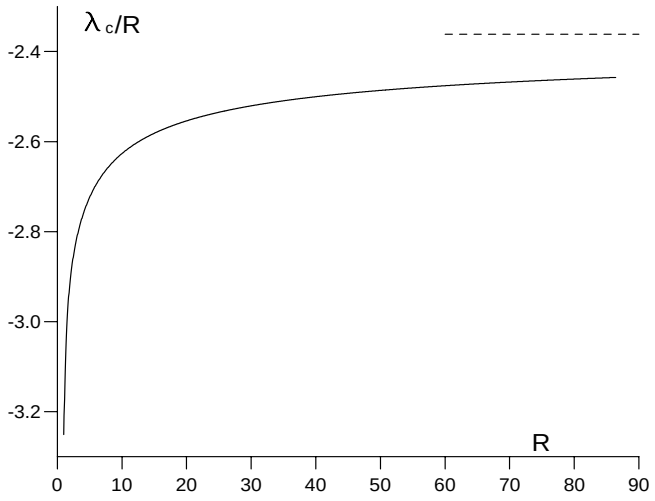

Figure 6: A plot of $\lambda_c R^{-1}$ against R for $\sigma = 1$. The asymptotic limit (30) for R large is shown by the broken line.

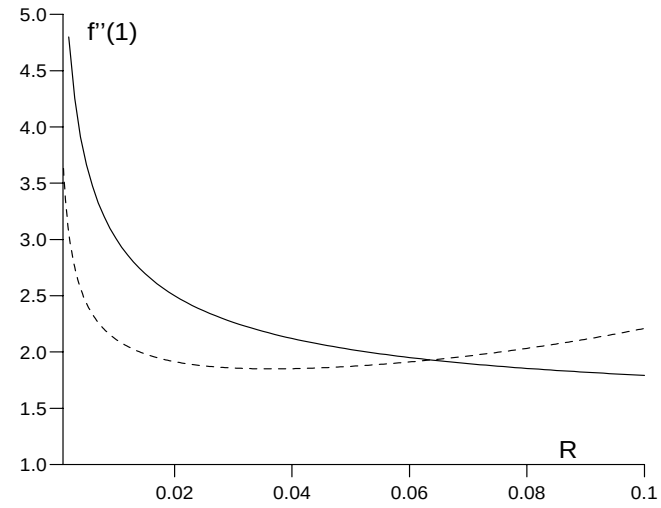

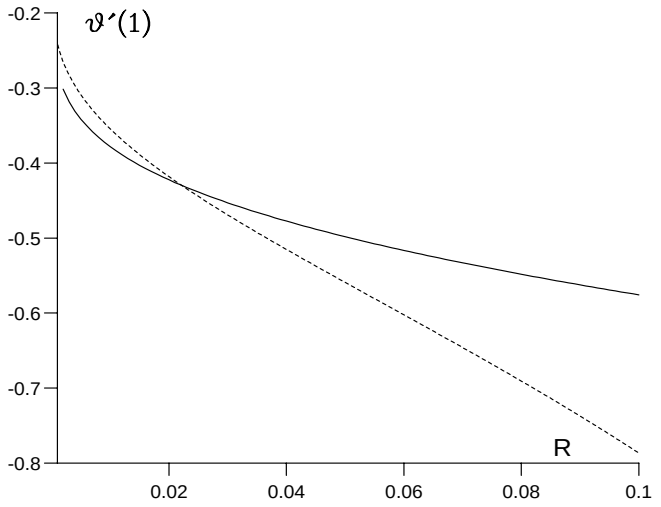

Figure 7: Plots of (a) $f''(1)$ and (b) $\theta'(1)$ against R for $\lambda = 1$, $\sigma = 1$ for small R obtained from the numerical solution of equations (3, 4) subject to boundary conditions (5). The asymptotic expressions (47) are shown by the broken lines.

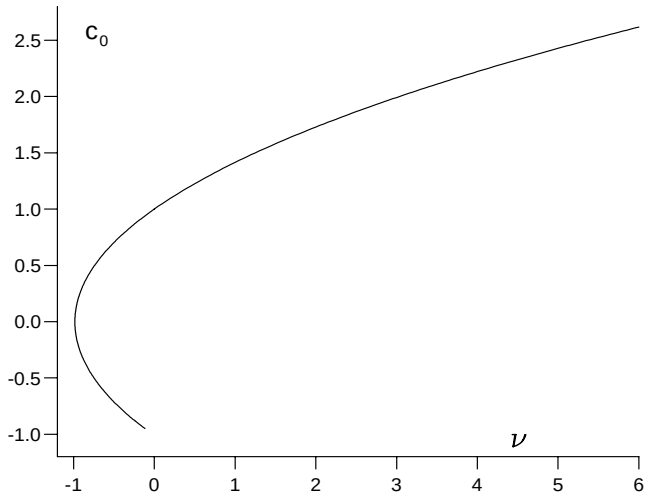

Figure 8: A plot of c_0 against ν, defined in (48), for $\sigma = 1$ arising in the small R, small λ problem (51 – 53).

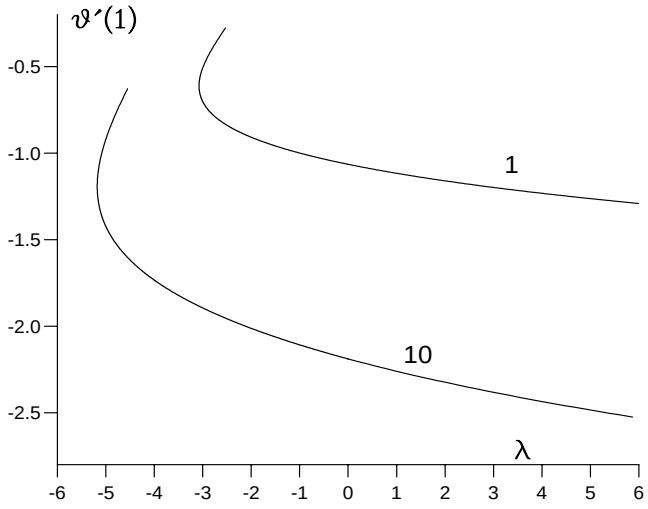

Figure 9: Plots of $\theta'(1)$ against λ for $R = 1$ and $\sigma = 1$, 10 obtained from the numerical solution of equations (3, 4) subject to boundary conditions (5).

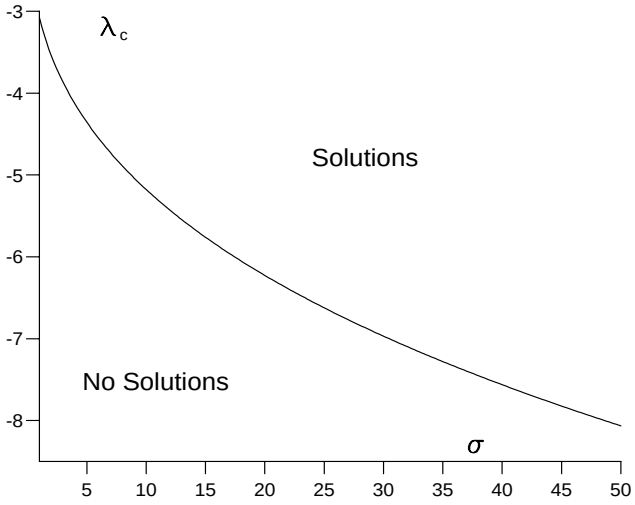

Figure 10: A plot of the critical value λ_c of λ against σ for $R = 1$. The region in the (λ, σ) parameter plane where solutions exist is labelled on the figure.

Brinkman Flow of a Viscous Fluid through a Spherical Porous Medium Embedded in another Porous Medium

A. Postelnicu[1,], T. Grosan[2] and I. Pop[2]

[1]*Department of Thermal Engineering and Fluid Mechanics, Transilvania University, 500036, Brasov, Romania*

[2]*Faculty of Mathematics, University of Cluj, R-3400 Cluj, CP 253, Romania*

Abstract A mathematical model for the two-dimensional steady viscous and incompressible flow past a permeable sphere embedded in another porous medium is presented under the assumption of the Darcy-Brinkman equation model and a uniform shear flow away from the sphere. Closed form analytical solutions are presented for streamlines inside and outside the sphere and shearing stress at the surface of the sphere. The streamlines and the shearing stress at any point on the surface of the sphere are shown in several graphs for different values of the governing parameters. It is shown that the dimensionless shearing stress on the sphere is periodic in nature and its absolute value increases with an increase in both porous parameters.

Keywords: permeable sphere · porous media · Darcy-Brinkman model · analytical solution

Nomenclature

a	radius of the sphere, *m*
K_i	permeability of the porous medium, m^2
$\bar{p}_i$	pressure, *Pa*
p_i	non-dimensional pressure
$\bar{r}$	radial coordinate, *m*
r	non-dimensional radial coordinate
$\bar{u}_i, \bar{v}_i$	radial and transversal coordinates, $m.s^{-1}$
u_i, v_i	non-dimensional radial and transverse components of velocity
U_∞	constant velocity away from the sphere, $m.s^{-1}$

Greek symbols

ϕ_i	porosity of the porous medium
ϕ	ratio of the porosities
θ	angular coordinate
σ_i	parameter of the porous medium, $a/\sqrt{K_i}$
$\tau_{r\theta(i)}, \tau_{rr(i)}$	non-dimensional skin friction at the surface of the sphere in the radial and transversal directions
ψ_i	non-dimensional stream function

Subscript

$i = 1, 2$

1. Introduction

Flow in porous media has been an area of intensive investigation for the last several decades. The growing emphasis on effective granular and fibrous insulation systems for the successful containment of the transport of radio-nuclide from deposits of nuclear waste materials has stimulated various studies in fluid saturated porous media and many results were obtained for the forced and convective flow in the fundamental geometries of internal (cavities, annulus, etc.) and external (flow over surfaces) flows. In comprehensive reviews of the heat transfer mechanisms in geothermal systems, Cheng (1987,1985) and Bejan (1987) presented the work in this field with emphasis on its applications in geothermal and energy systems research. Since then a very large number of practical applications, both industrial and environmental, have caused a rapid extension of the research, and a substantial number of papers, which relate the boundary-layer flow past surfaces of various configurations, have been published. Nield and Bejan (2006), Ingham and Pop (1998,2002), Pop and Ingham (2001), Vafai (2000,2005) Ingham *et al.* (2004) and Bejan *et al.* (2004) gathered many applications which highlight the directions where further theoretical and experimental developments are required.

Earlier studies of a uniform shear flow past a body embedded in a porous medium in the Stokes flow were mainly concerned with the use of the Darcy model because the

dimensionless particle diameter (i.e., the ratio of particle diameter to the characteristic length) is usually small. Flows in rocks, soil sand and other composite media encountered in hydrology and geothermal problems are usually studied using the Darcy flow model. Rudraiah (1984) and Rudraiah *et al.* (2003) have shown that in many practical applications of flow in porous media which involve porous materials, such as foam metals and fibrous media of high porosity, where dimensionless particle diameter is not small, the Darcy law is not adequate and the non-Darcy equation is more accurate to describe the flow. The non-Darcy equation which incorporates both boundary and inertia effects in addition to the Darcy resistance may alter the characteristics of flow past a body. Padmavathi *et al.* (1993), Masliyah *et al.* (1987) and Berman (1996) have studied the Stokes flow past a sphere embedded in a porous medium using Stokes and Brinkmann flow equations with specifying a uniform velocity far away from the sphere. Also, Srivastava and Srivastava (2005) have recently discussed the steady flow of an incompressible viscous fluid streaming past a porous sphere at small Reynolds number with a uniform velocity by dividing the flow in three regions. The region –I is the region inside the porous sphere in which the flow is governed by Brinkman equation with the effective viscosity different from that of the clear (non-porous) fluid. In regions II- and III- clear fluid flows and Stokes and Ossen solutions are respectively valid. In all the three regions Stokes stream function is expressed in powers of Reynolds number. Further, in a very recent paper, Rudraiah and Chandrashekhar (2005) have studied the two-dimensional steady incompressible flow past an impermeable sphere embedded in a porous medium using the Brinkman model with a uniform shear instead of a uniform velocity away from the sphere. This problem occurs in a wide variety of technological applications like removing impurities in the integrated circuits used in computers, lubrication process in porous bearings, etc.. However, results of this paper are, unfortunately, wrong because the authors have wrongly considered the expression for the stream function of the flow outside the porous sphere. The existence and uniqueness of the solution for the two-dimensional flow with porous inclusions based on Brinkman equation has been studied by Kohr and Raja Sekar (2006).

The aim of this paper is to study the flow of a viscous fluid past a permeable sphere embedded in another porous medium using the Brinkman equation model for the

flow inside and outside the sphere. A rigorous theoretical justification of Brinkman's equation was given by Tam (1969) and later by Lundgren (1972). It is important that we succeed to present a closed form solutions of the non-dimensional governing equations and the evolution of the flow field is demonstrated by plotting the streamlines, velocity and shearing stress for the flow inside and outside the sphere. These quantities are numerically computed and depicted graphically for various values of the porous medium parameters σ_1 and σ_2. By way of correspondence to a real physical phenomenon of such a situation, one may well consider the application to pollutants flow at the interface between two porous media or oil drilling in a porous medium having insertions with others porous media.

2. Basic equations

Consider the steady forced convection flow of a viscous and incompressible fluid past a permeable sphere of radius a with the constant velocity U_∞ away from the sphere. The sphere is filled with a porous medium of permeability K_1 placed in a fluid-saturated porous medium of permeability K_2. The problem is discussed by dividing the flow area in two zones. Zone I is the region inside the porous sphere and zone II is the region outside it. Let the index i in the subscript of any entity X_i, $i = 1, 2$ indicate the zone in which the entity is represented.

The continuity and Brinkman equations for this problem with inertial terms omitted are of the form, see Nield and Bejan (2006):

$$\overline{\nabla} \cdot \mathbf{v_i} = 0 \tag{1}$$

$$\overline{\nabla}\, \overline{p}_i = -\frac{\mu}{K_i} \overline{\mathbf{v}}_\mathbf{i} + \tilde{\mu}\, \overline{\nabla}^2\, \overline{\mathbf{v}}_\mathbf{i} \tag{2}$$

where $\overline{p}_i$ is the pressure, $\overline{\mathbf{v}}_\mathbf{i}$ is the superficial velocity vector, μ is the dynamic viscosity of the fluid, $\tilde{\mu}$ is an effective or Brinkman viscosity. It is common practice for $\tilde{\mu}$ to be taken equal with μ for high porosity medium, i.e. $\tilde{\mu}/\mu = 1$ (see Nield and Bejan, 2006). Further, we use a spherical coordinate system $(\overline{r}, \theta, \varphi)$ with the origin at

the centre of the sphere and the axis $\theta = 0$ along the direction of the undisturbed flow U_∞ as it is shown in Fig. 1. Due to the symmetry of the problem we have $\partial / \partial \varphi = 0$. It is convenient to non-dimensionalise all variable by writing

$$r = \bar{r} / a, \quad u_i = \bar{u}_i / U_\infty, \quad v_i = \bar{v}_i / U_\infty, \quad p_i = a\, \bar{p}_i / (\mu U_\infty) \tag{3}$$

where $\bar{u}_i$ and $\bar{v}_i$ are the radial and transverse components of velocity.

Using the new non-dimensional variables (3), Eqs. (1) and (3) can be written as

$$\frac{\partial}{\partial r}(r^2 u_i) + \frac{r}{\sin\theta}\frac{\partial}{\partial \theta}(v_i \sin\theta) = 0 \tag{4}$$

$$-\frac{\partial p_i}{\partial r} = \sigma_i^2 u_i - \left\{ \frac{\partial^2 u_i}{\partial r^2} + \frac{2}{r}\frac{\partial u_i}{\partial r} + \frac{1}{r^2}\frac{\partial^2 u_i}{\partial \theta^2} + \frac{\cot\theta}{r^2}\frac{\partial u_i}{\partial \theta} - \frac{2u_i}{r^2} - \frac{2}{r^2}\frac{\partial v_i}{\partial \theta} - \frac{2v_i \cot\theta}{r^2} \right\} \tag{5}$$

$$-\frac{1}{r}\frac{\partial p_i}{\partial \theta} = \sigma_i^2 v_i - \left\{ \frac{\partial^2 v_i}{\partial r^2} + \frac{2}{r}\frac{\partial v_i}{\partial r} + \frac{1}{r^2}\frac{\partial^2 v_i}{\partial \theta^2} + \frac{\cot\theta}{r^2}\frac{\partial v_i}{\partial \theta} + \frac{2}{r^2}\frac{\partial u_i}{\partial \theta} - \frac{v_i \operatorname{cosec}^2\theta}{r^2} \right\} \tag{6}$$

where $\sigma_i = a / \sqrt{K_i}$ are the parameters of the porous media. Permeabilities K_i of the porous media are given by Carman-Kozeny relationship, see Nield (2002),

$$K_i = \frac{d_i^{\,2} \phi_i^{\,3}}{180(1-\phi_i)^2} \tag{7}$$

where ϕ_i are the porosities and d_i are the mean particles diameters for the two porous media. Thus the parameters of the porous media are given by:

$$\sigma_i = \gamma_i \frac{\sqrt{180}(1-\phi_i)}{\phi_i^{\,3/2}} \tag{8}$$

where $\gamma_i = a / d_i$. In Eqs. (4) – (6) variables r and θ vary in zone I in the ranges $0 \le r \le 1, \ -180^\circ \le \theta \le 180^\circ$ and in zone II in the ranges $1 \le r < \infty, \ -180^\circ \le \theta \le 180^\circ$.

The matching conditions at the surface of the sphere can be written as (see, Merikh and Mohamad, 2002)

$$
\begin{aligned}
&u_1 = u_2 \quad \text{at} \quad r = 1 \\
&v_1 = v_2 \quad \text{at} \quad r = 1 \\
&\tau_{r\theta(1)} = \tau_{r\theta(2)} \quad \text{at} \quad r = 1 \\
&\tau_{rr(1)} = \tau_{rr(2)} \quad \text{at} \quad r = 1
\end{aligned}
\tag{9}
$$

where $\tau_{r\theta(i)}$ and $\tau_{rr(i)}$ are the non-dimensional shear stresses on the surface of the sphere.

We introduce now the stream function ψ_i defined in the usual way as

$$
u_i = \frac{1}{r^2 \sin\theta} \frac{\partial \psi_i}{\partial \theta}, \quad v_i = -\frac{1}{r \sin\theta} \frac{\partial \psi_i}{\partial r} \tag{10}
$$

Outsideb the porous sphere the stream function ψ_2 is given by

$$
\psi_2(r,\theta) = \frac{1}{2}\left(r^2 - \frac{1}{r}\right) \sin^2\theta \quad \text{for all} \quad r > 1 \tag{11}
$$

Using (10) and (11), the boundary conditions for the velocity components in zone II are

$$
u_2 \sim \cos\theta, \quad v_2 \sim -\sin\theta \quad \text{as} \quad r \to \infty \tag{12}
$$

The expression of $\tau_{r\theta(i)}$ and $\tau_{rr(i)}$ are given by

$$
\begin{aligned}
\tau_{r\theta(i)} &= \frac{1}{r}\frac{\partial u_i}{\partial \theta} + \frac{\partial v_i}{\partial r} - \frac{v_i}{r} \\
\tau_{rr(i)} &= -p_i + 2\frac{\partial u_i}{\partial r}
\end{aligned}
\tag{13}
$$

3. Mathematical analysis

We introduce now the stream function ψ_i defined in the usual way

$$
u_i = \frac{1}{r^2 \sin\theta} \frac{\partial \psi_i}{\partial \theta}, \quad v_i = -\frac{1}{r \sin\theta} \frac{\partial \psi_i}{\partial r} \tag{14}
$$

and eliminate the pressure p_i between Eqs. (5) and (6). Then, using (14), we get

$$
\Im^2 \left(\Im^2 - \sigma_i^2\right) \psi_i = 0 \tag{15}
$$

where the operator $\Im^2$ is defined as

$$
\Im^2 = \frac{\partial^2}{\partial r^2} + \frac{\sin\theta}{r^2} \frac{\partial}{\partial \theta}\left(\frac{1}{\sin\theta} \frac{\partial}{\partial \theta}\right) \tag{16}
$$

The boundary conditions far away from the sphere (12) in terms of ψ_2 become

$$\psi_2(r,\theta) \sim \frac{r^2}{2}\sin^2\theta \quad \text{as} \quad r \to \infty \tag{17}$$

The boundary condition (17) suggests the following similarity solution to Eq. (15)

$$\psi_i(r,\theta) = f_i(r)\sin^2\theta \tag{18}$$

Substituting (18) into Eq. (15), we obtain the following ordinary differential equation

$$f_i^{\,iv} - \frac{4}{r^2} f_i'' + \frac{8}{r^3} f_i - \frac{8}{r^4} - \sigma_i^2 \left(f_i'' - \frac{2}{r^2} f_i \right) = 0 \tag{19}$$

where primes denote differentiation with respect to r. If we make the transformation

$$f_i'' - \frac{2}{r^2} f_i = \sqrt{r}\, g_i(r) \tag{20}$$

the fourth order equation (19) reduces to the second order equation

$$r^2 g_i'' + r g' - \left[\left(\frac{3}{2} \right)^2 + (\sigma_i r)^2 \right] g_i = 0 \tag{21}$$

This is the modified Bessel differential equation and hence his general solution is given by

$$g_i(r) = A_i I_{3/2}(\sigma_i r) + B_i K_{3/2}(\sigma_i r) \tag{22}$$

where $I_{3/2}(\sigma_i r)$ and $K_{3/2}(\sigma_i r)$ are the modified Bessel functions of first and second kind of order 3/2, respectively, and A_i and B_i are arbitrary constants of integration. Thus on using (22), Eq. (20) becomes

$$f_i'' - \frac{2}{r^2} f_i = A_i I_{3/2}(\sigma_i r) + B_i K_{3/2}(\sigma_i r) \tag{23}$$

and has the general solution

$$f_i(r) = \frac{C_i}{r} + D_i r^2 + A_i \frac{\sqrt{r}}{\sigma_i^2} I_{3/2}(\sigma_i r) + B_i \frac{\sqrt{r}}{\sigma_i^2} K_{3/2}(\sigma_i r) \tag{24}$$

where C_i and D_i are also arbitrary constants of integration.

Using (18) and (24) we can describe the flow in the both zones I and II with a proper choice of the constants A_i, B_i, C_i and D_i. For the flow in zone I where $r<1$ and origin occurs, the constants $C_1 = B_1 = 0$ and the expression for $f_1(r)$ can be written as

$$f_1(r) = D_1 r^2 + A_1 \frac{\sqrt{r}}{\sigma_1^2} I_{3/2}(\sigma_1 r) \tag{25}$$

On the other hand, for the flow in zone II where $r>1$ and $f_2(r) \to \frac{1}{2} r^2$ as r $\to \infty$, we get $D_2 = 1/2$ and $A_2 = 0$ and the expression for $f_2(r)$ is given by

$$f_2(r) = \frac{C_2}{r} + \frac{1}{2} r^2 + B_2 \frac{\sqrt{r}}{\sigma_2^2} K_{3/2}(\sigma_2 r) \tag{26}$$

To determine the constants A_1, B_2, C_2 and D_1 we have to use the matching and boundary conditions (9). To do it, we have to determine the expression for $\tau_{r\theta(i)}$ and $\tau_{rr(i)}$ given by (13) and also the pressure p_i. Substituting (14) and (18) into Eqs. (5) and (6), we get after some algebra

$$p_i = \left(-2\sigma_i^2 \int \frac{f_i}{r^2} dr + 8\int \frac{f_i}{r^4} dr + \frac{2}{r^2} f_i' + \frac{4}{r^3} f_i \right) \cos\theta \tag{27}$$

where the constant of integration has been taken to be zero. Thus, relations (13) become

$$\begin{aligned} \tau_{r\theta(i)} &= \left(\frac{2}{r^2} f_i' - \frac{2}{r^3} f_i - \frac{1}{r} f_i'' \right) \sin\theta \\ \tau_{rr(i)} &= \left(2\sigma_i^2 \int \frac{f_i}{r^2} dr - \frac{12}{r^3} f_i - 8\int \frac{f_i}{r^4} dr + \frac{2}{r^2} f_i' \right) \cos\theta \end{aligned} \tag{28}$$

Now, the four matching conditions (9) in terms of $f_i(r)$ can be written as

$$\begin{aligned} & f_2(1) = f_1(1) \\ & f_2'(1) = f_1'(1) \\ & f_2''(1) = f_1''(1) \\ & \left(\sigma_2 \int \frac{f_2}{r^2} dr - 4\int \frac{f_2}{r^4} \right)_{r=1} = \left(\sigma_1 \int \frac{f_1}{r^2} dr - 4\int \frac{f_1}{r^4} dr \right)_{r=1} \end{aligned} \tag{29}$$

These relations can be used to determine the values of the constants A_1, B_2, C_2 and D_1 for some values of the parameters σ_1 and σ_2.

Thus, we have the stream functions $\psi_i(r,\theta)$ in the both zones I and II given by

$$\psi_1(r,\theta) = f_1(r)\sin^2\theta, \quad \psi_2(r,\theta) = f_2(r)\sin^2\theta \tag{30}$$

From these equations we obtain the normal and tangential components of velocities in zones I and II, using (14) as

$$\begin{aligned} u_1 &= 2\,\frac{f_1(r)}{r^2}\cos\theta, \quad v_1 = -\frac{f_1'(r)}{r}\sin\theta \\ u_2 &= 2\,\frac{f_2(r)}{r^2}\cos\theta, \quad v_2 = -\frac{f_2'(r)}{r}\sin\theta \end{aligned} \tag{31}$$

The case when the sphere is impermeable corresponds to $u_2 = 0$ and $v_2 = 0$ at the surface of the sphere. Thus, the values of B_2 and C_2 are given by $f_2(1) = 0$ and $f_2'(1) = 0$ from (29). On using (24) and the properties of the Bessel functions (Abramowitz and Stegun, 1972) calculation gives the following expressions for B_2 and C_2

$$B_2 = \frac{3\sigma_2}{2K_{1/2}(\sigma_2)}, \quad C_2 = -\frac{1}{2} - \frac{3K_{3/2}(\sigma_2)}{2\sigma_2 K_{1/2}(\sigma_2)} \tag{32}$$

Thus, $f_2(r)$ is given by

$$f_2(r) = \frac{1}{2}r^2 - \frac{1}{2}\left(1 + \frac{3K_{3/2}(\sigma_2)}{\sigma_2 K_{1/2}(\sigma_2)}\right)\frac{1}{r} + \frac{3\sqrt{r}}{2\sigma_2}\frac{K_{3/2}(\sigma_2 r)}{K_{1/2}(\sigma_2)} \tag{33}$$

This expression is exactly the same with that reported by Pop and Ingham (1996) for the problem of flow past an impermeable sphere embedded in a porous medium using the Brinkman model if we change σ_2 by $1/\sigma_2$. Thus, using (28) and (33) we get that the dimensionless shearing stress at any point on the surface of the sphere (i.e., $r = 1$) is given by

$$\tau_{r\theta(2)} = -\frac{3}{2}(1+\sigma_2)\sin\theta \tag{34}$$

Also this expression is identical with that found by Pop and Ingham (1996) if we change σ_2 by $1/\sigma_2$. Therefore, we can conclude that the present analysis is correct.

4. Results and discussion

Based on the governing equations of motion it is seen that the parameters affecting the flow in the present problem are the porous media parameters σ_1 and σ_2 given by Eq. (8). Values of the porosities for different porous materials can be found in the book by Nield and Bejan (2006). For a high porosity porous media a typical value is $\phi_i = 0.8$ so that Eq. (8) reduces to:

$$\sigma_i = 3.5\ \gamma_i \tag{35}$$

In most physical problems of interest γ_i is large and hence σ_i is large. In this paper calculation have been carried out using the symbolic calculus software Mathematica and it was found that for large values of the porous media parameters, except when $\sigma_1 = \sigma_2$, in all other cases, basically A_1 diminishes and B_2 takes a very large value. In an attempt to understand, from the numerical point of view, this fact, we have to examine Eq. (23). Thus, we remark from this equation that as r increases towards $r = 1$ and σ_1 takes large values, the weight of the second term becomes important, due to the behaviour of the Bessel function $I_{3/2}(\sigma_1 r)$, which grows very fast to infinity. On the other hand, the modified Bessel function $K_{3/2}(\sigma_2 r)$ in Eq. (24) decreases to zero as r increases. For example, $K_{3/2}(10)$ = 1.9793e-005. Therefore, the effect of the B_2 coefficient, which has a very large value, is damped, due to the above mentioned behavior of $K_{3/2}(\sigma_2 r)$. In order to have confidence in this analysis, we have determined both numerically and analytically the values of the coefficients A_1, B_2, C_2 and D_1, and it was found a very good agreement for large values of the parameters σ_1 and σ_2. However, in order to save space we will not present here this comparison.

Figures 2 to 4 illustrate the streamlines computed from Eq. (30) are drawn for some values of the parameters of the porous media σ_1 and σ_2, namely the cases of $\sigma_1 < \sigma_2$, $\sigma_1 > \sigma_2$ and $\sigma_1 = \sigma_2$ have been considered. Figure 2 shows the streamlines for $\sigma_1 = 1$ and $\sigma_2 = 10,\ 100$, Fig. 3 illustrates the streamlines for $\sigma_1 = 10$ and $\sigma_2 = 1,\ 10,\ 100$, and Fig. 4 show the streamlines for $\sigma_1 = 100$ and $\sigma_2 = 1,\ 10$. It is clearly seen from

these figures that there is a substantial difference between the cases considered when $\sigma_1 < \sigma_2$ and $\sigma_1 > \sigma_2$, respectively. Thus, it is noticed that the meandering of the streamlines near the surface of the sphere and approaching a constant value away from the sphere for both $\sigma_1 < \sigma_2$ and $\sigma_1 > \sigma_2$. In addition, in the case $\sigma_1 > \sigma_2$ a boundary layer near the surface of the sphere can be observed, see Figs.3a, 4a and 4b. Further we can notice from Figs. 2a, 2b and 3c that the streamlines are distorted towards the center of the porous sphere in the case $\sigma_1 < \sigma_2$. This is in accordance with the properties of the porous media. In the special case of $\sigma_1 = \sigma_2$, the flow is not perturbed by the presence of the porous sphere. This is again in accordance with the properties of the porous media that is because the two porous media have the same properties.

The variation of the dimensionless shearing stress $\tau_{r\theta(2)}$ at any point on the surface of the sphere (i.e., $r = 1$) with θ is illustrated in Figs. 5 to 7 for several values of the porous parameters σ_1 and σ_2. We can see that the absolute value of the shearing increases with an increase in both σ_1 and σ_2. It is also seen that at the front and rear points of the sphere, $\theta = 0^o$ and $\theta = 180^o$, the shearing stress vanishes, whereas it attains the maximum value at $\theta = \pm 90^o$. It should also be pointed out that there is no flow separation occurring for the flow past a sphere which is embedded in a constant porosity medium based on the Brinkman equation model. The positive or negative value of the shearing stress $\tau_{r\theta(2)}$ depend on the velocity direction at the interface between the interface of two porous media.

5. Conclusion

The flow of a viscous fluid past a permeable sphere embedded in another porous medium has been investigated using the Brinkman equation model. An exact analytical solution of the governing equations for the flow inside and outside the sphere has been calculated. It has been found that for a particular porous medium outside the sphere, the dimensionless shearing stress at any point on the surface of the sphere $\tau_{r\theta(2)}$ increases with the increase

of the parameter σ_2. It is shown that there is a substantial difference between the cases when $\sigma_1 < \sigma_2$, $\sigma_1 = \sigma_2$ and $\sigma_1 > \sigma_2$.

References

Bejan, A.: 1987, Convective heat transfer in porous media. In: *Handbook of Single-Phase Convective Heat Transfer* (Kakaç, S., Shah, R.K. and Aung, W.,eds.), Chapter 16. Wiley, New York.

Bejan, A., Dincer, I., Lorente, S., Miguel, A.F. and Reis, A.H., 2004, *Porous and Complex Flow Structures in Modern Technologies*, Springer, New York.

Berman, B.: 1996, Flow of a Newtonian fluid past an impervious sphere embedded in a porous medium, *Indian J. Pure Appl. Math*. **27**, 1249-1256.

Cheng, P.: Heat transfer in geothermal systems, in: *Adv. Heat Transfer* **14**, 1-105.

Cheng, P.: Natural convection in a porous medium: external flows, in: *Natural Convection: Fundamentals and Applications* (Kakç, S., Aung, W. and Viskanta, R. eds.), Hemisphere, Washington, DC, 1985.

Ingham, D.B. and Pop, I. (eds.): 1998, *Transport Phenomena in Porous Media*, Pergamon, Oxford.

Ingham, D.B. and Pop, I. (eds.): 2002, *Transport Phenomena in Porous Media*, Pergamon, Oxford, Vol. II.

Ingham, D.B. and Pop, I. (eds.): 2005, *Transport Phenomena in Porous Media. Elsevier*, Oxford, Vol. III.

Kohr, M. and Raja Sekar, G.P.: 2007, Existence and uniqueness result for two-dimensional porous media flows with porous inclusions based on Brinkman equation, *Engineering Analysis with Boundary Elements* (in press).

Lundgren, T.S.: 1972, Slow flow through stationary random beds and suspensions of spheres, *J. Fluid Mech*. **51**, 273-299.

Masliyah, J.H., Neale, G., Malysa, M. and Van De Ven, T.G.M.: 1987, Creeping flow over a composite sphere: Solid core with porous shell, *Chem. Engng. Sci*. **4**, 245-253.

Merrikh, A.A., Mohamad, A.A., 2002, Non-Darcy effects in buoyancy driven flows in an enclosure filled with vertically layered porous media, *Int. J. Heat Mass Transfer* **45**, 4305-4313.

Nield, D.A. and Bejan, A.: 2006, *Convection in Porous Media* (3nd edition), Springer, New York.

Niled, D.A., 2002, Modeling fluid flow in saturated porous media and at interfaces. In: *Transport Phenomena in Porous Media* (Ingham, D.B. and Pop, I., eds.), Pergamon, Oxford, 1-19.

Padmavathi, B.S., Amaranath, T. and Nigam, S.D.: 1993, Stoke's flow past a porous sphere using Brinkman model, *J. Appl. Math. Phys.* (*ZAMP*) **44**, 929-939.

Pop, I. and Ingham, D.B.: 1996, Flow past a sphere embedded in a porous medium based on the Brinkman model, *Int. Comm. Heat Mass Transfer* **23**, 865-874.

Pop, I. and Ingham, D.B.: 2001, *Convective Heat Transfer*: *Mathematical and Computational Modelling of Viscous Fluids and Porous Media*, Pergamon, Oxford.

Rudraiah, N.: 1984, Non-linear convection in porous medium with convective acceleration and viscous force, *Arab. J. Sci. and Engng*. **9**, 153-167.

Rudraiah, N., Pradeep, G.S. and Masuoka, T.: 2003, Non-linear convection in porous media: a review, *J. Porous Media* **6**, 1-32.

Rudraiah, N. and Chandrashekhar, D.V.: 2005, Flow past an impermeable sphere embedded in a porous medium with Brinkman model, *Int. J. Appl. Mech. Engng.* **10**, 145-158.

Srivastava, A.C. and Srivastava, N.: 2005, Flow past a porous sphere at small Reynolds Number, *J. Appl. Math. Phys.* (*ZAMP*) **56**, 821-835.

Tam, C.K.W.: 1969, The drag on a cloud of spherical particles in low Reynolds number flow, *J. Fluid Mech*. **38**, 537-546.

Vafai, K. (ed.): 2000, *Handbook of Porous Media*, Marcel Dekker, New York.

Vafai, K. (ed.): 2005, *Handbook of Porous Media*, Taylor & Francis, New York.

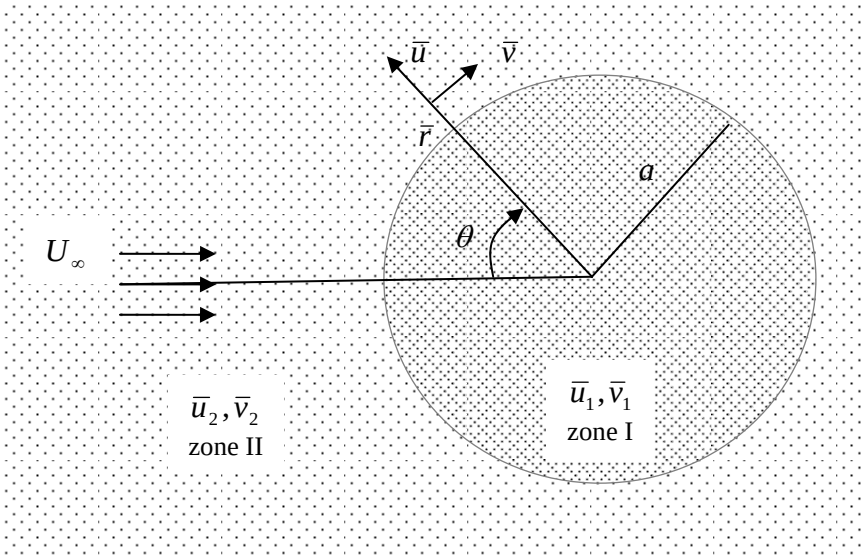

Fig. 1 Physical model and coordinate system.

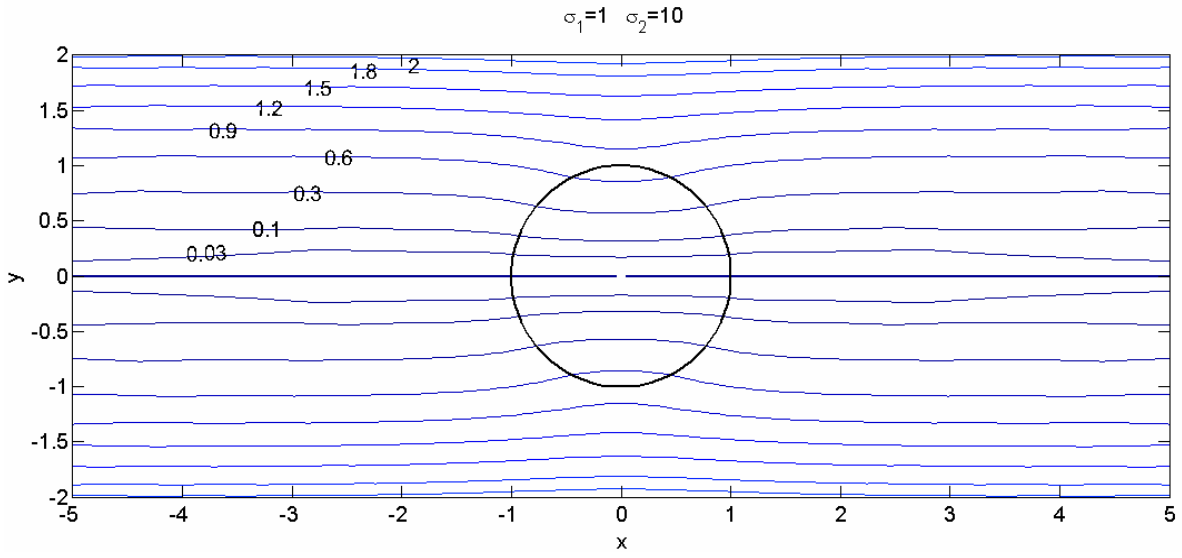

a)

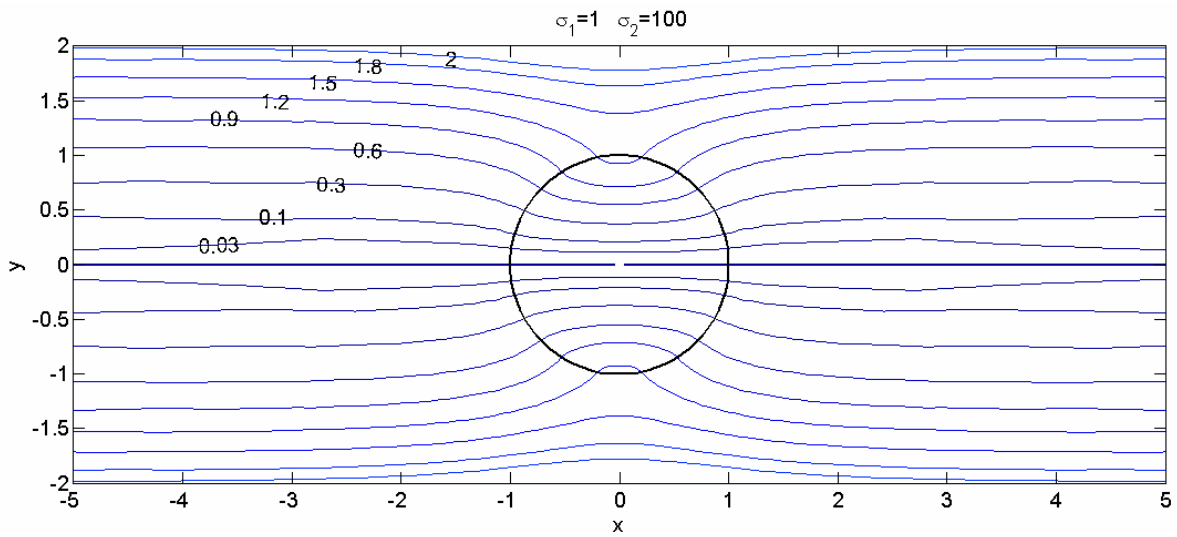

b)

Fig. 2. Streamlines for $\sigma_1 = 1$: a) $\sigma_2 = 10$; b) $\sigma_2 = 100$.

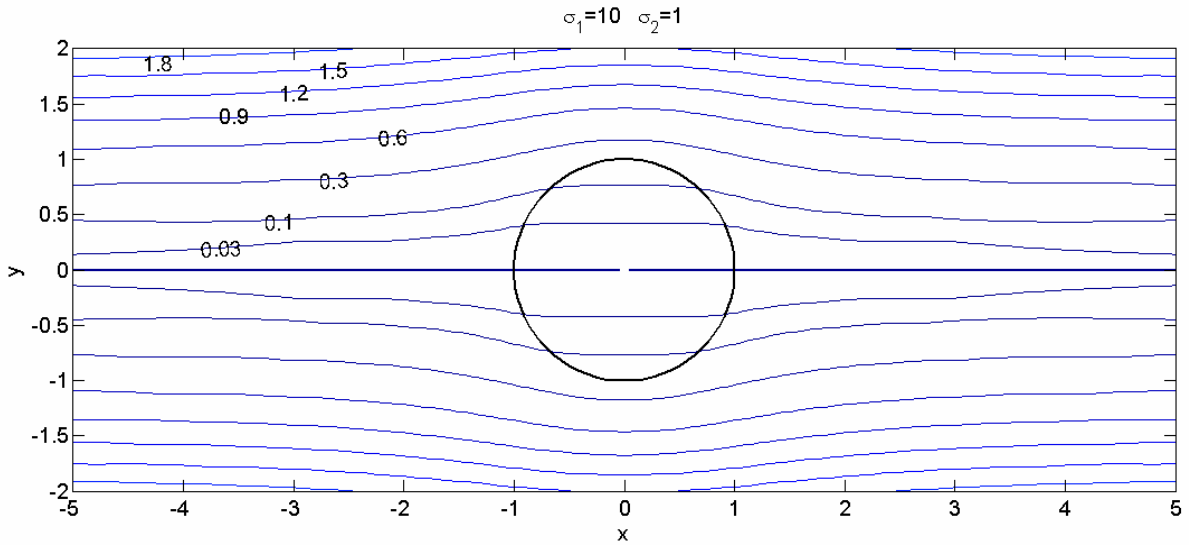

a)

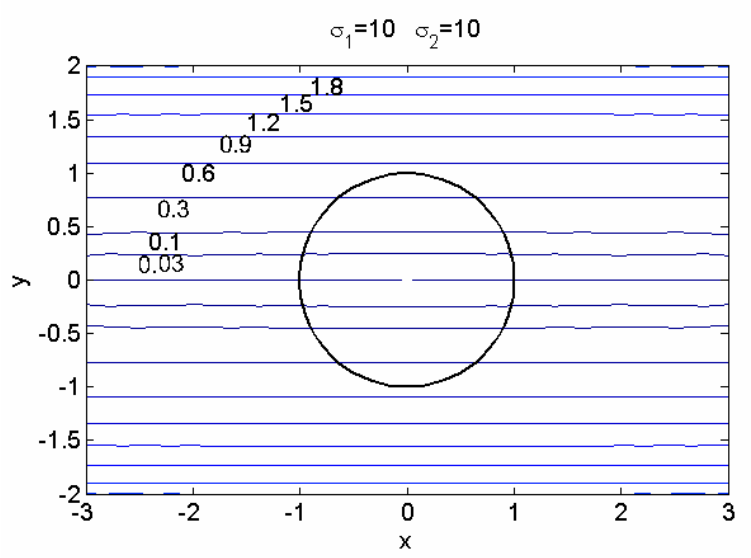

b)

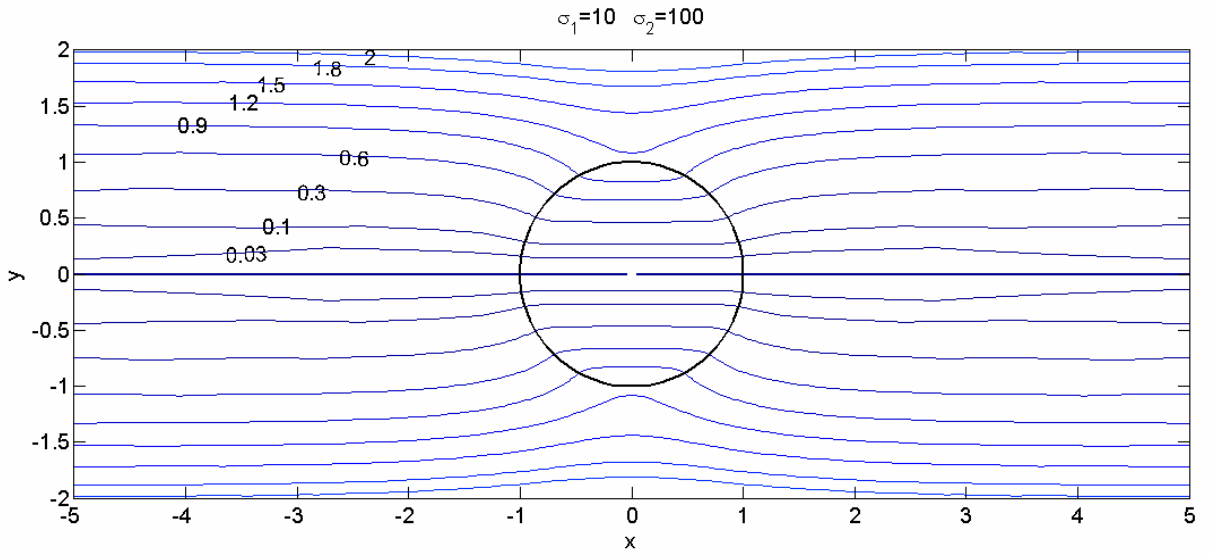

c)

Fig. 3. Streamlines for $\sigma_1 = 10$: a) $\sigma_2 = 1$; b) $\sigma_2 = 10$; c) $\sigma_2 = 100$.

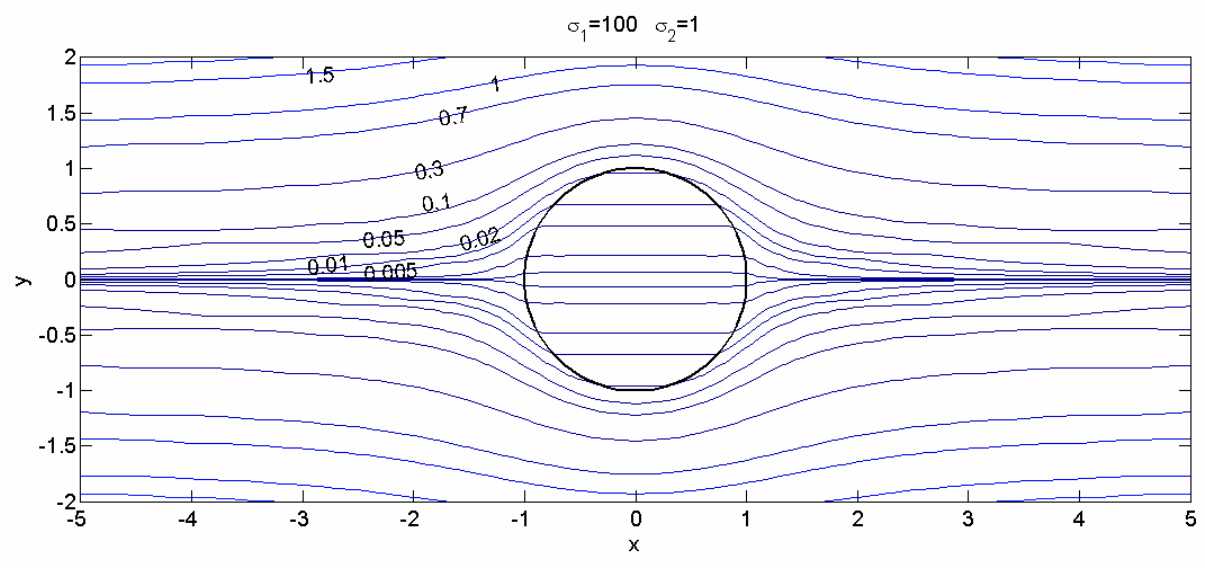

a)

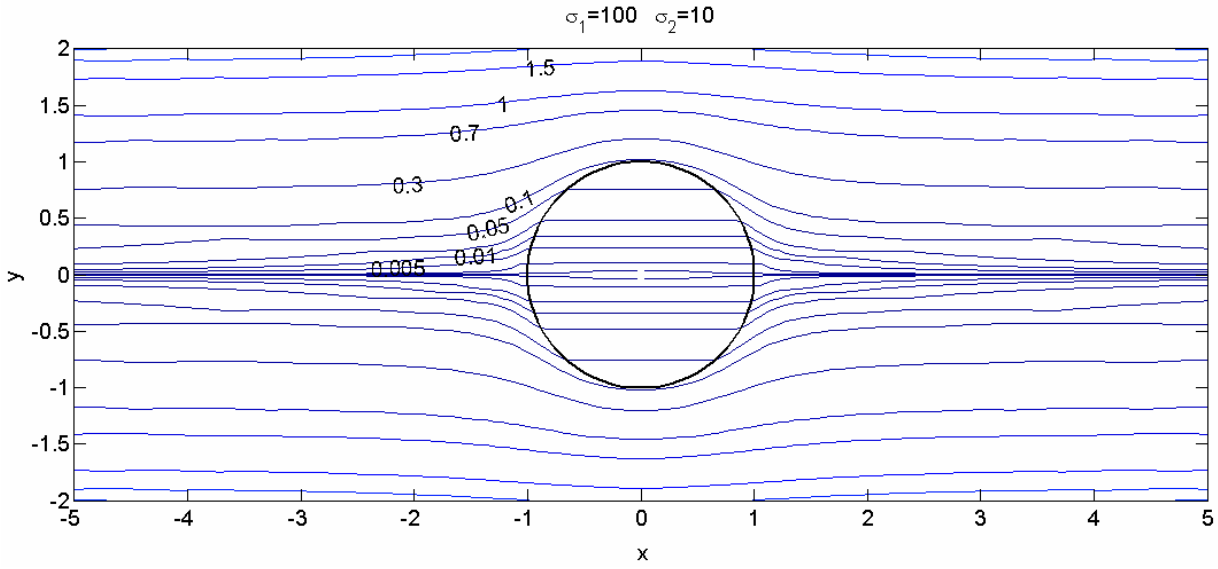

b)

Fig. 4. Streamlines for $\sigma_1 = 100$: a) $\sigma_2 = 1$; b) $\sigma_2 = 10$.

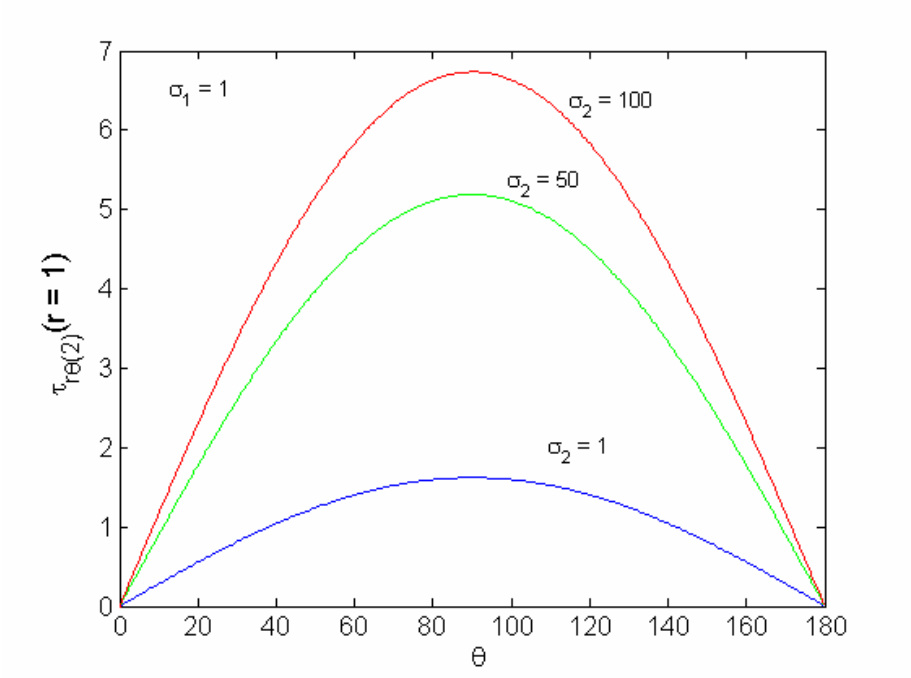

Fig. 5. Variation of tangential shear stress along the surface of the sphere for $\sigma_1 = 1$ and $\sigma_2 = 1, 50, 100$.

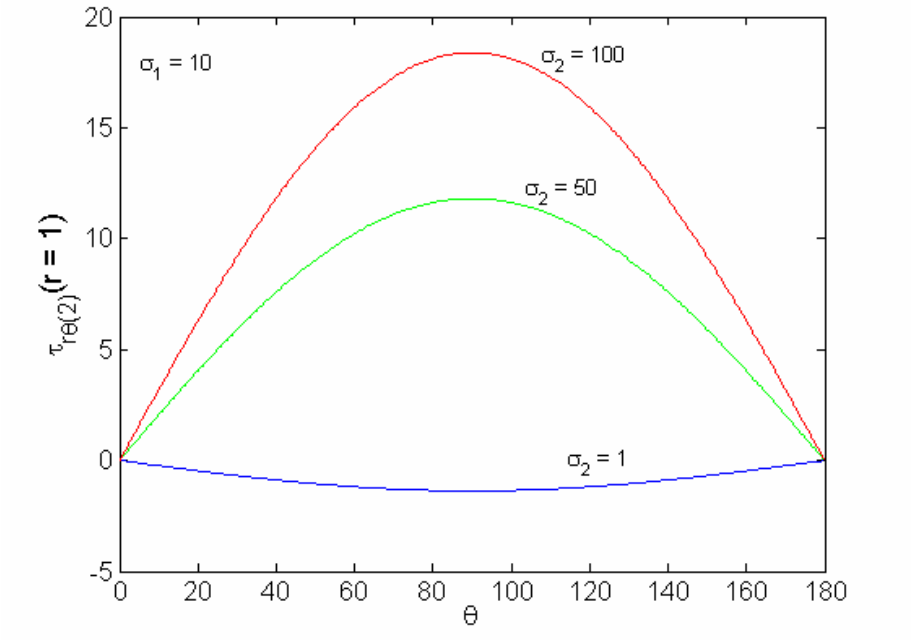

Fig. 6. Variation of tangential shear stress along the surface of the sphere

for $\sigma_1 = 10$ and $\sigma_2 = 1, 50, 100$.

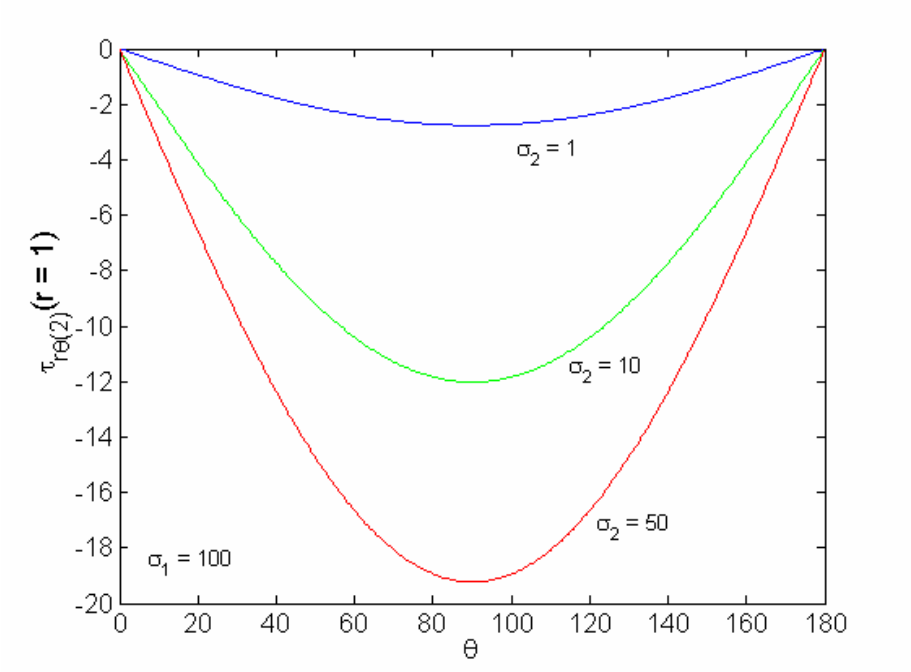

Fig. 7. Variation of tangential shear stress along the surface of the sphere for $\sigma_1 = 100$ and $\sigma_2 = 1, 10, 50$.

Magnetohydrodynamics oblique stagnation-point flow

T. Grosan · C. Revnic · I. Pop · D.B. Ingham

Abstract Laminar two-dimensional stagnation flow of an incompressible viscous electrically conducting fluid obliquely impinging on a flat plate is formulated as a similarity solution of the Navier-Stokes equations. The relative importance of this flow is measured by the dimensionless strain rate γ and magnetohydrodynamic M parameters. The viscous problem is reduced to a coupled pair of ordinary differential equations governed by γ and M. It is found that the parameter M causes a shift in the position of the point of zero skin friction along the plate.

Keywords Magnetohydrodynamics; Oblique stagnation-point flow; Similarity solution; Numerical methods

1 Introduction

The steady two-dimensional stagnation-point flow of an incompressible viscous fluid impinging obliquely on a plane rigid wall has been studied by many researchers. Stuart [1], Tamada [2], Dorrepaal [3,4], Labropulu et al. [5], Liu [6] and Tittleyand Weidman [7] have considered the case when the plane is fixed while Reza and Gupta [8], Lok et al. [9] and Mohapatra et al. [10] have considered the two-dimensional oblique stagnation-point flow towards a surface which is stretched with a velocity proportional to the distance stagnation-point flow towards a surface which is stretched with a velocity proportional to the distance from a fixed point. The case of axisymmetric flow stagnating obliquely on a circular cylinder has been considered by Weidman and Putkaradze [11]. Dorrepaal [3] and Labropolu et al.[5] have shown that for oblique flow impinging on a flat rigid wall that the slope of the dividing streamline at the wall divided by its slope at infinity is independent of the angle of incidence.

Several aspects of steady and unsteady two-dimensional stagnation-point flow of an electrically conducting fluid in the presence of a uniform applied magnetic field towards a fixed rigid plane wall or a stretching surface has been discussed in recent years by several authors, see for example Pavlov [12], Chakrabarti and Gupta [13], Andersson [14], Chiam [15], Mohapatra and Gupta [16], Ariel [17] and Xu *et al.*[18]. The study of magnetohydrodynamic (MHD) flow of an electrically conducting fluid caused by the deformation of the wall of a vessel containing a fluid is of considerable interest in modern metallurgical and metal-working processes.

The aim of the present paper is to discuss the steady two-dimensional oblique flow of a viscous and electrically conducting fluid impinging on a flat rigid wall in the presence of a constant applied magnetic field. It is found that the presence of the magnetic field causes a shift in the stagnation point and that this shift depends upon the magnetic parameter. To the best of our knowledge this problem has not been studied before.

2 Basic equations

Consider the steady two-dimensional MHD flow of an electrically conducting fluid near a stagnation point when an incompressible viscous fluid impinges obliquely on a rigid wall coinciding with the plane $\bar{y} = 0$ in the presence of a uniform transverse magnetic field, see Fig. 1, where $\bar{x}$ and $\bar{y}$ are the Cartesian coordinates along the wall and normal to it, respectively. It is assumed that the strength of the magnetic field is B_0 and that the magnetic Reynolds number is small. It is also assumed that the

T. Grosan · I. Pop (✉)
Faculty of Mathematics and Computer Science,
Babes-Bolyai University of Cluj, R-3400 Cluj,
Romania
email: popioan@yahoo.co.uk

C. Revnic
Institute of Mathematics of the Romanian Academy of Sciences, Cluj-Napoca, Romania

D.B. Ingham
Centre for Computational Fluid Dynamics, University of Leeds, Leeds LS2 9JT, UK

induced magnetic field is negligible. Under these assumptions the basic equations are given by

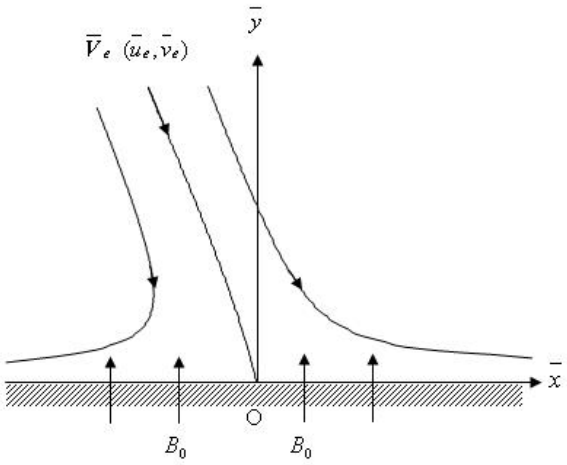

Fig. 1. Physical model and coordinate system.

$$\frac{\partial \bar{u}}{\partial \bar{x}} + \frac{\partial \bar{v}}{\partial \bar{y}} = 0 \tag{1}$$

$$\bar{u}\frac{\partial \bar{u}}{\partial \bar{x}} + \bar{v}\frac{\partial \bar{u}}{\partial \bar{y}} = -\frac{1}{\rho}\frac{\partial \bar{p}}{\partial \bar{x}} + \nu \bar{\nabla}^2 \bar{u} - \frac{\sigma {B_0}^2}{\rho}\bar{u} \tag{2}$$

$$\bar{u}\frac{\partial \bar{v}}{\partial \bar{x}} + \bar{v}\frac{\partial \bar{v}}{\partial \bar{y}} = -\frac{1}{\rho}\frac{\partial \bar{p}}{\partial \bar{y}} + \nu \bar{\nabla}^2 \bar{v} \tag{3}$$

where $\bar{u}$ and $\bar{v}$ are the velocity components along the $-\ \bar{x}$ and $-\ \bar{y}$ directions, respectively, $\bar{p}$ is the pressure, ρ is the density, ν is the kinematic viscosity, σ is the electrical conductivity and $\bar{\nabla}^2$ is the two-dimensional Laplacian. We consider an outer (inviscid) flow consisting of a linear superposition of an irrotational stagnation-point flow of strain rate a (> 0) and a uniform shear flow parallel to the wall of strain b. Thus, we assume that the boundary conditions appropriate to Eqs. (1) – (3) are given as

$$\begin{aligned} &\bar{u} = \bar{v} = 0 \quad \text{at} \quad \bar{y} = 0 \\ &\bar{u} = \bar{u}_e,\ \bar{v} = \bar{v}_e,\ \bar{p} = \bar{p}_\infty \quad \text{as} \quad \bar{y} \to \infty \end{aligned} \tag{4}$$

We introduce now the stream function $\bar{\psi}$ defined as

$$\bar{u} = \frac{\partial \bar{\psi}}{\partial \bar{y}},\ \bar{v} = -\frac{\partial \bar{\psi}}{\partial \bar{x}} \tag{5}$$

Substituting (5) into Eqs. (2) and (3), and eliminating the pressure $\bar{p}$ from the resulting equations, we obtain

$$\frac{\partial \bar{\psi}}{\partial \bar{x}}\frac{\partial}{\partial \bar{y}}\left(\bar{\nabla}^2 \bar{\psi}\right) - \frac{\partial \bar{\psi}}{\partial \bar{y}}\frac{\partial}{\partial \bar{x}}\left(\bar{\nabla}^2 \bar{\psi}\right) + \nu \bar{\nabla}^4 \bar{\psi} - \frac{\sigma {B_0}^2}{\rho}\frac{\partial^2 \bar{\psi}}{\partial \bar{y}^2} = 0 \tag{6}$$

and the boundary conditions (4) become

$$\begin{aligned} &\bar{\psi} = 0,\ \frac{\partial \bar{\psi}}{\partial \bar{y}} = 0 \quad \text{at} \quad \bar{y} = 0 \\ &\bar{\psi} = a\bar{x}\bar{y} + b\bar{y}^2 \quad \text{as} \quad \bar{y} \to \infty \end{aligned} \tag{7}$$

Further we define the following non-dimensional variables

$$x = \bar{x}/l,\quad y = \bar{y}/l,\quad \psi = \bar{\psi}/\left(al^2\right) \tag{8}$$

where $l = \left(\nu / a\right)^{1/2}$ is a characteristic length. Substituting (8) into (6), we obtain the following equations, in non-dimensional form,

$$\frac{\partial \psi}{\partial x}\frac{\partial}{\partial y}\left(\nabla^2 \psi\right) - \frac{\partial \psi}{\partial y}\frac{\partial}{\partial x}\left(\nabla^2 \psi\right) + \nu \nabla^4 \psi - M\frac{\partial^2 \psi}{\partial y^2} = 0 \tag{9}$$

and the boundary conditions (7) become

$$\begin{aligned} &\psi = 0,\ \frac{\partial \psi}{\partial y} = 0 \quad \text{at} \quad y = 0 \\ &\psi = xy + \gamma y^2 \quad \text{as} \quad y \to \infty \end{aligned} \tag{10}$$

Where γ is the shear parameter and M is the magnetic parameter which are defined as

$$\gamma = \frac{b}{a},\quad M = \frac{\sigma {B_0}^2}{\rho a} \tag{11}$$

A physical quantity of interest is the skin friction, or the shear stress $\bar{\tau}_w$ at the wall, which is defined as

$$\bar{\tau}_w = \mu\left(\frac{\partial^2 \bar{\psi}}{\partial \bar{x}^2} + \frac{\partial^2 \bar{\psi}}{\partial \bar{y}^2}\right)_{\bar{y}=0} \tag{12}$$

or in non-dimensional form

$$\tau_w = \mu\left(\frac{\partial^2 \psi}{\partial x^2} + \frac{\partial^2 \psi}{\partial y^2}\right)_{y=0} \tag{13}$$

where $\tau_w = \bar{\tau}_w/(a\mu)$.

3..Solution procedure

The boundary conditions (10) suggest that $\psi(x,y)$ has the form

$$\psi(x,y) = xF(y) + G(y) \tag{14}$$

Substituting (14) into Eq. (9), we obtain the following ordinary differential equations

$$FF''-F'F''+F^{IV} - MF'' = 0 \tag{15}$$

$$FG'''-G'F''+G^{IV} - MG'' = 0 \tag{16}$$

which have to be solved subject to the boundary conditions

$$\begin{aligned} &F(0) = F'(0) = 0, \quad G(0) = G'(0) = 0 \\ &F'(\infty) = 1, \quad G''(\infty) = 2\gamma \end{aligned} \tag{17}$$

where primes denote differentiation with respect to *y*. Integrating Eqs. (15) and (16) once, we obtain

$$F'''+FF''-F'^2-MF' = C_1 \tag{18}$$

$$G'''+FG''-G'F'-MG' = C_2 \tag{19}$$

where C_1 is a constant and $C_2 = C_2(y)$. Using the boundary conditions (17) for $F(y)$, we obtain $C_1 = -(1+M)$ so that Eq. (18) becomes

$$F'''+FF''+1-F'^2-M(1-F') = 0 \tag{20}$$

This equation describes the classical MHD boundary layer flow near a two-dimensional orthogonal stagnation-point, see Ariel [17]. Equation (20) gives

$$F(y) \approx y + A \quad \text{as} \quad y \to \infty \tag{21}$$

where *A* is a constant which depends on *M*. Further, using (21) we obtain from Eq. (19) that $C_2 = 2A\gamma - 2M\gamma y$ and Eq.(19) becomes

$$G'''+FG''-G'F'+M(2\gamma y - G') = 2A\gamma \tag{22}$$

Finally, we have to solve Eqs.(20) and (22) subject to the boundary conditions

$$\begin{aligned} &F(0) = F'(0) = 0, \quad G(0) = G'(0) = 0 \\ &F'(\infty) = 1, \quad G''(\infty) = \gamma \end{aligned} \tag{23}$$

Introducing the new variable

$$G'(y) = 2\gamma H(y) \tag{24}$$

then Eq. (22) becomes

$$H''+FH'-HF'+M(y-H) = A\gamma \tag{25}$$

which has to be solved subject to the boundary conditions

$$H(0) = 0, \quad H(\infty) = 1 \tag{26}$$

Further, from (24) we have

$$G(y) = 2\gamma \int_0^y H(s)ds \tag{27}$$

Integrating numerically Eq. (25) with the boundary conditions (26), we obtain

$$H'(0) = C \tag{28}$$

where *C* is a constant which depends on *M*.

The non-dimensional skin friction (13) can be written as

$$\tau_w = xF''(0) + 2\gamma H'(0) \tag{29}$$

The dimensionless velocity components (u,v) are defined as $u = \bar{u}/(al)$ and $v = \bar{v}/(al)$ which give, from (14)

$$u = xF'(y) + G'(y), \quad v = -F(y) \tag{30}$$

The streamline $\psi = 0$ meets the wall at the point $x = x_0$ where $\tau_w = 0$ (point of zero skin friction), which from (29) is given by

$$x_0 = -\frac{2\gamma H'(0)}{F''(0)} \tag{31}$$

On the other hand, following Labropulu *et al.* [5], we expand $F(y)$ and $G(y)$ in Taylor series about $y \approx 0$ (near the wall) and Eq. (29) gives for $\tau_w = 0$

$$\frac{1}{2}\left[xF''(0) + G''(0)\right]y + \frac{1}{6}\left[xF'''(0) + G'''(0)\right]y^2 + \text{h.o.t} = 0 \tag{32}$$

where $F''(0) = B$, $G''(0) = 2\gamma C$, $F'''(0) = -(1+M)$ and $G'''(0) = 2A\gamma$. Dividing

(31) by $F''(0) \neq 0$ and letting $X = x + 2\gamma C / B$, we obtain

$$\frac{B}{2}\left\{X + \frac{2}{3}\left[\frac{A\gamma}{B} + \frac{\gamma C(1+M)}{B}\right]y + \text{h.o.t}\right\} = 0 \qquad (33)$$

From (33) we can see that the dividing streamline meets the wall $y = 0$ at $X = 0$ or $x = -2\gamma C / B$ and its slope m_0 near the wall is given by

$$m_0 = -\frac{3B^2}{2\gamma\left[AB + C(1+M)\right]} \qquad (34)$$

On the other hand, the dividing streamline which comes into the wall from infinity is defined by $\psi(x, y) = 0$ and its slope at infinity is m_∞ given by

$$m_\infty = -\frac{1}{\gamma} \qquad (35)$$

The ratio $R = m_0 / m_\infty$ is found to be

$$R = \frac{3B^2}{2\left[AB + C(1+M)\right]} \qquad (36)$$

which is independent of the parameter γ.

4 Results and discussion

Equations (20) and (22) subject to the boundary conditions (23) have been solved numerically using the Runge-Kutta method for several values of the parameters γ and *M*. Values of *A*, *B* and *C* are given in Table 1 for $\gamma = 0$ (orthogonal stagnation-point flow) and different values of *M*. The corresponding values reported by Labropulu *et al.* [5] and Ariel [17] have also been included in this table. It is seen that the present results are in very good agreement with those determined by Labropulu *et al.* [5] and Ariel [17]. We are therefore confident that the present results are accurate. It is seen, as expected, that $F''(0)$ increases steadily as *M* increased from zero and this appears to be more plausible physically. Also some values of *R* given by (36) for several values of *M* are given in Table 1. The value of *R* = 3.748513 for *M* = 0 reported by Dorrepaal [3] and Labropulu *et al.* [5] has been also included in this table.

Figure 2 shows the variation of the velocity profiles $u(x, y)$ with y at a fixed value of x = 1.0 for several values of *M* and γ. It is seen that at a given location (x = 1.0) the velocity (which is simply taken to represent a typical result) increases with increasing *M*.

Figures 3 to 7 show the streamline pattern for orthogonal ($\gamma = 0$) and oblique ($\gamma \neq 0$) flows for several values of *M*. The location of the point of zero skin friction on the axis, x_0, is also shown in these figures. It can be seen that for a fixed value of γ that these locations are at a larger distance from the stagnation point as the value of *M* increases. Further, it is clear from these figures that for a fixed value of γ that the streamlines become more and more closer to the wall with increasing *M*.

Further, for a given value of *M* the streamlines are more and more oblique towards the left of the stagnation-point with increasing γ. On the other hand, for a fixed value of *M* the streamlines are more and more oblique towards the right of the stagnation-point with increasing γ when $\gamma < 0$. This is consistent with the fact that increasing the shear in the γ results in an increase in the shearing motion which in turn leads to increased obliquity of the flow towards the surface. However, it should be noticed that the streamlines for negative values of γ are not shown in Figs. 5 to 7 because they are almost mirror images in the plane y = 0 to the streamlines for positive values of γ.

5 Conclusions

A numerical solution of the steady oblique flow of a viscous and electrically conducting fluid impinging on a flat plate has been investigated. The governing partial differential equations are reduced to a set of two ordinary differentials equation which are solved numerically for different values of the governing parameters *M* and γ. This solution provides useful information about the MHD stagnation-point flow and, in limited cases that have already been investigated when the magnetic field is absent, there is quantitatively good agreement.

Acknowledgements

The authors I. Pop and D.B. Ingham wish to express their thanks to the Royal Society for partial financial support. The work of the authors T. Grosan and C. Revnic was supported form the grant CEEX-ET90/2006-2008.

M	$F''(0)$		$H'(0)$		A		R	
	present	Ariel [17]	present	Labropulu *et al.* [5]	present	Labropulu *et al.* [5]	Present	Labropulu *et al.* [5]
0.00	1.232588	1.232588	1.406616	1.406544	-0.647900	-0.647900	3.748069	3.748513
0.16	1.295368	1.295368	1.373280		-0.626277		3.219676	
0.64	1.467976	1.467976	1.300013		-0.572893		2.503764	
1.00	1.585331	1.585331	1.261685		-0.541007		2.263267	
4.00	2.346663	2.346663	1.127294		-0.393590		1.752707	
25.00	5.147965	5.147965	1.027863		-0.190725		1.544224	
100.00	10.074741	10.074741	1.007358		-0.098774		1.481927	

Table 1. Values of $F''(0)$, $H'(0)$, A and R for several values of M.

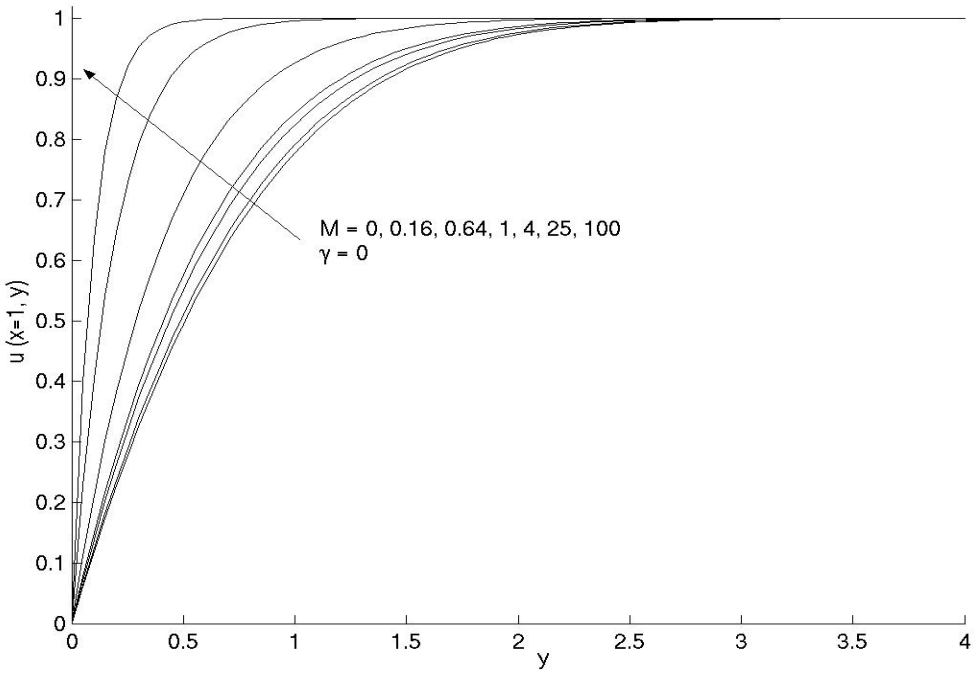

(a)

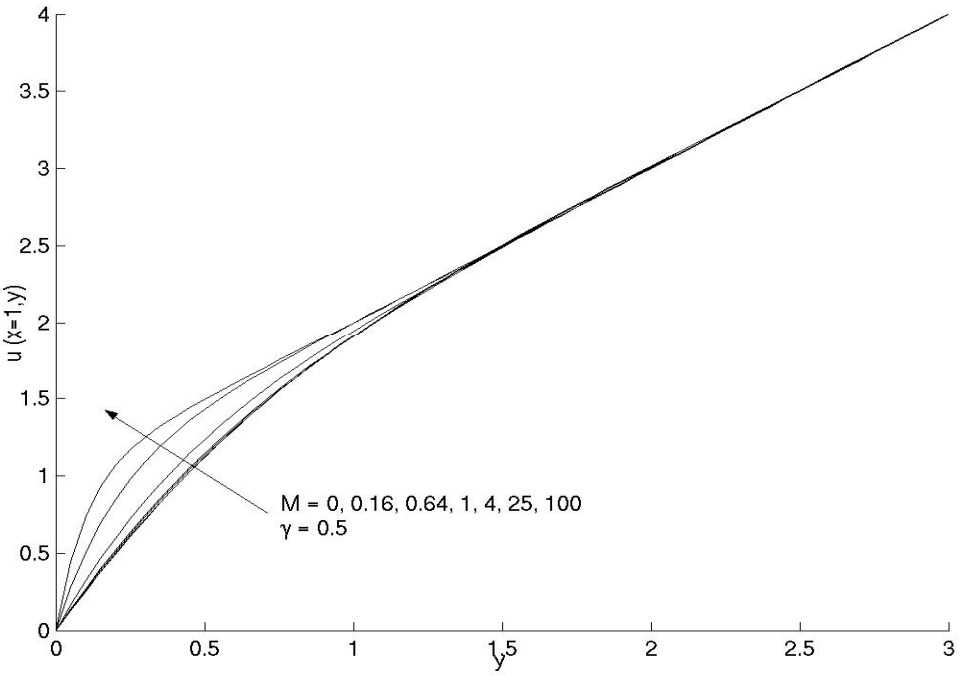

(b)

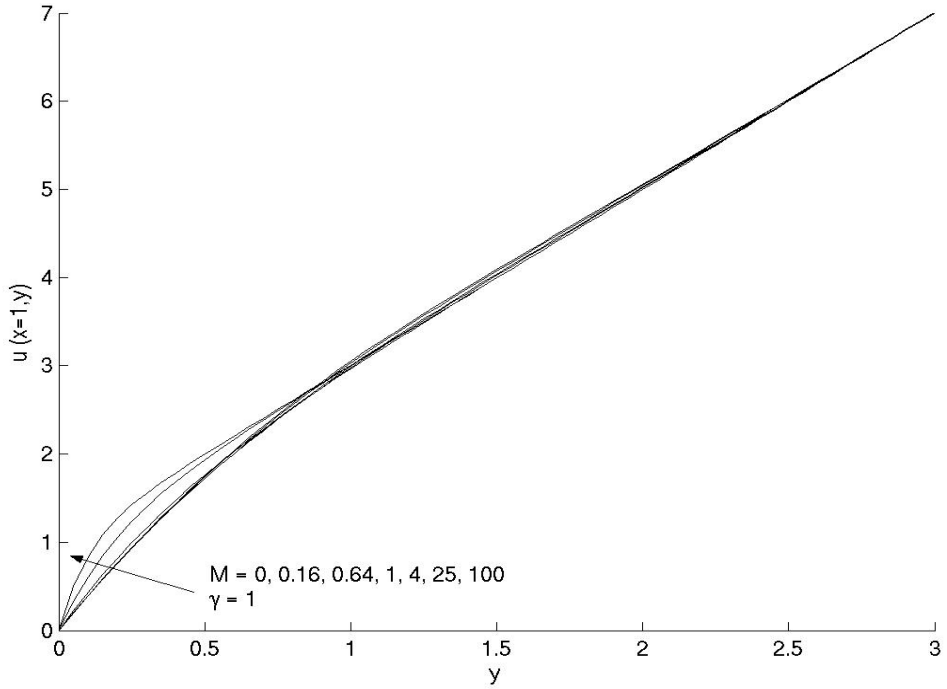

(c)

Fig. 2. Velocity profile for $x = 1$ and several values of M :
(a) $\gamma = 0$ (orthogonal stagnation-point flow); (b) $\gamma = 0.5$ (c) $\gamma = 1$.

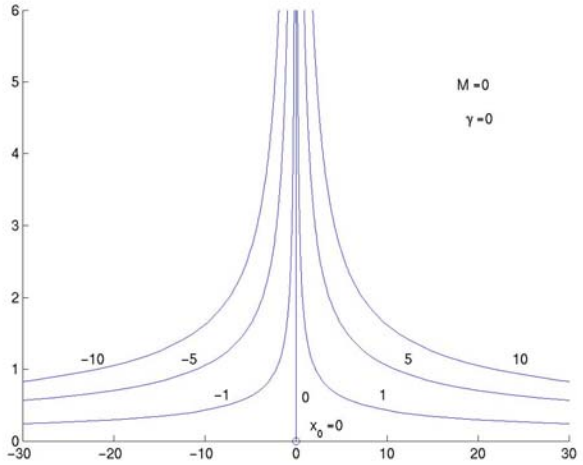

Fig.3. Streamline pattern for $M = 0$, $\gamma = 0$ (orthogonal stagnation point).

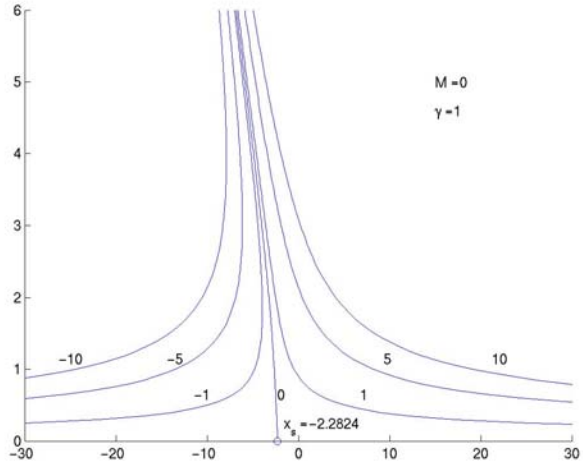

Fig. 5. Streamlines for $M = 0$ and $\gamma = 1$.

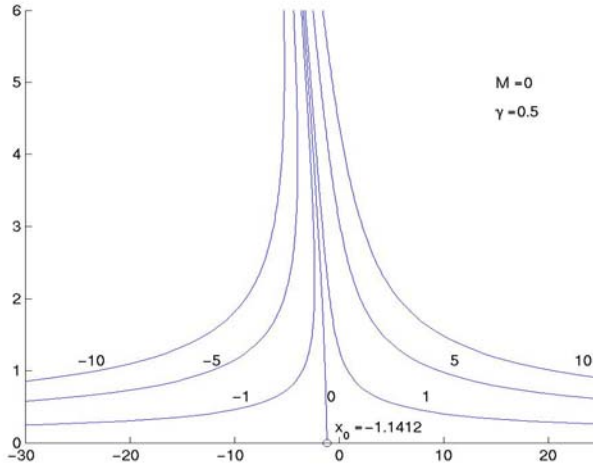

(a)

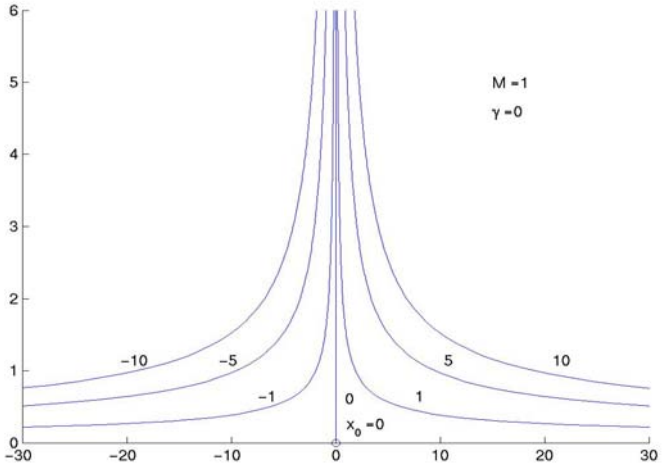

(a)

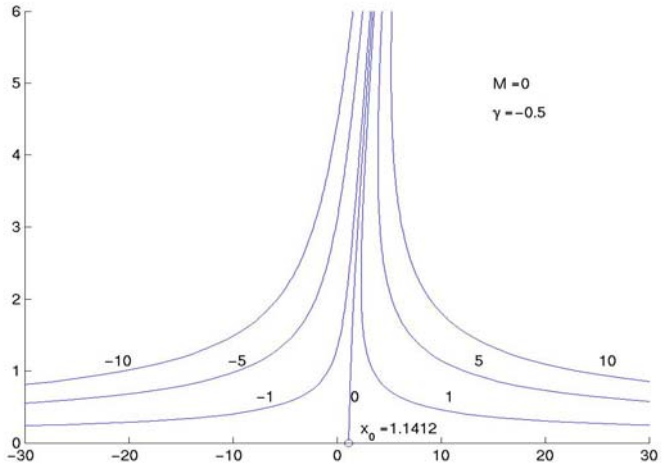

(b)

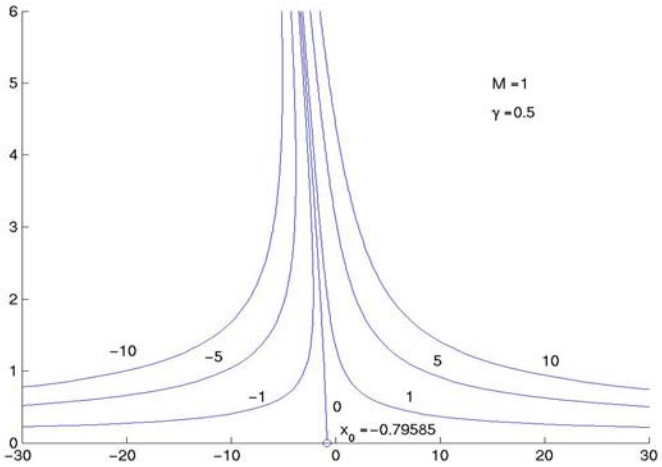

(b)

Fig. 4.Streamlines for $M = 0$; (a) $\gamma = 0.5$ (b) $\gamma = -0.5$

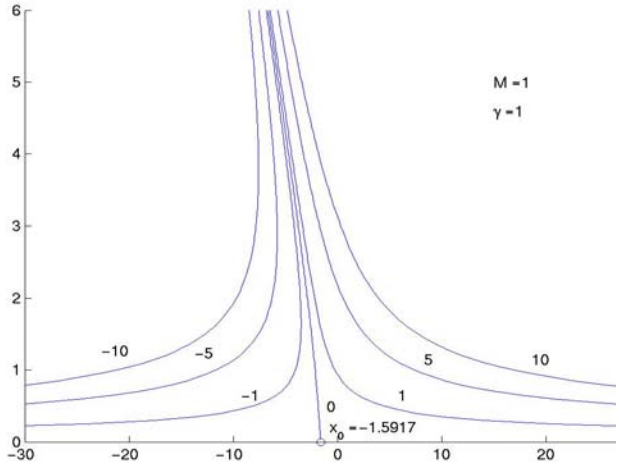

(c)

Fig. 6. Streamline pattern for $M = 1$; (a) $\gamma = 0$ (b) $\gamma = 0.5$ (c) $\gamma = 1$.

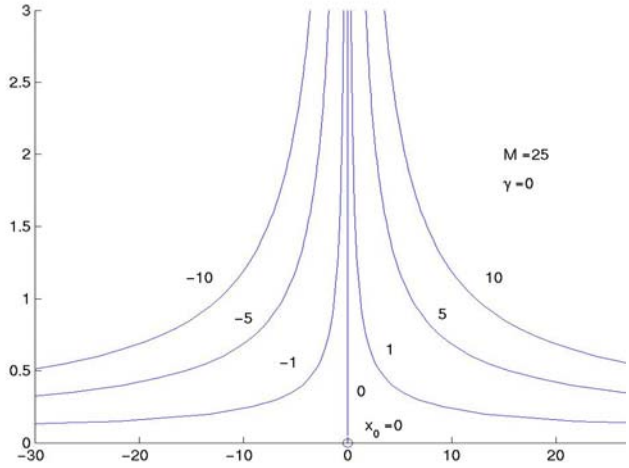

(a)

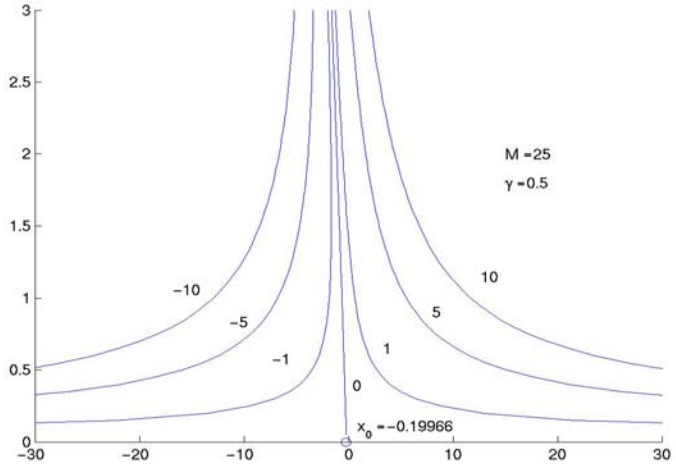

(b)

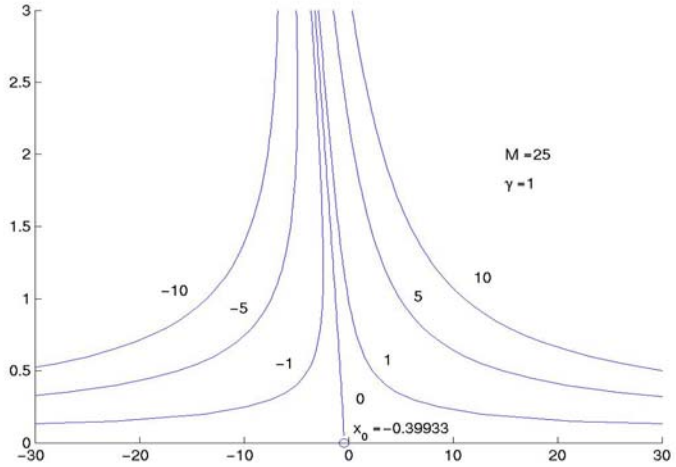

(c)

Fig. 7. Streamline pattern for $M = 25$; (a) $\gamma = 0$ (b) $\gamma = 0.5$ (c) $\gamma = 1$.

References

1. J.T. Stuart (1959) The viscous flow near a stagnation point when the external flow has uniform vorticity. J. Aerospace Sci. 26:124-125
2. K.J. Tamada (1979) Two-dimensional stagnation point flow impinging obliquely on a plane wall. J. Phys. Soc. Jpn. 46: 310-311
3. J.M. Dorrepaal (1986) An exact solution of the Navier-Stokes equation which describes non-orthogonal stagnation-point flow in two dimensions. J. Fluid Mech. 163:141-147
4. J.M. Dorrepaal (2000) Is two-dimensional oblique stagnation point flow unique?. Canadian Appl. Math. Quart. 8:61-66
5. F. Labropulu, J.M. Dorrepaal, O.P. Chandna (1996) Oblique flow impinging on a wall with suction or blowing. Acta Mech. 115:15-25
6. T. Liu (1992) Nonorthogonal stagnation flow on the surface of a quiescent fluid - an exact solution of the Navier-Stokes equation. Quart. Appl. Math. 50:39-47
7. B.S. Tittley, P.D. Weidman (1998) Oblique two-fluid stagnation-point flow. Eur. J. Mech. B/Fluids 17:205-217
8. M. Reza, A.S. Gupta (2005) Steady two-dimensional oblique stagnation-point flow towards a stretching surface. Fluid Dyn. Res. 27:334-340
9. Y.Y. Lok, N. Amin, I. Pop (2007) Comments on: “Steady two-dimensional oblique

stagnation-point flow towards a stretching surface": M. Reza and A.S. Gupta. Fluid Dynamics Research 37 (2005) 334–340, Fluid Dyn. Res. 39:505-510
10. P.D. Weidman, V. Putkaradze (2003) Axisymmetric stagnation flow obliquely impinging on a circular cylinder. Eur. J. Mech. B/Fluids 22:123-131
11. K.B. Pavlov (1974) Magnetohydrodynamic flow of an incompressible viscous fluid caused by deformation of a plane surface. Magnitnaya Gidrodinamika 4:146-147
12. Chakrabarti, A.S. Gupta (1979) Hydromagnetic flow and heat transfer over a stretching sheet. Quart. Appl. Math. 37:73-78
13. H.I. Andersson (1992) MHD flow of a viscoelastic fluid past a stretching surface. Acta Mech. 95:227-230
14. T.C. Chiam (1994) Stagnation-point flow towards a stretching plate. J. Phys. Soc. Japan 63: 2443-2444
15. T.R. Mahapatra, A.S. Gupta (2001) Magnetohydrodynamic stagnation-point flow towards a stretching sheet. Acta Mech. 152:191-196
16. T. Ray Mahatra, S. Dholey, A.S. Gupta (2007) Heat transfer in oblique stagnation point flow of an incompressible viscous fluid towards a stretching surface. Heat Mass Transfer 43:767-773
17. P.D. Ariel (1994) Hiemenz flow in hydromagnetics. Acta Mechanica 103:31-43
18. H. Xu, S.-J. Liao, I. Pop (2007) Series solutions of unsteady three dimensional MHD flow and heat transfer in a boundary layer over an impulsively streatching plate. Eur. J. Mech. B/Fluids 26:15-27

Unsteady Boundary Layer Flow and Heat Transfer Over a Stretching Sheet

Cornelia Revnic*, Teodor Grosan† and Ioan Pop[1†]

* *"Tiberiu Popoviciu" Institute of Numerical Analysis, P.O.Box. 68-1, 400110, Cluj-Napoca, Romania*
† *Babes-Bolyai University, Applied Mathematics, R-3400 Cluj, CP 253, Romania*

Abstract. Unsteady two-dimensional boundary layer flow and heat transfer over a stretching flat plate in a viscous and incompressible fluid of uniform ambient temperature is investigated in this paper. It is assumed that the plate is isothermal and is stretched in its own plane. Using appropriate similarity variables, the basic partial differential equations are transformed into a set of two ordinary differential equations. These equations are solved numerically for some values of the governing parameters, using Rungge-Kutta method of fourth order. Flow and heat transfer characteristics are determined and represented in some tables and figures. It is found that the structure of the boundary layer depends on the ratio of the velocity of the potential flow near the stagnation point to that of the velocity of the stretching surface. In addition, it is shown that the heat transfer from the plate increases when the Prandtl number increases. Our results are shown to include the steady situation as a special case considered by other authors. Comparison with known results is very good.

Keywords: heat transfer, stretching surface, the external inviscid flow, stagnation-point flow, boundary layer.
PACS: 02.60Lj, 44.20+b, 44.27+g, 47,10Ad, 47.85-g

INTRODUCTION

The unsteady boundary layers are important in several physical problems in aero - nautics, missile dynamics, acoustics etc. The work in this area was initiated by Moore [1], Lighthill [2] and Lin [3]. Critical reviews of unsteady boundary layers were presented by Stuart [4], Riley [5], Telionis [6], [7] and Pop [8]. In recent years certain aspects of the unsteady flows were investigated by Ma and Hui [9] and Ludlow et al. [10] using the classical method of Lie-group. The essence of the Lie-group method is that each of the variables in the initial equation is subjected to an infinitesimal transformation and the demand that the equation is invariant under these transformations leads to the determination of the possible symmetries (see Ludlow et al. [10]). The fundamental governing equations for fluid mechanics are the Navier-Stokes equations. This nonlinear set of partial differential equations have no general solutions, and only a small number of exact solutions have been found (see Wang [11]). Exact solutions are important for the following reasons: (i) the solutions represent fundamental fluid-dynamic flows. Also, owing to the uniform validity of exact solutions, the basic phenomena described by the Navier-Stokes equations can be more closely studied. (ii) the exact solutions serve as standards for checking the accuracies of the many approximate methods, whether they are numerical, asymptotic, or empirical.

Flow of a viscous fluid over a stretching sheet has an important bearing on several technological processes. In particular in the extrusion of a polymer in a melt-spinning process, the extruded from the die is generally drawn and simultaneously stretched into a sheet which is then solidified through quenching or gradual cooling by direct contact with water. Further, glass blowing, continuous casting of metals and spinning of fibres involve the flow due to a stretching surface, see Lakshmisha et al. [12]. In all these cases, a study of the flow field and heat transfer can be of significant importance since the quality of the final product depends to a large extent on the skin friction coefficient and the surface heat transfer rate. Crane [13] presented a simple closed form exponential solution of the steady two-dimensional flow caused solely by a linearly stretching sheet in an otherwise quiescent incompressible fluid. The simplicity of the geometry and the possibility of obtaining further exact solutions through simple generalizations have generated a lot of interest in extending it to more general situations. Such extensions include consideration of more general stretching velocity, application to non-Newtonian fluids, and inclusion of other physical effects such as suction or blowing, magnetic fields, etc. Unsteady two-dimensional boundary layer flow over a stretching surface

[1] Corresponding author: Tel.:-40-264594315; fax:+40-264591906; E-mail adress: pop.ioan@yahoo.co.uk (Pop Ioan)

has been studied by Na and Pop [14], Wang et al. [15], Elbashbeshy and Badiz [16], Sharidan et al. [17] and Ali and Magyari [18], while Lakshmisha et al. [12], Devi et al. [19] and Takhar et al. [20] have considered the unsteady three-dimensional-flow due to the impulsive motion of a stretching surface. The aim of the present analysis is to study the unsteady flow and heat transfer in the stagnation-point flow on a heated stretched surface in a viscous and incompressible fluid when both velocities of the stretching sheet and of the external flow (inviscid flow) are proportional to the distance from the stagnation-point and inversely to time. The geometry is similar to that proposed by Mahapatra and Gupta [21] for the steady two-dimensional stagnation-point flow towards a stretching sheet. The parabolic partial differential equations governing the flow and heat transfer have been reduced to a system of two ordinary differential equations which are solved using an implicit finite-difference scheme in combination with the shooting method.

PROBLEM FORMULATION

We consider the unsteady two-dimensional forced convection flow and heat transfer of a viscous and incompressible fluid near a stagnation point on a surface coinciding with the plain $y = 0$, the flow being confined to $y > 0$. Two equal and opposite forces are applied along the x - axis at the initial time $t = 0$, so that the surface is stretched keeping the origin fixed as shown in Fig.1. It is assumed that the uniform temperature of the plane is T_w , while the temperature of the ambient fluid is T_∞, where $T_w > T_\infty$ (heated plate). It is also assumed that the viscous dissipation effects are neglected. Under these assumptions, the system of boundary layer equations are given by

$$\frac{\partial u}{\partial x}+\frac{\partial v}{\partial y} = 0 \tag{1}$$

$$\frac{\partial u}{\partial t}+u\frac{\partial u}{\partial x}+v\frac{\partial u}{\partial y} = \frac{\partial u_e}{\partial t}+u_e\frac{\partial u_e}{\partial x}+\nu\frac{\partial^2 u}{\partial y^2} \tag{2}$$

$$\frac{\partial T}{\partial t}+u\frac{\partial T}{\partial x}+v\frac{\partial T}{\partial y} = \alpha\frac{\partial^2 T}{\partial y^2} \tag{3}$$

subject to the initial and boundary conditions are of the form:

$$\begin{aligned} t &< 0: \ u = 0,\ v = 0,\ T = T_\infty \ \ for\ \ any \ \ y > 0 \\ t &> 0: \ u = u_w(t,x),\ v = 0,\ T = T_w \ \ for \ \ y = 0 \\ t &= 0: \ u = u_{ws}(x),\ v = 0,\ T = T_w \\ & \quad u \to u_e(t,x),\ T \to T_\infty \ \ as \ \ y \to \infty \end{aligned} \tag{4}$$

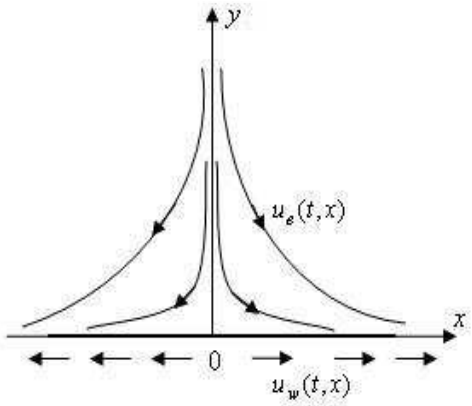

FIGURE 1. Physical model and coordinate system.

where u and v are the velocity components along the $x-$ and $y-$ axis, T is the fluid temperature, ν is the kinematic viscosity, $u_{ws} = cx$ (c is a positive constant) and α is the thermal diffusivity. Following Surma Devi [19] et al., we assumed that $u_w(t,x)$ and $u_e(t,x)$ are given by

$$u_w(t,x) = \frac{cx}{(1-\gamma t)}, \;\; u_e(t,x) = \frac{ax}{(1-\gamma t)} \tag{5}$$

where a is a positive constant. The momentum and energy equations can be transformed to the corresponding ordinary differential equations by the following substitutions:

$$\begin{aligned} \psi &= (c\nu/(1-\gamma t))^{1/2} x f(\eta), \\ \theta(\eta) &= (T-T_\infty)/(T_w - T_\infty), \\ \eta &= (c/\nu(1-\gamma t))^{1/2} y \end{aligned} \tag{6}$$

where ψ is the stream function which is defined in the usual way as $u = \partial\psi/\partial y$ and $v = -\partial\psi/\partial x$.
Substituting (6) into Eqs. (2) and (3), we obtain the following two ordinary differential equations:

$$f''' + f\, f'' + \frac{a^2}{c^2} - f'^2 + \frac{\gamma}{c}\left(\frac{a}{c} - \frac{\eta}{2} f'' - f'\right) = 0 \tag{7}$$

$$\frac{1}{Pr}\theta'' + f\, \theta' - \frac{\gamma}{2c}\eta\theta' = 0 \tag{8}$$

subject to the boundary conditions (4) which become

$$f(0) = 0, f'(0) = 1, \theta(0) = 1 \tag{9}$$

$$f'(\infty) = \frac{a}{c}, \theta(\infty) = 0 \tag{10}$$

where Pr is the Prandtl number and primes denote differentiation with respect to η.
The physical quantities of interest are the skin friction coefficient C_f and the local Nusselt number Nu_x, which are defined as

$$C_f = \frac{\tau_w}{\rho u_{ws}^2}, \; Nu_x = \frac{x q_w}{k(T_w - T_\infty)}, \tag{11}$$

where τ_w is the skin friction and q_w is the heat transfer from the plate which are given by

$$\tau_w = \mu \left(\frac{\partial u}{\partial y}\right)_{y=0}, \; q_w = -k\left(\frac{\partial T}{\partial y}\right)_{y=0} \tag{12}$$

with μ and k being the dynamic viscosity and thermal conductivity, respectively. Using (6), we get

$$\begin{aligned} (1-\gamma t)^{3/2} Re_x^{1/2} C_f &= f''(0), \\ (1-\gamma t)^{1/2} Re_x^{-1/2} Nu_x &= -\theta'(0) \end{aligned} \tag{13}$$

Where $Re = (cx)x/\nu$ is the low Reynolds number. It is important to notice that for the steady-state case,Eqs. (7) and (8) reduced to

$$f''' + f\, f'' - f'^2 + \frac{a^2}{c^2} = 0 \tag{14}$$

$$\frac{1}{Pr}\theta'' + f\, \theta' = 0 \tag{15}$$

with the boundary conditions (9)-(10). Equations (14) and (15) with the boundary conditions (9)-(10) where established by Mahapatra and Gupta [21].

TABLE 1. Values of $f''(0)$ for some values of a/c when the flow is steady. ( ) values reported by Mahapatra and Gupta [21].

a/c	**0.10**	**0.20**	**0.50**	**2.00**
$f''(0)$	-0.9696	-0.9182	-0.6673	2.0175
	(-0.9694)	(-0.9181)	(-0.6673)	(2.0175)

TABLE 2. Values of $\theta'(0)$ for some values of a/c and Pr when the flow is steady. ( ) values reported by Mahapatra and Gupta [21].

a/c / Pr	**0.05**	**0.5**	**1**	**1.5**
0.1	-0.081	-0.381	-0.603	-0.777
	(-0.081)	(-0.383)	(-0.603)	(-0.777)
0.5	-0.137	-0.472	-0.691	-0.863
	(-0.136)	(-0.473)	(-0.692)	(-0.863)
2	-0.248	-0.711	-0.978	-1.171
	(-0.241)	(-0.709)	(-0.974)	(-1.171)

SOLUTION

The systems of ordinary differential equations (7)-(8) and (14)-(15) subject to the boundary condition (9)-(10) have been solved numerically for some values of the parameters a/c, t and Pr using Rungge-Kutta method of fourth order combined with the shooting technique. For the physical considearation we take $\gamma = -1$. Some values of $f''(0)$ and $\theta'(0)$ are given in Tables 1 and 2 for the case of the steady flow.

We can see from these tables that there is a very good agreement between our results and those obtained by Mahapatra and Gupta [21]. Therefor, we are confident that the results obtained using the present method are accurate.

Figures 2 - 5 show the velocities profiles f and f' along with the corresponding streamlines patterns for the case of unsteady flow, Eqs. (7) and (8). The values of the parameters are $a = 0.1$, $c = 1$ and $t = 0, 1, 2, 3$. It is interesting to notice that the solution of Eq. (7) is not unique. Thus, there are two solutions, one Fig. 2 representing an attached flow and the other one Fig. 4 the reversed flow. These is in agreement with the results obtained by Ma and Hui [9] for the unsteady two-dimensional boundary layer flow near a stagnation point of a fixed plat plate.

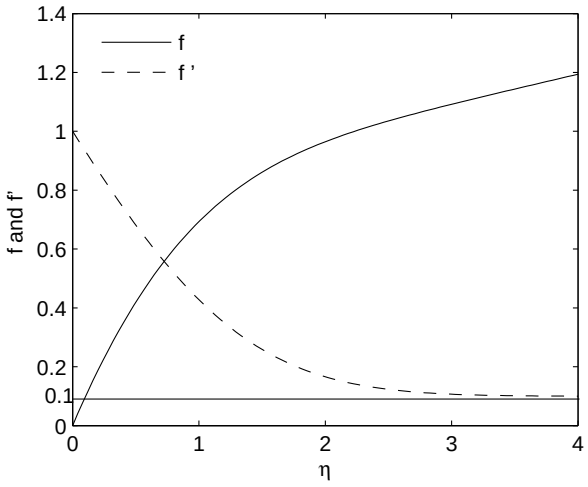

FIGURE 2. The first solution of $f(\eta)$ and $f'(\eta)$ for $a/c = 0.1$.

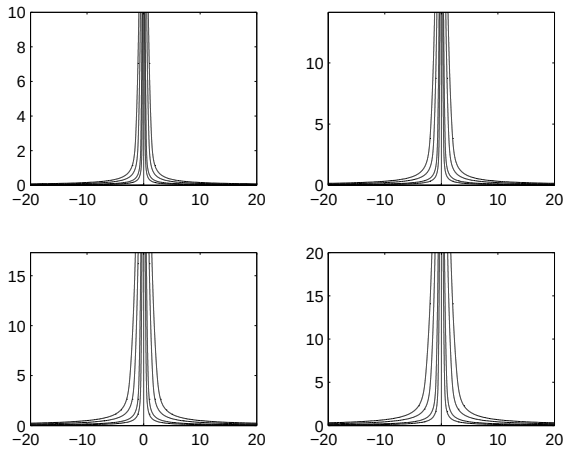

FIGURE 3. The streamlines function for: $t = 0, 1, 2$ and 3 corresponding to the first solution for $a/c = 0.1$.

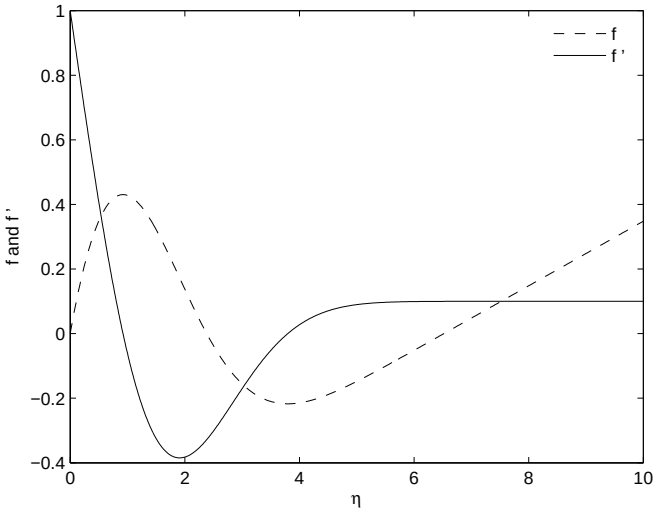

FIGURE 4. The second solution of $f(\eta)$ and $f'(\eta)$ for $a/c = 0.1$.

Fig. 6 illustrates the dimensionless temperature profiles $\theta(\eta)$ for some values of Pr when $a/c = 2$. We notice that temperature profile increase when Pr decreases. Further, Fig. 7 shows the variation of the heat transfer from the wall $-\theta'(0)$ with a/c and different values of Pr. It is evident from Fig. 7 that an increase in Pr result in a decrease in the thermal boundary layer thickness and as a consequence the heat transfer from the wall increases with Pr.

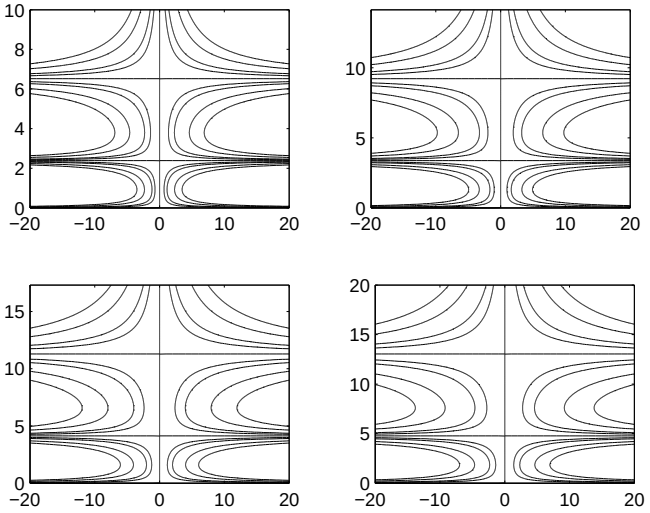

FIGURE 5. The streamlines function for: $t = 0, 1, 2$ and 3 corresponding to the second solution for $a/c = 0.1$.

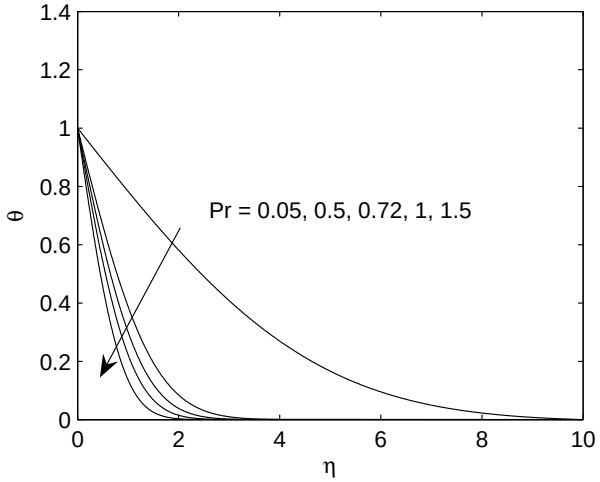

FIGURE 6. Temperature profiles of $\theta(\eta)$ for several values of Pr and $a/c = 2$ in respect with η.

CONCLUSION

The unsteady two-dimensional stagnation-point flow and heat transfer of a viscous and incompressible fluid over an isothermal stretching flat plate in its own plane has been numerically analyzed in detailed. Following Surma Devi et al. [19] similarity variables where used to reduced the governing partial differential equations to ordinary differential equations. Solving numerically these equations, we have been able to determine the velocity and temperature profiles, skin friction and heat transfer from the plate. For the case of steady-state flow, we have compared our present results with those of Mahapatra and Gupta [21]. The agreement between the results is excelent. Effects of a/c and Pr on the flow and heat transfer characteristic have been examened and discussed in detail. It is shown that for small values of a/c the solution of the ordinary differential equation is not unique. One solution represents an attached flow and the other one a reversed flow. It shoud be noticed that we have determined solutions of the problem for more values of the governing parameters but in order to save space, the reported results are limited only to some values of these parameters.

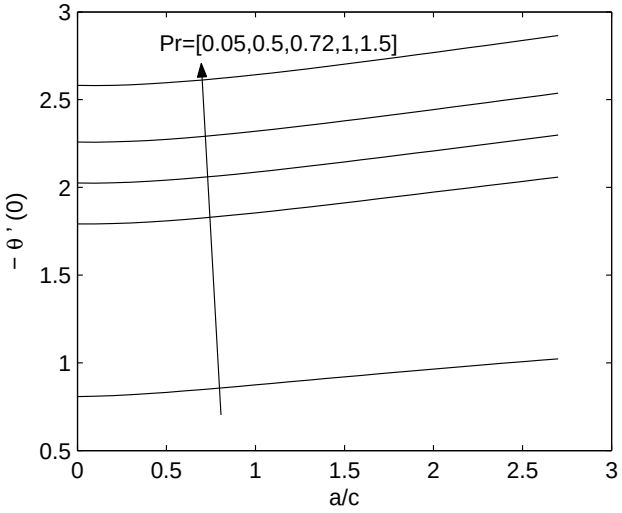

FIGURE 7. Variation of the heat transfer with a/c for several values of Pr.

REFERENCES

1. F. K. Moore, *Unsteady laminar boundary layer flow*, NACA TN, 1951, 3471.
2. M. J. Lightill, Proc. Roy. Soc. **224A**, 1–23 (1954).
3. C. C. Lin, Proc. 9th Int. Cong. Appl. Mech **4**, 155–168 (1956).
4. J. T. Stuart **1**, 1–40 (1971).
5. N. Riley, SIAM Review **17**, 274–297 (1975).
6. D. P. Telionis, J. Fluids Engng. **101**, 29–43 (1979).
7. D.P. Telionis, *Unsteady Viscous Flows*, Springer, Berlin, 1981.
8. I. Pop, *Theory of Unsteady Boundary Layers* (in Romanian), Ed. Stiintifica si Enciclopedica, Bucuresti–Romania, 1983.
9. P.K.H. Ma, and W.H. Hui, J. Fluid Mech **216**, 537–559 (1990).
10. D. K. Ludlow, P. A. Clarkson, and A.–P. Bassom, Q. Jl. Mech. Appl. Math. **53**, 175–206 (2000).
11. C. Y. Wang, Annu. Rev. Fluid Mech **23**, 159–177 (1991).
12. K. N. Lakshmisha, S. Venkateswaran, and G. Nath, ASME J. Heat Transfer **110**, 590–595 (1988).
13. L.J. Crane, J. Appl. Math. Phys, (ZAMP) **21**, 645–647 (1970).
14. I. Pop, and T.Y. Na, **23**, 413–422 (1996).
15. C. Y. Wang, Q. Du, M. Miklavčič, and C.–C. Chang, SIAM J. Appl. Math. **57**, 1–14 (1997).
16. E. M. A. Elbashbeshy, and M.A.A. Bazid, Heat Mass Transfer **41**, 1–4 (2004).
17. S. Sharidan, T. Mahmood, and I. Pop, Int. J. Appl. Mech. Engng., **11**, 647–654 (2006).
18. M. E. Ali, and E. Magyari, Int. J. Heat Mass Transfer **50**, 188–195 (2007).
19. C. D. Surma Devi, H.S. Takhar, and G. Nath, Int. J. Heat Mass Transfer **29**, 1996– 1999 (1986).
20. H. S. Takhar, A.J. Chamkha, and G. Nath, Acta Mechanica **146**, 59–71 (2001).
21. T. Ray Mahapatra, and A. S. Gupta, Heat Mass Transfer **38**, 517–521 (2002).

Magnetic field and internal heat generation effects on the free convection in a rectangular cavity filled with a porous medium

T. Grosan, [a] C. Revnic, [b] I. Pop [a,*] and D.B. Ingham [c]

[a] *Babes-Bolyai University, Applied Mathematics, R-3400 Cluj, CP 253, Romania*

[b] *"Tiberiu Popoviciu" Institute of Numerical Analysis, P.O.Box 68-1, 400110, Cluj, Romania*

[c] *Centre for Computational Fluid Dynamics, University of Leeds, Leeds LS2 9JT, UK*

Abstract

A numerical investigation of the steady magnetohydrodynamics free convection in a rectangular cavity filled with a fluid-saturated porous medium and with internal heat generation has been performed. A uniform magnetic field, inclined at an angle γ with respect to the horizontal plane, is externally imposed. The values of the governing parameters are the inclined angle $\gamma = 0, \pi/6, \pi/4$ and $\pi/2$, Hartmann number $Ha = 0, 1, 5, 10$ and 50, Rayleigh number $Ra = 10, 10^3$ and 10^5, and the aspect ratio $a = 0.01, 0.2, 0.5$ and 1(square cavity). It is shown that the intensity of the core convection is considerably affected by the considered parameters. It is also found that the local Nusselt number Nu_Y decreases on the bottom wall as γ increases (magnetic field changes its direction from the horizontal to the vertical direction) and vice-versa for the top wall of the cavity. The reported results are in good agreement with all the available published work in the literature.

Key words: Porous media, Natural convection, Heat generation, MHD

* Corresponding author. Tel:+40 264 594 315; fax: +40 264 591 906. *Email address:* pop.ioan@yahoo.co.uk (I.Pop).

Nomenclature

a	aspect ratio
$\mathbf{B}$	applied magnetic field, $Wb \cdot m^{-2}$
c_p	specific heat at constant pressure, $KJ \cdot kg^{-1} \cdot K^{-1}$
$\mathbf{g}$	gravitational acceleration vector, $m \cdot s^{-2}$
Ha	Hartmann number
h	height of the cavity, m
k	thermal conductivity, $W \cdot m^{-1} \cdot K^{-1}$
K	permeability of the porous medium, m^2
l	width of the cavity, m
Nu	mean Nusselt number
Nu_y	local Nusselt number
q_0'''	heat generation, $W \cdot m^{-3}$
Ra	Rayleigh number
u, v	velocity components along the x and y directions, respectively $m \cdot s$
$\mathbf{V}$	velocity vector, $m \cdot s^{-1}$
T_0	temperature of the vertical wall, K
x	dimensional Cartesian coordinate along the bottom wall, m
y	dimensional Cartesian coordinate along the left vertical wall, m
X, Y	dimensionless Cartesian coordinates

Greek symbols

α_m	effective thermal diffusivity, $m^2 \cdot s^{-1}$
β	coefficient of thermal expansion, K^{-1}
γ	angle of inclination to the horizontal of applied magnetic field, radians
μ	dynamic viscosity, $kg \cdot m^{-1} \cdot s^{-1}$
θ	dimensionless temperature
ρ	fluid density, $kg \cdot m^{-3}$
ρ_0	reference density, $kg \cdot m^{-3}$
σ	electrical conductivity, $\Omega^{-1} \cdot m^{-1}$

1 Introduction

Natural convective heat transfer in viscous fluids and fluid-saturated porous media has occupied the central stage in many fundamental heat transfer analyses and has received considerable attention over the last few decades. This interest is due to its wide range of applications in, for example, packed sphere beds, high performance insulation for buildings, chemical catalytic reactors, grain storage and such geophysical problems as frost heave. Porous media are also of interest in relation to the underground spread of pollutants, solar power collectors, and to geothermal energy systems. The literature concerning convective flow in porous media is abundant and representative studies in this may be found in the recent books by Nield and Bejan [1], Ingham and Pop [2], Vafai [3], Bejan *et al.* [4], Pop and Ingham [5], de Lemos [6] and Vadasz [7]. Further, a valuable reference on convective fluids in cavities filled with viscous fluids can be found in the recent book by Martynenko and Khramtsov [8]. Natural convection in enclosures in which internal heat generation is present

is of prime importance in certain technological applications. Examples are post-accident heat removal in nuclear reactors and geophysical problems associated with the underground storage of nuclear waste, among others (Acharya and Goldstein [9], Ozoe and Maruo [10], Lee and Goldstein [11], Fusegi *et al.* [12], Venkatachalappa and Subbaraya, [13], Shim and Hyun, [14] , Hossain and Wilson [15]).

The present paper investigates the effect of a magnetic field on the steady free convection in a rectangular cavity filled with a porous medium saturated with an electrically conducting fluid. This type of problem arises in geophysics when a fluid saturates the earth's mantle in the presence of a geomagnetic field. Natural convection flow in the presence of a magnetic field in an enclosure filled with a viscous and incompressible fluid has been studied by Garandet *et al.* [16], Alchaar *et al.* [17], Kanafer and Chamka [18], Chamkha and Al-Naser [19], Mahmud *et al.* [20], Hossain and Ress [21], Hossain *et al.* [22], and Ece and Büyük [23]. However, there are very few studies on the natural convection of a conducting fluid saturating a porous medium in the presence of a magnetic field in an enclosure. To the best of our knowledge, the first investigation of this problem is due to Alchar *et al.* [17] who considered the stability of a conducting fluid saturating a porous medium in the presence of a uniform magnetic field using the Brinkman model. However, some comments on the MHD convection in a porous medium have been done very recently by Nield [24]. Also a very recent paper by Barletta *et al.* [25] has studied the mixed convection with heated effect in a vertical porous annulus with the radially varying magnetic field.

2 Mathematical model

In this paper we consider the steady natural convection flow in a rectangular cavity filled with an electrically conducting fluid-saturated porous medium with internal heat generation. We assume that the enclosure is permeated by a uniform inclined magnetic field. The geometry and the Cartesian coordinate system are schematically shown in Fig. 1, where the dimensional coordinates x and y are measured along the horizontal bottom wall and normal to it along the left vertical wall, respectively. The height of the cavity is denoted by h and the width by l. Further, the angle of inclination of the magnetic field $\mathbf{B}$ from the horizontal plane, and measured positively in the counterclockwise direction is denoted by γ. It is assumed that the vertical walls are maintained at a constant temperature T_0 , while the horizontal walls are adiabatic. A uniform source of heat generation in the flow region with a constant volumetric rate of $q_0'''[W \cdot m^{-3}]$ is also considered. Further, it is assumed that the effect of buoyancy is included through the well-known Boussinesq approximation. The

viscous, radiation and Joule heating effects are neglected. The resulting convective flow is governed by the combined mechanism of the driven buoyancy force, internal heat generation and the retarding effect of the magnetic field. The magnetic Reynolds number is assumed to be small so that the induced magnetic field can be neglected compared to the applied magnetic field.

Under the above assumptions, the conservation equations for mass, momentum under the Darcy approximation, energy and electric transfer are give by

$$\nabla.\mathbf{V} = 0 \tag{1}$$

$$\mathbf{V} = \frac{K}{\mu}\left(-\nabla p + \rho\mathbf{g} + \mathbf{I}\times\mathbf{B}\right) \tag{2}$$

$$\left(\mathbf{V}.\nabla\right)T = \alpha_m\nabla^2 T + \frac{q_0'''}{\rho_0 c_p} \tag{3}$$

$$\nabla.\mathbf{I} = 0 \tag{4}$$

$$\mathbf{I} = \sigma\left(-\nabla\phi + \mathbf{V}\times\mathbf{B}\right) \tag{5}$$

$$\rho = \rho_0[1-\beta(T-T_0)] \tag{6}$$

where $\mathbf{V}$ is the fluid velocity vector, T is the fluid temperature, p is the pressure, $\mathbf{B}$ is the external magnetic field, $\mathbf{I}$ is the electric current, ϕ is the electric potential, $\mathbf{g}$ is the gravitational acceleration vector, K is the permeability of the porous medium, α_m is the effective thermal diffusivity, ρ is the density, μ is the dynamic viscosity, β is the coefficient of thermal expansion, c_p is the specific heat at constant pressure, σ is the electrical conductivity, ρ_0 is the reference density and -$\nabla\phi$ is the associated electric field. As discussed by Garandet *et al.* [16], Eqs. (4) and (5) reduce to $\nabla^2\phi = 0$. The unique solution is $\nabla\phi = 0$ since there is always an electrically insulating boundary around the enclosure. Thus, it follows that the electric field vanishes everywhere (see, Alchaar *et al.*, [17]).

Eliminating the pressure term in Eq. (2) in the usual way, the governing equations (1) to (3) can be written as

$$\frac{\partial u}{\partial x} + \frac{\partial v}{\partial y} = 0 \tag{7}$$

$$\frac{\partial u}{\partial y} - \frac{\partial v}{\partial x} = \tag{8}$$
$$- \frac{gK\beta}{\upsilon}\frac{\partial T}{\partial x} + \frac{\sigma K B_0^2}{\mu}\left(-\frac{\partial u}{\partial y}\sin^2\gamma + 2\frac{\partial v}{\partial y}\sin\gamma\cos\gamma + \frac{\partial v}{\partial x}\cos^2\gamma\right)$$

$$u\frac{\partial T}{\partial x} + v\frac{\partial T}{\partial y} = \alpha_m\left(\frac{\partial^2 T}{\partial x^2} + \frac{\partial^2 T}{\partial y^2}\right) + \frac{q_0'''}{\rho c_p} \tag{9}$$

which has to be solved subject to the boundary conditions

$$u = 0, T = T_0 \quad \text{at} \quad x = 0 \quad \text{and} \quad x = l, \quad 0 \le y \le h \tag{10}$$
$$v = 0, \frac{\partial T}{\partial y} = 0 \quad \text{at} \quad y = 0 \quad \text{and} \quad y = h, \quad 0 \le x \le l$$

where B_0 is the magnitude of $\mathbf{B}$ and υ is the kinematic viscosity of the fluid. Further, we introduce the following non-dimensional variables

$$X = \frac{x}{l}, Y = \frac{y}{h}, U = \frac{h}{\alpha_m}u, V = \frac{l}{\alpha_m}v, \theta = \frac{T - T_0}{(q_0''' l^2/k)} \tag{11}$$

where k is the thermal conductivity. Introducing the stream function ψ defined as $U = \partial\psi/\partial Y$ and V =-$\partial\psi/\partial X$, and using expressions (11) in Eqs. (7) - (9), we obtain the following partial differential equations in non-dimensional form:

$$\frac{\partial^2\psi}{\partial X^2} + a^2\frac{\partial^2\psi}{\partial Y^2} = -Ra\frac{\partial\theta}{\partial X} - Ha^2\left(a^2\frac{\partial^2\psi}{\partial Y^2}\sin^2\gamma + 2a\frac{\partial^2\psi}{\partial X\partial Y}\sin\gamma\cos\gamma + \frac{\partial^2\psi}{\partial X^2}\cos^2\gamma\right) \tag{12}$$

$$\frac{\partial^2\theta}{\partial X^2} + a^2\frac{\partial^2\theta}{\partial Y^2} + 1 = a\left(\frac{\partial\psi}{\partial Y}\frac{\partial\theta}{\partial X} - \frac{\partial\psi}{\partial X}\frac{\partial\theta}{\partial Y}\right) \tag{13}$$

which have to be solved subject to the boundary conditions

$$\psi = 0, \theta = 0, \quad \text{at} \quad X = 0 \quad \text{and} \quad X = 1, \quad 0 \le Y \le 1 \tag{14}$$
$$\psi = 0, \frac{\partial\psi}{\partial Y} = 0, \frac{\partial\theta}{\partial Y} = 0 \quad \text{at} \quad Y = 0 \quad \text{and} \quad Y = 1, \quad 0 \le X \le 1$$

where $a = l/h$ is the aspect ratio of the cavity, Ra is the Rayleigh number and $Ha = \sigma K B_0^2/\mu$ is the Hartmann number for the porous medium. It should

mentioned that $\gamma = 0$ corresponds to a horizontal magnetic field and $\gamma = \pi/2$ corresponds to a vertical magnetic field, respectively.

Once we know the temperature we can obtain the rate of heat transfer from each of the vertical walls, which are given in terms of the local Nusselt number Nu_Y and the mean Nusselt number Nu which are defined as

$$Nu_Y = -\left(\frac{\partial\theta}{\partial X}\right)_{X=0}, Nu = -\int_0^1 \left(\frac{\partial\theta}{\partial X}\right)_{X=0} dY \tag{15}$$

3 Numerical method and validation

To obtain the numerical solution of Eqs (12) and (13) a central finite-difference scheme was used and the system of discretized equations has been solved using a Gauss-Seidel iteration technique. The unknowns θ and ψ were calculated iteratively until the following criteria of convergence was fulfilled:

$$|\max[\chi_{new}(i,j) - \chi_{old}(i,j)]| \leq \varepsilon \tag{16}$$

where χ represents the temperature or the stream function and ε is the convergence criteria. In all the results presented in this paper, $\varepsilon = 10^{-7}$ was found be sufficiently small such that any smaller value produced results which were graphically the same. In order to choose the size of the grid, accuracy tests using the finite different method and Richardson extrapolation [26] for mesh sensitivity analysis were perform for $Ra = 10^3$, $Ha = 0$, and aspect ratio $a = 1$, using three sets of grids: $26 \times 26, 51 \times 51$, 101×101 and 201×201 as shown in Table 1. Reasonably good agreement was found between the 51×51 and 101×101 grids and therefore the grid used in this problem was 101×101 and these give accurate results for $Ra \leq 10^3$. We have also found that 201×201 grids give accurate results for $Ra \leq 10^5$.

Table 1
Accuracy test for $Ra = 10^3$, $Ha = 0$ and $a = 1$

Nodes	$\psi(0.24, 0.24)$	$\theta(0.24, 0.24)$
26×26	2.6368	0.0389
51×51	2.5987	0.0384
101×101	2.5800	0.0382
201×201	2.5707	0.0381
Richardon extrapolation	2.5614	0.0380

Further, in order to verify the accuracy of the code we compared the obtained results for the case when the magnetic field is absent ($Ha = 0$), $a = 0.5$ and $Ra = 10$ and 10^3, respectively, with those obtained by Haajizadeh *et al.* [27]. These results are shown in Table 2. It can be concluded from this table that the results are in good agreement and we can be confident that the present analysis and the code used are correct.

Table 2
Comparison of ψ_{max} and θ_{max} for $Ha = 0$ and $a = 0.5$

Ra	Haajizadeh *et al.* [27]		Present (Richardson extrapolation)	
	$\psi_{\max}$	$\theta_{\max}$	$\psi_{\max}$	$\theta_{\max}$
10	0.078	0.130	0.079	0.127
10^3	4.880	0.118	4.833(4.832)	0.116(0.116)

4 Analytical solution

For small values of $a(\ll 1)$, the solution of Eqs. (12) and (13) is given by the leading order terms, $\psi = \psi_0(x)$ and $\theta = \theta_0(x)$, see Mandar *et al.* [28]

$$(1 + Ha^2 cos^2\gamma)\frac{\partial^2\psi_0}{\partial X^2} = -Ra\frac{\partial\theta_0}{\partial X} \tag{17}$$

$$\frac{\partial^2\theta_0}{\partial X^2} + 1 = 0 \tag{18}$$

with the boundary conditions

$$\psi_0 = \theta_0 = 0 \qquad \text{at} \qquad X = 0 \qquad \text{and} \qquad X = 1 \tag{19}$$

On solving Eqs. (17) and (18) with the boundary conditions (19), we obtain

$$\begin{aligned} \theta_0(X) &= \frac{X(1-X)}{2} \\ \psi_0(X) &= \frac{Ra}{2(1 + Ha^2\cos^2\gamma)}\left(\frac{1}{6}X - \frac{1}{2}X^2 + \frac{1}{3}X^3\right) \end{aligned} \tag{20}$$

5 Results and discussions

In this section we present numerical results for the streamlines, isotherms and velocity profiles on the left wall, for various values of the magnetic field parameter Ha, inclination angle γ of the magnetic field and the Rayleigh number Ra. In addition, the local Nusselt numbers Nu_Y have been calculated. Figures (2) -(6) show plots of the streamlines and isotherms for an aspect ration $a = 1$, Rayleigh number $Ra = 10^3$ and 10^5, magnetic field parameter $Ha = 0, 1, 10$ and 50 and values of the inclined angle $\gamma = 0, \pi/6, \pi/4$ and $\pi/2$. It is seen from these figures that the intensity of the convection in the core is considerable affected by the magnetic field. A weak convective motion with a bicellular structure is induced, see Figs. 2 to 5. The two cells are symmetrical with respect to the central plane according to the value of γ. It is also observed that these two cells rotate for $\gamma = \pi/6$ and $\pi/4$. It is seen from Fig. 2 that the pattern of the streamlines and isotherms are similar to those predicted by Haajizadeh *et al.* [27]. On the other hand, Fig. 3 illustrates that for relative small values of Ha ($Ha = 1$) the maximum stream function increases and the maximum temperature decreases as γ increases. However, for larger values of Ha ($Ha >> 1$) the maximum of both the stream function and the temperature increase as γ increases. Therefore, the presence of the magnetic force tends to accelerate the fluid motion inside the cavity when the direction of the magnetic field changes from the horizontal to the vertical direction. Further, for $Ra = 10^3$ and higher values of Ha, the isotherms are almost parallel and this implies that conduction is dominant, see Figures 4 and 5. Also, these figures show that when the magnetic field is horizontal ($\gamma = 0$) and $Ra = 10^3$ the core vortex is elongated vertically as the Hartmann number increase. For the value of Ra and γ considered, the core streamlines start to flatten at the top and bottom of the cavity, while the isotherms are almost parallel. This indicates that conduction is dominated, see Fig. 5. For high Rayleigh numbers, the flow and heat transfer regime is characterized by a thermally stratified core region and two thin boundary layers on the vertical walls, see Fig. 6(a). Also, as the Raigleigh number and magnetic field increase ($Ra = 10^5$ and $Ha = 10, 50$), stronger convective motion takes place and the core vortex breaks up into three cells. There is also a weak distortion of the isotherms, as indicated in Figs. 6(b)-(c). This occurs at smaller inclination angles of the magnetic field ($\gamma = \pi/6$). This is in agreement with the results reported by Al-Najem *et al.* [29] for the case of natural convection in a two-dimensional square cavity filled with a viscous fluid with a transverse magnetic field.

Typical velocity profiles at the vertical walls, U_w for $Ra = 10^3$ and different values of γ and Ha are shown in Fig. 7. We observe that for a fixed value of Ha that the minimum of the wall velocity is attained when the magnetic field is in the vertical direction ($\gamma = \pi/2$). On the other hand, for $\gamma = \pi/4$ the wall velocity decreases as Ha increases. We observe that for all the values of

Ra considered, the maximum temperature profiles do not overshoot the limit prescribed by the analytical solution ($\theta_{\max} = 1/8$), see Fig. 8. Numerical and analytical solutions for the streamlines on the horizontal centerline plane of the cavity are shown in Figs. 9 for a small value of the aspect ratio, namely $a = 0.01$ and for $Ra = 10^3$ when $Ha = 0, 1, 5$ and $\gamma = 0$ (Fig. 9a) and when $Ha = 1$ and $\gamma = 0, \pi/4, \pi/2$ (Fig. 9b). We observe from these figures that there is very good agreement between the analytical and numerical solution.

Figure 10 shows the variation of the local Nusselt number Nu_Y with Y for $Ra = 100$ and $\gamma = 0$. In order to compare the present results with those obtained by Haajizadeh *et al.* [27] when the magnetic field is absent($Ha = 0$) the value of $2Nu_Y$ for $a = 0.2$ is presented in this figure. It is observed that the results are in very good agreement and therefore we are confident that the present results are accurate. Finally, Fig. 11 presents the variations of the local Nusselt number Nu_Y with Y for $Ra = 100$, $Ha = 1$ and for several values of γ when $a = 1$. It is also found that the local Nusselt number Nu_Y decreases at the bottom wall as γ increases (magnetic field changes its direction from the horizontal to the vertical direction) and vice-versa for the top wall of the cavity.

6 Conclusion

The present numerical study exhibits many interesting features concerning the effect of the inclined magnetic fields on the free convection flow and heat transfer characteristics in a rectangular cavity filled with a porous medium. Detailed numerical results for the temperature distribution and heat transfer have been presented in graphical and tabular form. The main conclusions of the present analysis are as follows:

- In general, it has been found that the effect of the magnetic field is to reduce the convective heat transfer inside the cavity.
- The convection modes within the cavity were found to depend upon both the strength and the inclination of the magnetic field. The applied magnetic field in the horizontal direction was found to be most effective in suppressing the convection flow for a stronger magnetic field in comparison with the vertical direction.
- It is found that strong boundary layers are formed near the vertical walls for $Ra = 10^5$ and $\gamma = \pi/6$ and the intensity increases as Ha increases. The flat isotherms in the core region indicate that there is negligible lateral heat conduction and the equal spacing of the streamlines implies a uniform vertical velocity in this region, as predicted by boundary layer theory, see Fig. 6(a).

- The magnetic field has a negligible effect on the heat transfer mechanism for small values of γ and $Ha >> 1$. This is true since pure conduction becomes dominant when the magnetic field is applied in the horizontal direction ($\gamma = 0$). However, for $Ra = 10^5$ the the parabolic profile is distroyed.
- For Rayleigh number $Ra = 10^3$, and small Hartmann numbers, the flow and heat transfer are characterized by a parallel flow structure in the central region of the cavity. The conduction is the dominant mode of heat transfer and vertical velocity profiles and temperatures are almost parabolic.
- It should be pointed out that the general analysis described in this work can represent a useful starting point to treat more complex problems, such as, for example, time-dependent flows.

Acknowledgements

The work done by T. Grosan and C. Revnic is supported by the MEDCT under Grant Ceex 90/2006. D.B. Ingham and I. Pop wishes to express their thanks to the Royal Society for partial financial support.

References

[1] D.A. Nield, A. Bejan, Convection in Porous Media (3th edition), Springer, New York, 2006.

[2] D.B. Ingham, I. Pop (eds.), Transport Phenomena in Porous Media, Elsevier, Oxford, 2005.

[3] K. Vafai (ed.), Hanbook of Porous Media, (2nd edition), Taylor&Francis, Boca Raton, 2005.

[4] A. Bejan, I. Dincer, S. Lorente, A. F. Miguel, A. H. Reis, Porous and Complex Flows Structures in Modern Technologies, Springer, New York, 2004.

[5] I. Pop, D.B. Ingham, Convective Heat Transfer: Mathematical and Computational Modelling of Viscous Fluids and Porous Media, Pergamon, Oxford, 2001.

[6] M.J.S. de Lemosm, Turbulence in Porous Media: Modeling and Applications, Elsevier, Oxford, 2006.

[7] P. Vadasz (ed.), Emerging Topics in Heat and Mass Transfer in Porous Media, Springer, New York, 2008.

[8] O. Martynenko, P. Khramtsov, Free-Convective Heat Transfer, Springer, Berlin, 2005.

[9] S. Acharya, R.J. Golstein, Natural convection in an externally heated vertical or inclined square box containing internal energy sources, J. Heat Transfer 107 (1985) 855-866.

[10] H. Ozoe, K. Okada, The effect of the direction of the external magnetic field on the three-dimensional natural convection in cubical enclosure, Int. J. Heat Mass Transfer 32(1989) 1939-1954.

[11] J.-H. Lee, R.J. Goldstein, An experimental study on natural convection heat transfer in an inclined square enclosure containing internal energy sources, J. Heat Transfer 110 (1988) 345-349.

[12] T. Fusegi, J. M. Hyun, K. Kuwahara, Natural convection in a differentially heated square cavity with internal heat generation, Numer. Heat Transfer, Part A 21 (1992) 215-229.

[13] M. Venkatachalappa, C.K. Subbaraya, Natural convection in a rectangular enclosure in the presence of a magnetic field with uniform heat flux from the side walls, Acta Mechanica 96 (1993) 13-26.

[14] Y.M. Shim, J.M. Hyun, Transient confined natural convection with internal heat generation, Int. J. Heat Fluid Flow 18 (1997) 328-333.

[15] M.A. Hossain, M. Wilson, Natural convection flow in a fluid-saturated porous medium enclosed by non-isothermal walls with heat generation, Int. J. Thermal Sci. 41 (2002) 447-454.

[16] J.P. Garandet, T. Albussoiere, R. Moreau, Buoyancy driven convection in a rectangular enclosure with a transverse magnetic field, Int. J. Heat Mass Transfer 35 (1992) 741-748.

[17] S. Alchaar, P. Vasseur, E. Bilgen, Natural convection heat transfer in a rectangular enclosure with a transverse magnetic field, J. Heat Transfer 117 (1995) 668-673.

[18] K. Kanafer, A.J. Chamkha, Hydromagnetic natural convection from an inclined porous square enclosure with heat generation, Numer. Heat Transfer, Part A 33 (1998) 891-910.

[19] A.J. Chamkha, H. Al-Naser, Double-diffusive convection in an inclined porous enclosure with opposing temperature and concentration gradients, Int. J. Thermal Sci. 40 (2001) 227-244.

[20] S. Mahmud, S.H. Tasnim, M.A.H.Mamun,Thermodynamic analysis of mixed convection in a channel with transverse hydromagnetic effect, Int. J. Thermal Sci. 42 (2003) 731-740.

[21] Md.A. Hossain, D.A.S.Rees, Natural convection flow of water near its density maximum in a rectangular enclosure having isothermal walls with heat generation, Heat Mass Transfer 41 (2005) 367-374.

[22] M.A. Hossain, M.Z. Hafiz, D.A.S. Rees, Buoyancy and thermo capillary driven convection flow of an electrically conducting fluid in an enclosure with heat generation, Int. J. Thermal Sci. 44 (2005) 676-684.

[23] M.C. Ece, E. Büyük, Natural-convection flow under a magnetic field in an inclined rectangular enclosure heated and cooled on adjacent walls, Fluid Dyn. Res. 38 (2006) 564-590.

[24] D.A. Nield, Impracticality of MHD Convection in a Porous Medium, Transport Porous Media 73 (2008) 379-380.

[25] A. Barletta, S. Lazzari, E. Magayri, I. Pop, Mixed convection with heating effect in a vertical porous annulus with a radially varying magnetic field, Int. J. Heat Mass Transfer (online).

[26] G.D. Smith, Numerical Solution of Partial Differential Equations. Finite Difference Method, Oxford university Press, New York, 2004.

[27] M. Haajizadeh, A. F. Ozguc,C. L. Tien, Natural convection in a vertical porous enclosure with internal heat generation, Int. J. Heat Mass Transfer 27 (1984) 1893-1902.

[28] N.M. Al-Najem, K.M. Khanafer, and M.M. El-Refaee, Numerical study of laminar natural convection in tilted enclosure with transverse magnetic field, Int. J. Numer. Methods Heat Fluid Flow 8 (1998) 651-672

[29] V.J. Mandar, U. N. Gaitonde and K.M. Sushanta, Analytical study of natural convection in a cavity with volumetric heat generation, J. Heat Transfer 128 (2006) 176-182.

List of Figures

Figure 7. The velocity profile in the vicinity of the vertical wall for different values of γ and Ha.

Figure 8. Temperature profiles for $a = 0.01$ and $Ra = 1000$.

Figure 9. Comparison between the streamlines obtained analytical and numerical:
(a) for $\gamma = 0$ and different values of Ha;
(b) for $Ha = 1$ and different values of γ.

Figure 10. Nusselt number for $Ra = 100, a = 0.2, \gamma = 0$ and different values of Ha.

Figure 11. Nusselt number for $Ra = 100, a = 1, Ha = 1$ and different values of γ.

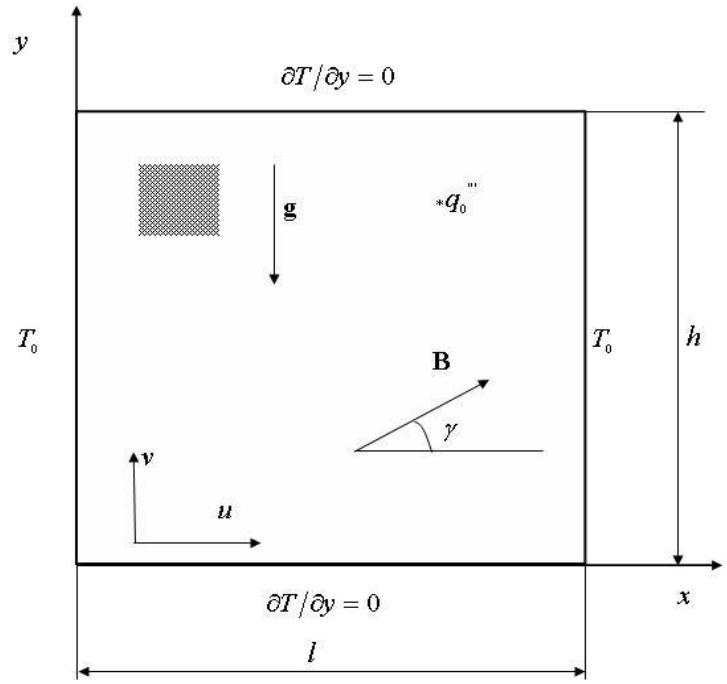

Fig. 1. Geometry of the problem and co-ordinate system.

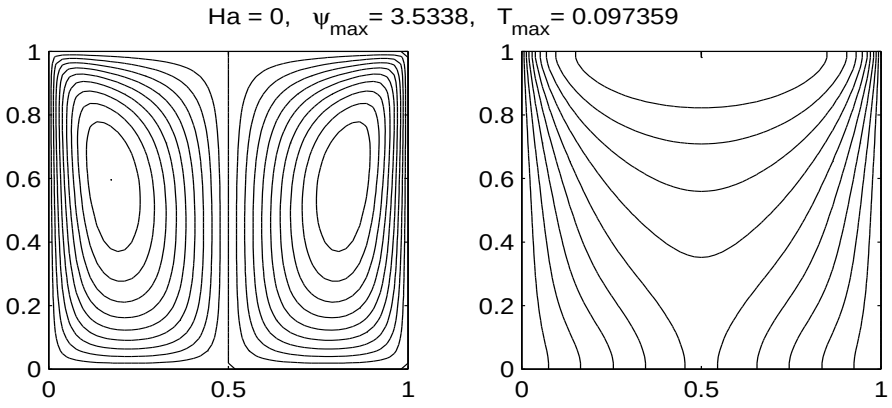

Fig. 2. Streamlines and isotherms for $Ra = 10^3$, $Ha = 0$ and when the magnetic field is in horizontal direction ($\theta = 0^0$).

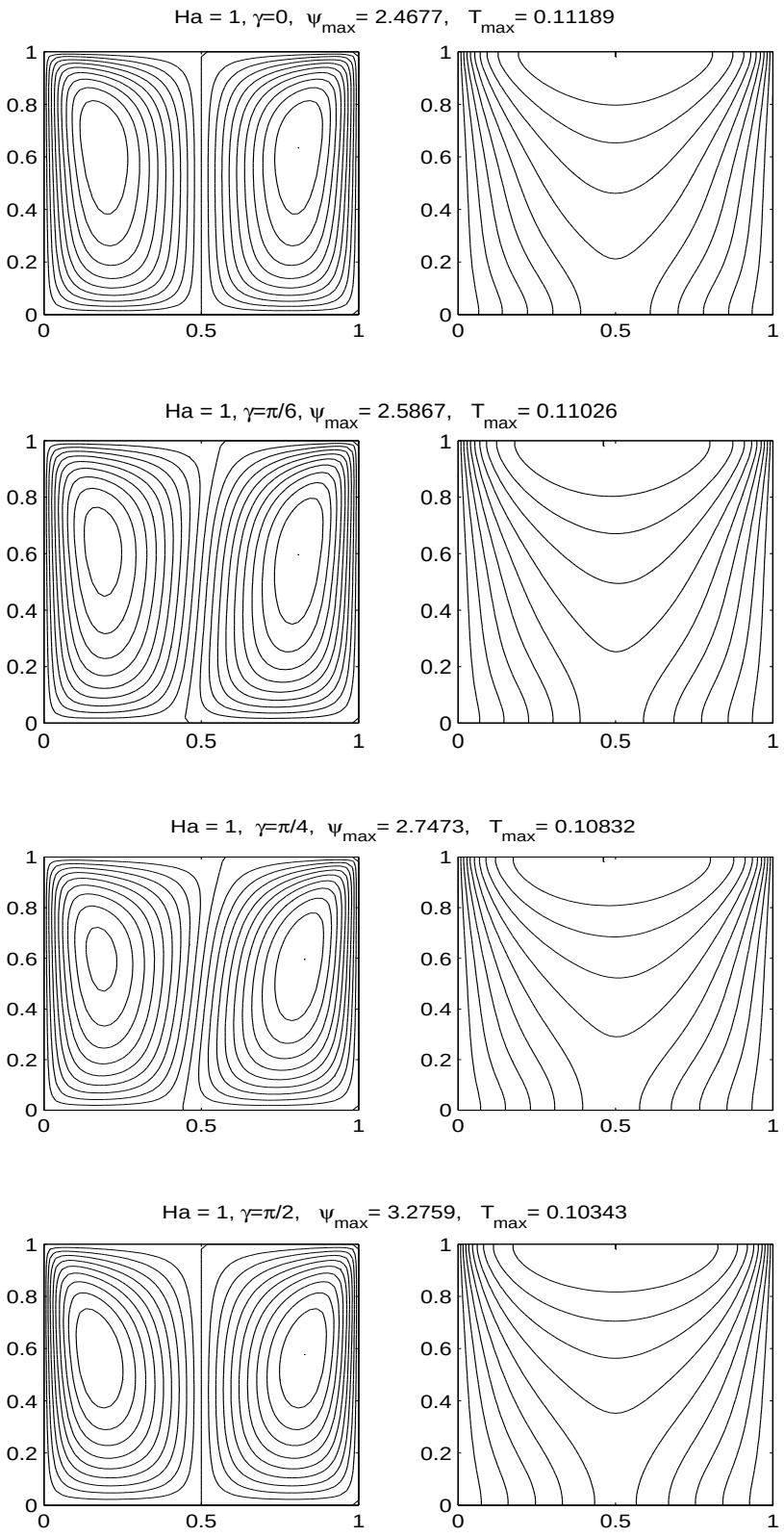

Fig. 3. Streamlines and isotherms for $Ra = 10^3$, $Ha = 1$ and for different values of γ.

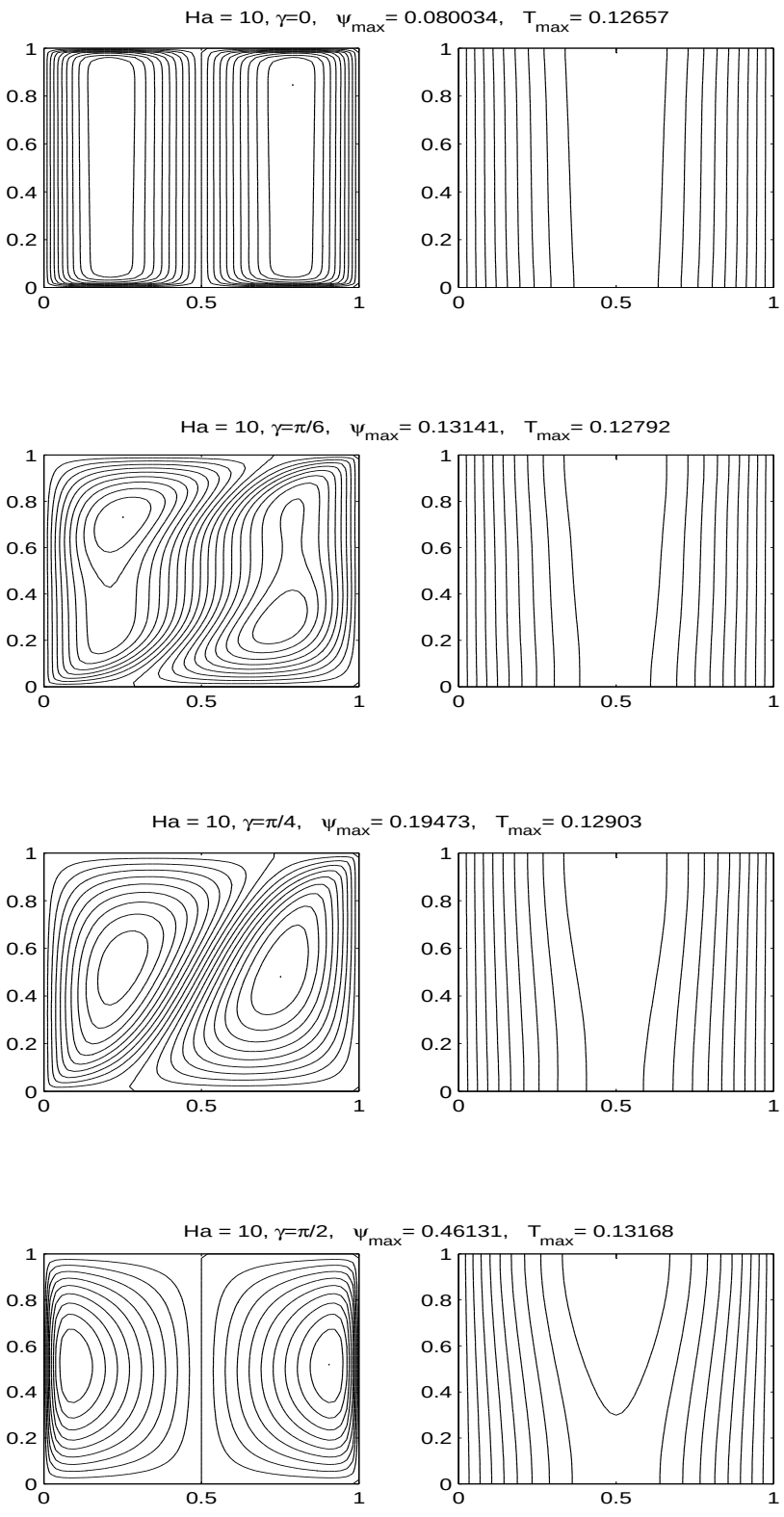

Fig. 4. Streamlines and isotherms for $Ra = 10^3$, $Ha = 10$ and for different values of γ.

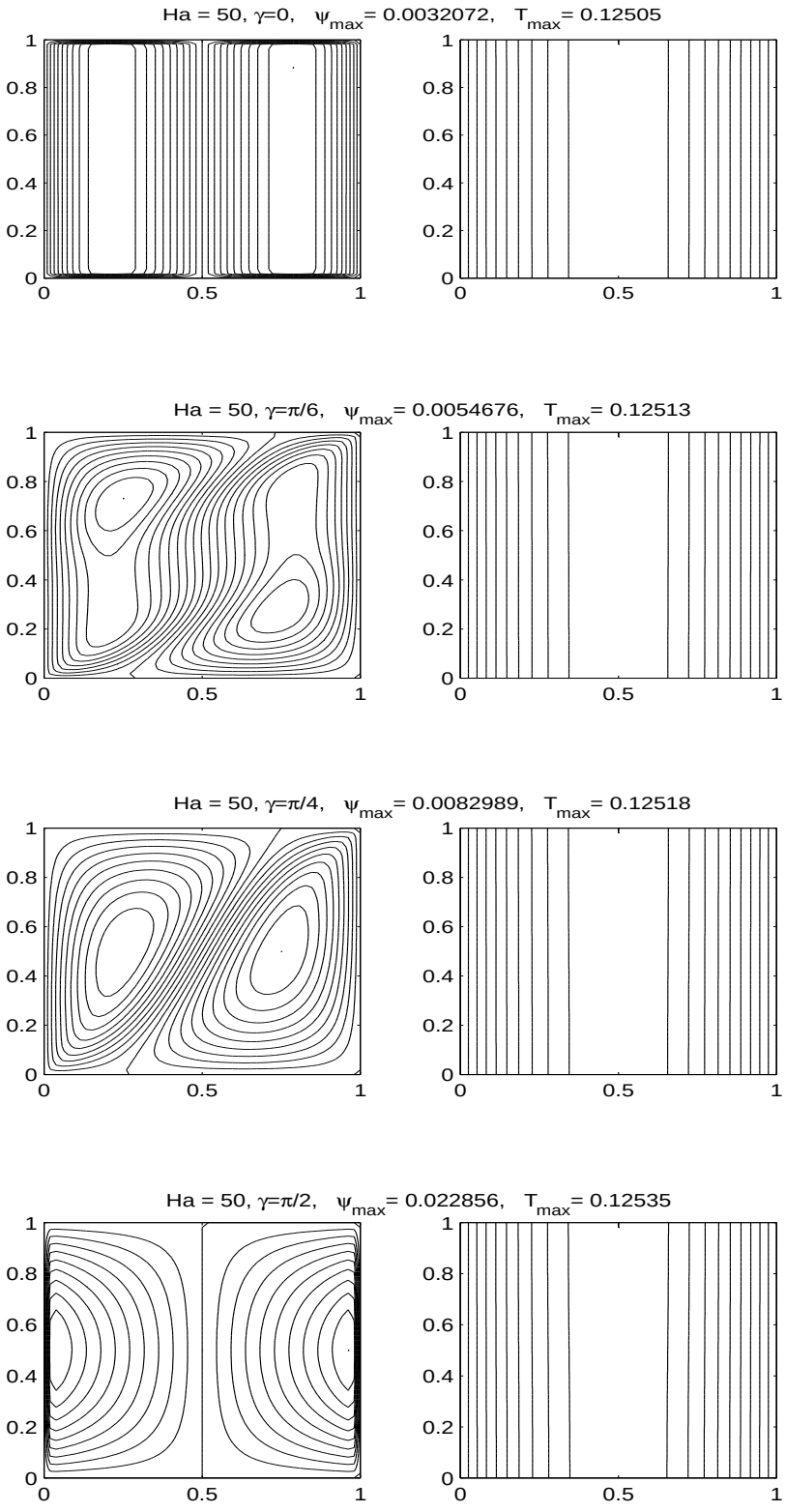

Fig. 5. Streamlines and isotherms for $Ra = 10^3$, $Ha = 50$ and for different values of γ.

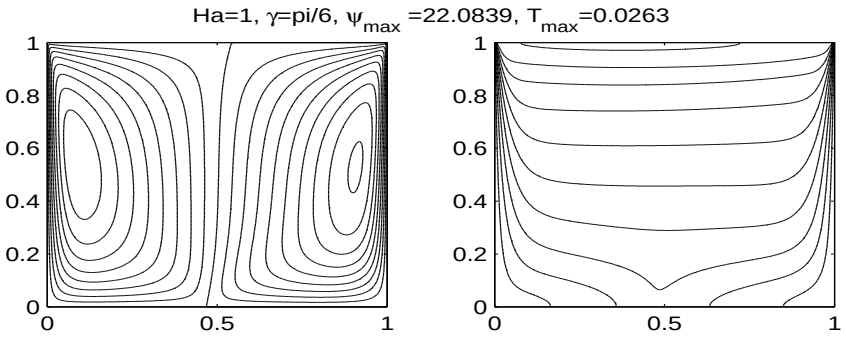

(a)

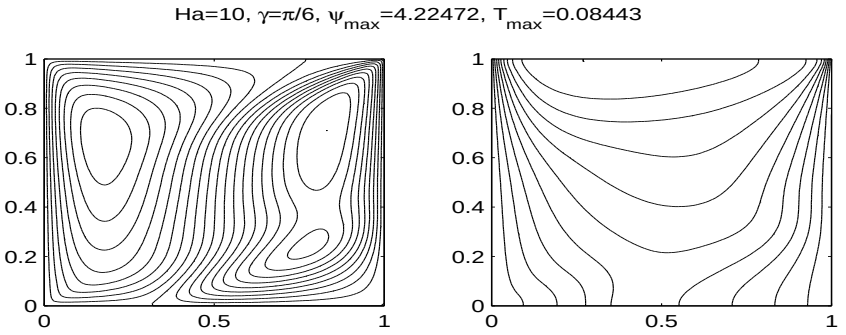

(b)

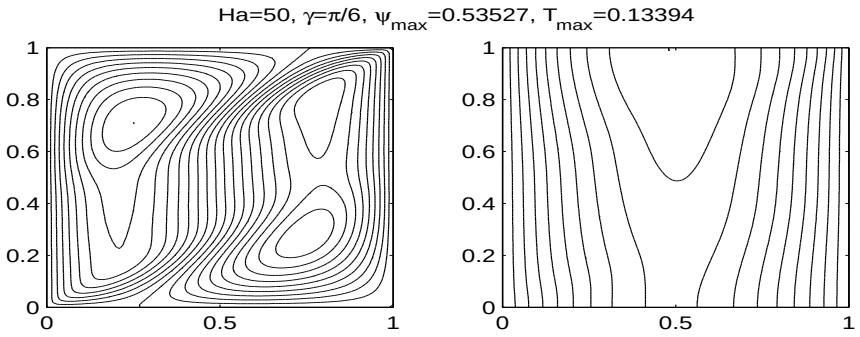

(c)

Fig. 6. Streamlines and isotherms for $Ra = 10^5$, $\gamma = \pi/6$ and for different values of Ha.

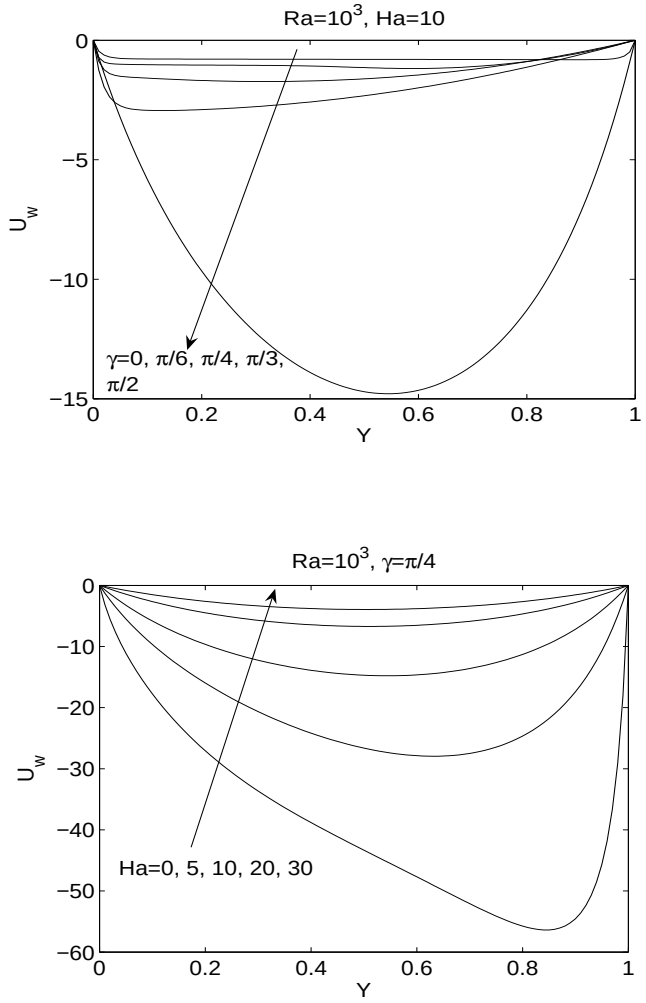

Fig. 7. The velocity profile in the vicinity of the vertical wall for different values of γ and Ha.

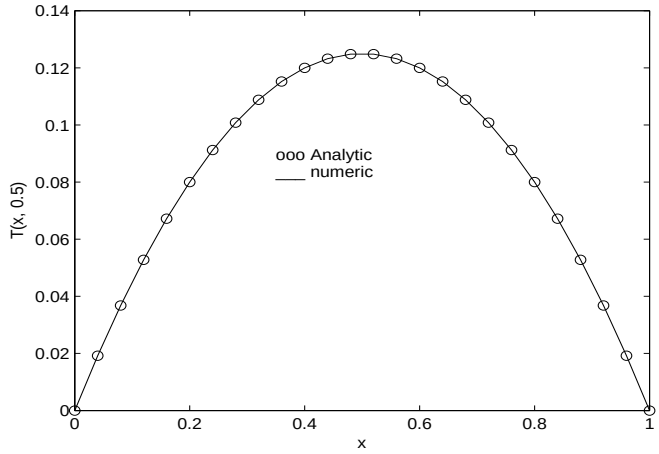

Fig. 8. Temperature profiles for $a = 0.01$ and $Ra = 1000$.

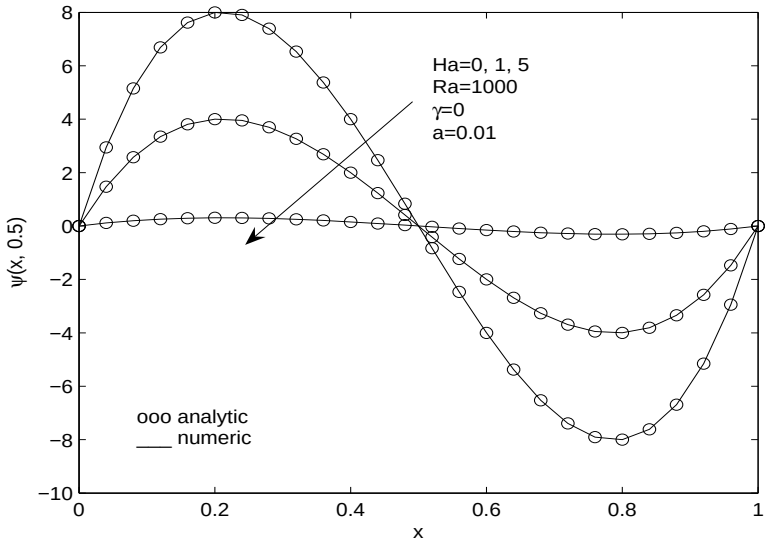

(a)

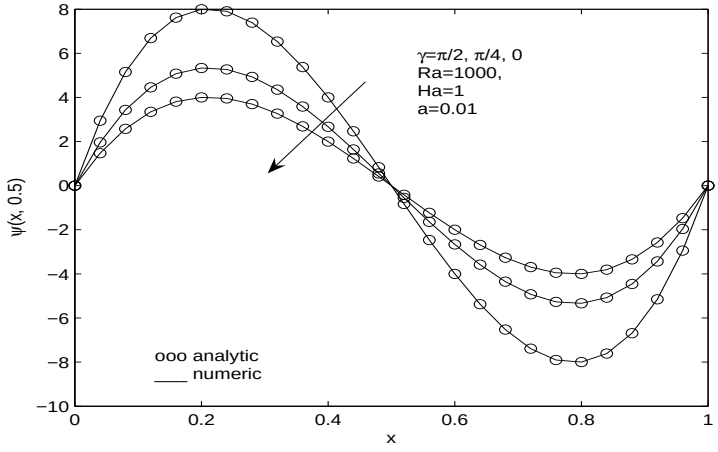

(b)

Fig. 9. Comparison between the streamlines obtained analytical and numerical:
(a) for $\gamma = 0$ and different values of Ha;
(b) for $Ha = 1$ and different values of γ.

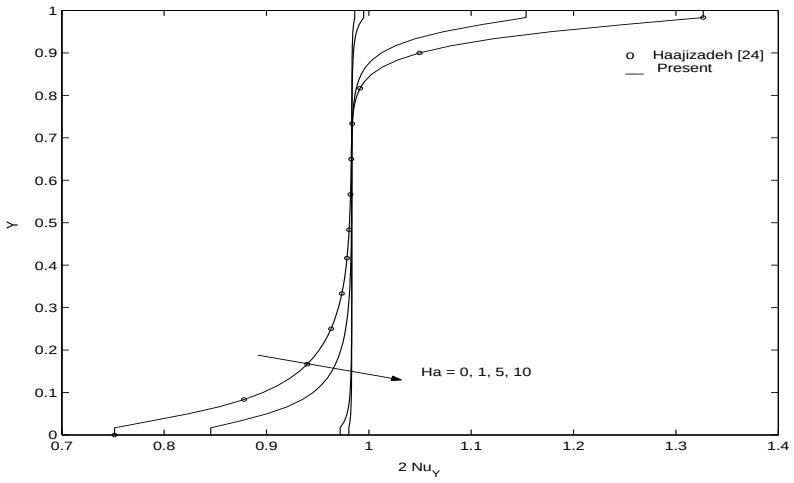

Fig. 10. Nusselt number for $Ra = 100, a = 0.2, \gamma = 0$ and different values of Ha.

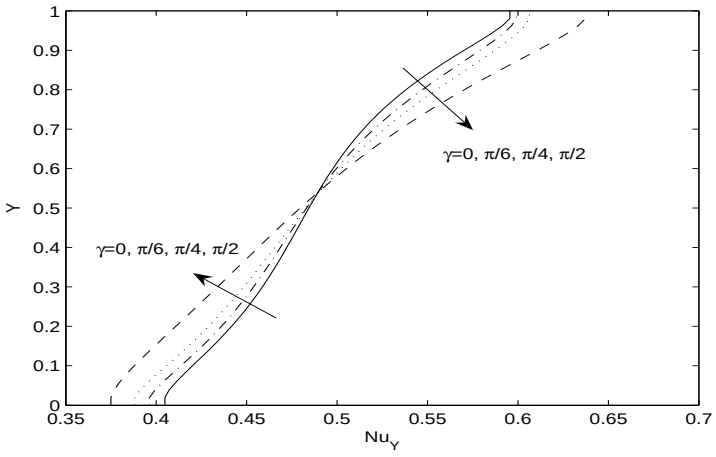

Fig. 11. Nusselt number for $Ra = 100, a = 1, Ha = 1$ and different values of γ.

Anexa II

Abstractul articolelor publicate în jurnale neindexate ISI

Int. J. of Applied Mechanics and Engineering, 2006, vol.11, No.3, pp.715-722

Letter to the Editor

A NOTE ON THE EFFECT OF RADIATION ON FREE CONVECTION OVER A VERTICAL FLAT PLATE EMBEDDED IN A NON-NEWTONIAN FLUID SATURATED POROUS MEDIUM

T. GROSAN and I. POP*
Faculty of Mathematics and Computer Science
Babeş-Bolyai University, R-3400 Cluj-Napoca, ROMANIA
e-mail: popi@math.ubbcluj.ro

The effect of radiation on the free convection from a vertical plate embedded in a power-law fluid saturated porous media has been considered. Similarity equations have been obtained and solved numerically. It was found that there is an increase in the boundary layer thickness with an increase in the radiation parameter N and a decrease in the power-law index n was observed.

Key words: porous media, non-Darcy law, boundary layer, radiation.

TECHNISCHE MECHANIK, Band 26, Heft 1, (2006), 11-19
Manuskripteingang: 03. November 2005

Rotating Flow of Power-Law Fluids over a Stretching Surface

M. Kumari, T. Grosan , I. Pop

The steady flow of a non-Newtonian power-law fluid due to a stretching surface in a rotating fluid has been investigated in this paper. After a similarity transformation, the set of non-linear ordinary differential equations have been solved numerically using the Keller-box method for some values of the parameter λ which is the ratio of the rotation rate to the stretching rate and the power-law index n. It is found that both the skin frictions coefficients in the x and y directions decrease with the increase of the parameter λ. However, for smaller values of λ the skin friction coefficients are higher for the dilatant fluid and smaller for the pseudoplastic fluid, respectively.

STUDIA UNIV. "BABEŞ-BOLYAI", MATHEMATICA, Volume LI, Number 4, December 2006

THERMAL RADIATION EFFECT ON FULLY DEVELOPED FREE CONVECTION IN A VERTICAL RECTANGULAR DUCT

T. GROŞAN, T. MAHMOOD, AND I. POP

Dedicated to Professor Gheorghe Coman at his 70^{th} anniversary

Abstract. The effect of radiation on the steady free convection flow, i.e. the case of purely buoyancy-driven flow, in a vertical rectangular duct is investigated for laminar and fully developed regime. The Rosseland approximation is considered and temperatures of the walls are assumed constants. The governing equations are expressed in non-dimensional form and are solved both analytically and numerically. It was found that the governing parameters have a significant effect on the velocity and temperature profiles.

BULLETIN OF THE TRANSILVANIA UNIVERSITY OF BRAŞOV

NON-LINEAR DENSITY VARIATION EFFECTS ON THE FULLY DEVELOPED MIXED CONVECTION FLOW IN A VERTICAL CHANNEL

T. GROŞAN* I. POP*

Abstract: *The effect of the quadratic term of density variation with temperature on the steady mixed convection flow in a vertical channel is investigated for laminar and fully developed flow regime .In the modelling of the heat transfer the viscous dissipation term was considered and temperatures of the walls are assumed constants. The governing equations are expressed in non-dimensional form and are solved both analytically and numerically. It was found that there is a decrease in reversal flow with an increase in the mixed convection parameters.*

Keywords: *fully developed flow, mixed convection, viscous dissipation*

Mixed convection flow along a thin vertical cylinder with localized heating or cooling in a porous medium

M. Kumari
Department of Mathematics, Indian Institute of Bangalore, Bangalore, India

C. Bercea and I. Pop*
Faculty of Mathematics University of Cluj, Cluj CP 253, Romania

The effects of localized cooling/heating on the steady mixed convection boundary layer flow over a thin vertical cylinder embedded in a fluid saturated porous medium under the assumption of Darcy law has been theoretically studied. The localized cooling/heating introduces a finite discontinuity in the mathematical formulation of the problem, which increases its complexity. In order to overcome this difficulty, a non-uniform distribution of the wall temperature is considered at certain sections of the cylinder. The nonlinear coupled parabolic partial differential equations have been solved numerically by using an implicit finite-difference scheme similar to that proposed by Blottner [23].

Key words: mixed convection, vertical cylinder, porous medium, boundary layer

Seria B1, Vol 13, pag 31-38, 2006

FORCED CONVECTION BOUNDARY LAYER FLOW OVER A FLAT PLATE WITH VARIABLE THERMAL CONDUCTIVITY EMBEDDED IN A POROUS MEDIUM

C. BERCEA* I. POP*

Abstract: *The effect of variable thermal diffusivity on the steady forced convection boundary layer flow past a flat plate which is embedded in a fluid-saturated porous medium has been studied in this paper. The basic partial differential equations of continuity, Darcy law and the energy are transformed into a single ordinary differential equation using a simple similarity transformation. This equation is solved analytically and numerically.*

Keywords: *forced convection, boundary layer flow, variable thermal conductivity, Keller – box method.*

TECHNISCHE MECHANIK, Band 27, Heft 1, (2007), 37 – 47
Manuskripteingang: 6. Juli 2006

Thermal Radiation Effect on Fully Developed Mixed Convection Flow in a Vertical Channel

T. Grosan, I. Pop

The effect of radiation on the steady mixed convection flow in a vertical channel is investigated for laminar and fully developed flow regime. The Rosseland approximation is considered in the modelling of the conduction-radiation heat transfer and temperatures of the walls are assumed constants. The governing equations are expressed in non-dimensional form and are solved both analytically and numerically. It was found that there is a decrease in reversal flow with an increase in the radiation parameters.

Effect of non-uniform suction or injection on mixed convection flow over a vertical cylinder embedded in a porous medium

M. Kumari[1], C. Bercea and I. Pop[2*]

[1]*Department of Mathematics, Indian Institute of Bangalore, Bangalore, India*

[2]*Faculty of Mathematics University of Cluj, R-3400 Cluj, Cluj CP 253, Romania*

Abstract. The effect of steady non-uniform suction or injection on mixed convection boundary layer flow over a vertical heated or cooled permeable cylinder, which is embedded in a fluid-saturated porous medium, is studied numerically using the Darcy law approximation. Both assisting and opposing flow cases are considered. Using suitable transformations, the coupled governing boundary layer equations are transformed into a form suitable for a numerical solution. The effects of the suction or injection, transverse curvature and mixed convection parameters on the local Nusselt number and temperature profiles are studied. The obtained results are presented graphically and discussed in details.

Keywords boundary layer, heat transfer, mixed convection, porous medium suction/injection, vertical cylinder

Int. J. of Applied Mechanics and Engineering, 2008, vol.13, No.1, pp.203-215

BOUNDARY LAYERS GROWTH ON A MOVING SURFACE DUE TO AN IMPULSIVE MOTION AND A SUDDEN INCREASE OF WALL HEAT FLUX

M. KUMARI
Department of Mathematics
Indian Institute of Bangalore
Bangalore, INDIA

T. GROSAN and I. POP*
Faculty of Mathematics
University of Cluj
R-3400 Cluj, CP 253, ROMANIA
e-mail: pop.ioan@yahoo.co.uk

In this paper we investigate the development of the momentum and thermal boundary layers over a continuous moving semi-infinite flat plate when the external stream starts impulsively from rest at time $t = 0$ with a constant velocity u_∞. It is assumed that the plate starts to supply heat to the fluid at a constant rate q_w at time $t = 0$ and maintained at this rate. The problem has been formulated in a new system of scaled coordinates such that for $t^* = 0$ it reduces to Rayleigh type of equation and for $t^* \to \infty$ (large time) it reduces to Blasius or Sakiadis type of equation. A new scale of dimensionless time ξ has been used which reduces the region of time integration from an infinite region $(0 \le t < \infty)$ to a finite time region $(0 \le \xi \le 1)$ which reduces the computational time considerably. The governing partial differential equations are transformed into a singular parabolic partial differential equations which have been solved numerically for a range of values of the governing parameters using an implicit finite-difference scheme. The results show that there is a smooth transition from Rayleigh solution to Blasius or Sakiadis solution as the dimensionless time ξ increases from zero to one.

Key words: continuously moving plate, unsteady boundary layer, heat flux rate, numerical solution.

STUDIA UNIV. "BABEŞ–BOLYAI", MATHEMATICA, Volume xxx, Number 1, March xxxx

Radiation and variable viscosity effects in forced convection from a horizontal plate embedded in a porous medium

T. GROSAN, I. POP, S.R. POP

Abstract. Radiation and temperature dependent viscosity effects on forced convection boundary layer flow over a horizontal plate embedded in a fluid-saturated porous media is studied in this paper. Darcy's law model, Rosseland model for radiation and an inverse proportional law for temperature dependent viscosity have been considered. The transformed ordinary differential equations are solved numerically, and a very good agreement between the present results and those reported for particular situations were found.

Proceedings of 3ICAMP
3rd International Conference on Applications of Porous Media
May 29 – June 3, 2006, Marrakesch, MOROCCO
Paper number "4"

MIXED CONVECTION ALONG A VERTICAL WAVY SURFACE WITH A DISCONTINUOUS TEMPERATURE PROFILE IN A POROUS MEDIUM

M. Kumari[(a)], C.Bercea[(b)*] and I. Pop[(b)]
[(a)]Department of Mathematics, Indian Institute of Bangalore, Bangalore, India
[(b)]Faculty of Mathematics, University of Cluj, R-3400 Cluj, CP 253, Romania

ABSTRACT

The steady mixed convection boundary layer flow along a vawy vertical wall with a discontinuous temperature profile and embedded in a fluid-saturated porous medium is considered in this paper. The overall surface is equally divided into a heated section succeeded by an unheated section alternately. The basic continuity equation, the Darcy law and the energy equation are transformed using a simple coordinate transformation which transforms the irregular surface into a flat surface. These equations are solved numerically using a very efficient implicit finite-difference method. The influence of the mixed convection and wavy geometry parameters on the skin friction coefficient, local Nusselt number and velocity and temperature profiles have been studied in details. The numerical results demonstrate that values of the local Nusselt number are positive (heat is transferred from the wall to the fluid) in the heated regions and it is negative (heat is transferred from the fluid to the wall) in the unheated regions, respectively. The obtained results for the heat transfer from the wall are also compared with the corresponding results for a vertical flat plate embedded in a porous medium with a uniform temperature distribution.

STUDIA UNIV. "BABEŞ–BOLYAI", MATHEMATICA, Volume LIII, Number 2, June 2008

HEAT TRANSFER IN AXISYMMETRIC STAGNATION FLOW ON A THIN CYLINDER

CORNELIA REVNIC, TEODOR GROŞAN, AND IOAN POP

Abstract. The steady axisymetric stagnation flow and heat transfer on a thin infinite cylinder of radius a is studied in this paper. Both cases of constant wall temperature and constant wall heat flux are considered. Using similarity variables the governing partial differential equations are transformed into ordinary differential equations. The resulting set of two equations is solved numerically using Runge-Kutta method combined with a shooting technique. For the special case of the Reynolds number $Re >> 1$ (boundary layer approximation), we obtained an asymptotic solution which include the Hiemenz solution. The present results are compared in some particular cases with existing results from the open literature and with the asymptotic approximation, and we found a very good agreement. It is shown that the Nusselt number and the skin friction increase and the boundary layer thickness decreases with the increase of the Reynolds number. Some graphs for the velocity and temperature profiles are presented. Also, tables with values related to the skin friction and Nusselt number are given.